Stimuli-Responsive Polymer-Based Materials and Devices for Controlled and Triggered
Release of Small Molecules

by

Siyuan Guo

A thesis submitted in partial fulfillment of the requirements for the degree of

Doctor of Philosophy

Department of Chemistry
University of Alberta

Abstract

This thesis covers the general scope of stimuli-responsive polymers and the concept of controlled drug delivery, with special focus on controlled/triggered release applications of temperature-responsive poly (*N*-isopropylacrylamide) (pNIPAm)-based hydrogels, microgels, their assemblies, and composites.

Chapter 2 focuses on investigating the methodology and mechanism of a controlled release system, i.e., a pNIPAm-based microgel-based assembly. Surface modification was utilized to build a chemical barrier to control the molecular interchange between the inside and the outside of the device. The small-molecule diffusion behaviors of the device were studied, and mathematical models were used to describe the behaviors.

Chapter 3 focuses on the development of a small-molecule controlled release system, based on the stimuli-responsive hydrogel–microgel composite (HMC). In this work, the small hydrophilic molecule release kinetics were tuned by changing the chemical composition of the material, and the mechanism of the controlled release was investigated based on the interactions between the small molecules and the polymer materials. As a further study of the HMC in controlled drug delivery applications, Chapter 4 discusses the idea of applying the HMC to a multi-drug controlled release system.

In addition, four appendices, A, B, C, and D have been added to the end of this dissertation. They contain supporting information for the main chapters, previous related work done before my PhD program, and preliminary experimental results on related research projects.

Preface

This thesis is an original work by Siyuan Guo (S. Guo) under the supervision of Dr. Michael J. Serpe (M. J. Serpe).

Chapter 2 of this thesis has been published as Guo, S.; Carvalho, S. W.; Wong, D.; and Serpe, J. M., *ACS Appl. Mater. Interfaces* 2019, 11, 50, 47446-47455. I was responsible for designing and executing experiments, data collection and analysis, and manuscript composition. W. S. Carvalho assisted with the data analysis and D. Wong assisted with the data collection. M. J. Serpe was the supervisory author and was involved in the concept formation and manuscript composition.

Appendix B of this thesis has been published as Guo, S.; Gao, Y.; Wei, M.; Zhang, Q. M.; and Serpe, J. M., *J. Mater. Chem. B* 2015, *3* (12), 2516-2521. Y. Gao and I contributed equally to this publication. I was responsible for the data collection, data analysis, and the manuscript composition, while Y. Gao was responsible for the experiment design and assisted with the manuscript composition. M. Wei assisted with the data collection and Q. Zhang assisted with the manuscript composition. M. J. Serpe was the supervisory author and was involved with research design and manuscript composition.

I would like to dedicate this thesis to my late grandfather Zuze Guo. It was his tireless

effort and unreserved dedication that have brought me this far. May his soul rest in

perfect peace!

Acknowledgement

I would like to express my most sincere gratitude to my supervisor, Dr. Michael J. Serpe, for providing me the opportunity to work in his laboratory on interesting and fascinating projects. As a great supervisor, he is enthusiastic about science, thoughtful to the students, and helpful in guiding us to pursue our goals. For me, he is not only a supervisor, but also a life mentor and a friend, as he was always by my side to extend my knowledge, support my research, and discuss the philosophy of life with me. I thank him for all of these. There is no doubt that it is my luck to have met him.

I would like to thank my supervisory committee members, Prof. Jillian M. Buriak and Prof. Jonathan G. C. Veinot, for their valuable suggestions and constructive criticism on my research. I am grateful also to Prof. Anastasia Elias and Prof. Elizabeth R. Gillies for agreeing to serve as the arm's length examiners for my doctoral examination. I also would like to thank Prof. Xi Zhang, who provided me with a wonderful project when I was visiting Tsinghua University. Special thanks are given to Dr. Qiao Song, who collaborated and discussed a lot with me on supramolecular chemistry research and helped me during my stay in Tsinghua. I also thank Prof. Qiang Matthew Zhang for his invaluable suggestions that helped me to get through difficulties in my research. In addition, I want to express my sincere appreciation to Dr. Anna Jordan for her tireless effort in editing this thesis and for her patient teaching on my writing.

I would like to express my gratitude to all the past and current Serpe group members and all the undergraduate students who worked with me. I feel so lucky to be one of this big family over the past five years. I also want to extend my gratitude to Mr. Gareth Lambkin from Biological Services, Ms. Kim Do from the Electronic Shop, Mr. Jason Dibbs

from the Glass Shop, and Mr. Dirk Kelm, Mr. Vincent Bizon, Mr. Paul Crothers, and Mr. Dieter Starke from the Machine Shop for their support and help on my research.

I would like to thank my parents, grandparents, and the rest of my family for their unconditional love, support, and encouragements. Last, but certainly not least, I would like to express my deepest gratitude to my lovely wife, Ruohan Gong, who has been there for me through the tough times and encouraged me over all the years since we have known each other, who has sacrificed so much to make my life go this far, and who has been giving me the unconditional love and support that brings me power and happiness. Ruohan, I appreciate your sincere love towards me, and I love you.

Table of Contents

List of Figures

List of Tables

List of Schemes

List of Abbreviations

VPTT: volume phase transition temperature

LCST: lower critical solution temperature

UCST: upper critical solution temperature

NIPAm: *N*-isopropylacrylamide

pNIPAm: poly (*N*-isopropylacrylamide)

pVCL: poly (*N*-vinyl caprolactam)

pEGMA: poly (ethylene glycol methacrylate)

pDEA: poly (*N,N*-diethylacrylamide)

pDMAEMA: poly (2-(dimethylamino)ethylmethacrylate)

AAc: acrylic acid

GIT: gastrointestinal tract

GOx: glucose oxidase

IDDS: implantable drug delivery systems

PU: polyurethane

PMMA: poly (methyl methacrylate)

PE: polyethylene

PET: poly (ethylene terephthalate)

ABT: abdominal trauma

PLA: poly (lactic acid)

PCL: polycaprolactone

PLGA: poly (lactic-*co*-glycolic acid)

PVA: poly vinyl alcohol

BIS: N,N'-methylene bis acrylamide

APS: ammonium persulfate

KPS: potassium persulfate

TEMED: N,N,N',N'-tetramethylethylenediamine

HEMA: 3-hydroxyethyl methacrylate

AIBI: 2,2′-azobis N, N'-dimethylene iso butyramidine

EDC: 1-ethyl-3-(-3-dimethylaminopropyl) carbodiimide hydrochloride

NHS: N-hydroxysuccinimide

1D: one dimensional

2D: two dimensional

3D: three dimensional

DTT: dithiothreitol

GSH: glutathione tripeptide

HMC: hydrogel–microgel composite

CV: crystal violet

AY: acid yellow 17

RhB: rhodamine B

DI: deionized

pNIPAm-co-AAc microgel: poly (N-isopropylacrylamide)-co-acrylic acid) microgel

2-OH: 2-mercapto-1-ethanol

6-OH: 6-mercapto-1-hexanol

11-OH: 11-mercapto-1-undecanol

6-CH$_3$: 1-heptanethiol

11-CH$_3$: 1-dodecanethiol

15-CH$_3$: 1-hexadecanethiol

HEAm: *N*-hydroxyethyl acrylamide

AMPS: 2-acrylamido-2-methyl-1-propanesulfonic acid

OMA: *N*-octyl methacrylate

BVB: 1-benzyl-3-vinylimidazolium bromide

SEM: scanning electron microscope

DSC: differential scanning calorimetry

XPS: X-ray photoelectron microscope

FTIR: Fourier-transform infrared spectroscopy

UV-Vis: ultraviolet-visible light absorbance spectrometry

HMC-BIS: HMC having BIS in its hydrogel matrix

HMC-BISa: HMC having BIS in its hydrogel matrix

HMC-OMA: HMC having OMA in its hydrogel matrix

HMC-HEAm: HMC having HEAm in its hydrogel matrix

HMC-AMPS: HMC having AMPS in its hydrogel matrix

HMC-BVB: HMC having BVB in its hydrogel matrix

pNIPAm-AMPS: poly (*N*-isopropylacrylamide)-*co*-2-acrylamido-2-methyl-1-propanesulfonic acid)

pNIPAm-BIS: poly (*N*-isopropylacrylamide)-*co*-N,N′-methylene bis acrylamide)

pNIPAm-BVB: poly (*N*-isopropylacrylamide)-*co*-1-benzyl-3-vinylimidazolium bromide)

pNIPAm-OMA: poly (*N*-isopropylacrylamide)-*co*-N-octyl methacrylate)

pNIPAm-HEAm: poly (*N*-isopropylacrylamide)-*co-N*-hydroxyethyl acrylamide)

APMAH: 3-aminopropyl methylacryamide hydrochloride

APBA: 3-(acrylamido) phenylboronic acid

PBS: phosphate buffer solution

HMC-AAc: HMC entrapping CV-loaded pNIPAm-*co*-AAc microgels

HMC-APMAH: HMC entrapping AY-loaded pNIPAm-*co*-APMAH microgels

HMC-APBA: HMC entrapping RhB-loaded pNIPAm-*co*-APBA microgels

TEOS: tetraethyl orthosilicate

SIMS: second ionization mass spectroscopy

MV: methyl viologen

Nap: naphthalene

CB [8]: cucurbituril [8]

SH: supramolecular hydrogel

MCH: microgel-crosslinked hydrogel

CT: charge transfer

Chapter 1

Introduction

1.1 Stimuli-responsive Polymers

In nature, stimuli-responsive materials and systems that endow organisms with competitiveness and survival skills can be found widely. Some examples are: chameleons can tune the color of their skin depending on the surrounding environment to camouflage themselves; *Mimosa pudica* contracts its leaflets in response to mechanical stimulus, which protects itself from potential damage from raindrops; many mammals have sudoriparous glands that secrete sweat under thermal stimuli to help organisms to maintain a constant body temperature in a hot environment. To mimic those responsive systems found in nature and take advantage of the stimuli-responsive functions, scientists have developed materials whose physical/chemical properties can respond to external stimuli; these are referred to as stimuli-responsive materials or "smart" materials.[1-3] Stimuli-responsive polymers, including synthetic polymers and natural polymers, are macromolecules that can undergo dramatic changes, such as conformation, structure, color, solubility, charge density, and refractive index, etc., in response to environmental variations.

There are many stimuli, such as temperature,[4-6] pH,[7-9] ionic strength,[6, 10-11] light,[12-13] electric and magnetic fields,[14-16] redox reagents,[17-20] and biomolecules (e.g. enzymes, antibodies),[21-24] that yield a response stimuli-responsive polymers as a consequence of the interaction between the stimuli and certain functional groups/structures in the polymer

materials. In other words, stimuli-responsive polymers can be designed and tailored by introducing specific stimuli-responsive functional groups into the polymers. In this chapter, polymers that respond to different stimuli will be introduced, focusing on temperature-responsive polymers and pH-responsive polymers.

1.1.1 Temperature-responsive Polymers

Among different types of temperature-responsive polymers,[25] the most widely studied are the polymers exhibiting a volume phase transition at a certain temperature. This temperature is known as the volume phase transition temperature (VPTT). Around the VPTT, the polymer can transform from a soluble state in the solvent to an insoluble state, accompanied by a transition in solution appearance from clear to cloudy. However, there are two main groups of temperature-responsive polymers that have a VPTT with an opposite phase transition behavior in their response to the temperature variation. If the phase transition occurs as the temperature is elevated, such polymers are called lower critical solution temperature (LCST) polymers, while if the polymers undergo the phase transition as the temperature is decreased are called upper critical solution temperature (UCST) polymers.

Here, we will focus mainly on poly (N-isopropyl acrylamide) (pNIPAm),[4] which has been the most extensively studied LCST polymer during the past few decades, as its LCST, ~32 °C, is close to the physiological temperature range and endows it with more advantages in biomedical applications. There are some other LCST polymers that also are investigated widely, including poly (N-vinyl caprolactam) (pVCL),[26] poly (ethylene glycol methacrylate) (pEGMA),[27] poly (N,N'-diethylacrylamide) (pDEA),[28] and poly (2-

(dimethylamino)ethyl methacrylate) (pDMAEMA).[29] Their chemical structures are shown in Figure 1-1.
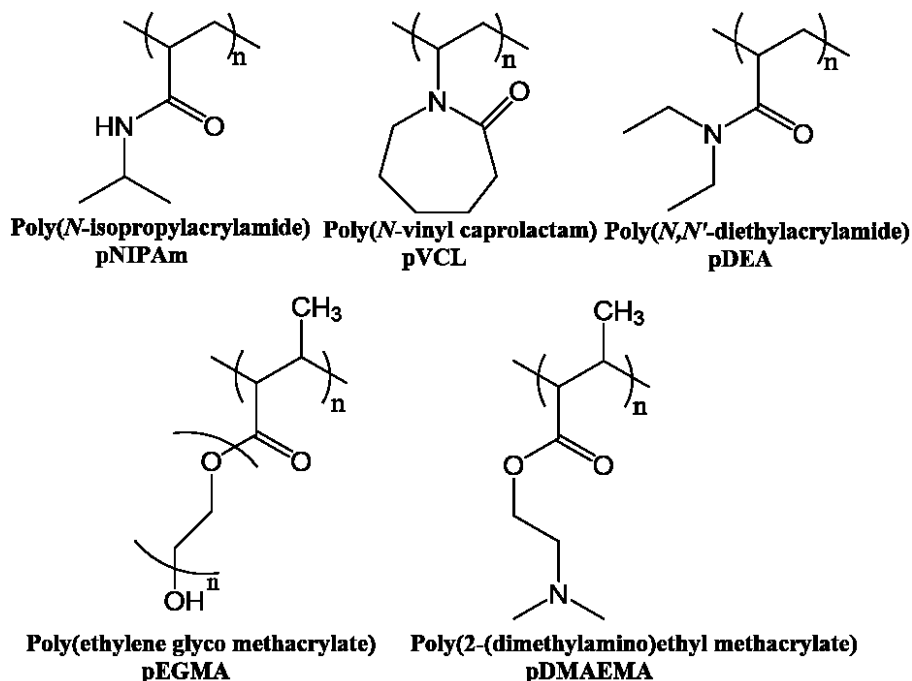
Figure 1-1. Structures of some other common temperature-responsive polymers that exhibit an LCST.

Generally, the LCST of polymers in aqueous solutions is determined by the temperature at which the mixing of two phases turns from spontaneous to non-spontaneous due to the unfavorable entropy of mixing.[30] In the following paragraphs, the detailed mechanism in terms of inter/intra-molecular interactions and thermodynamics of the phase transition of LCST polymers will be explained in the context of pNIPAm.

In 1968, Heskins and Guillet firstly explained this process as an entropically driven transition, which can be described using the Gibbs free energy equation, Equation 1-1

$$\Delta G = \Delta H - T\Delta S \tag{1-1}$$

where ΔG is free energy change of the polymer dissolution, ΔH is the enthalpy change of the dissolution, T is the temperature in Kelvin, and ΔS is the entropy change of the system

due to the interaction between the water molecules and the polymer.[31] In a polymer-water mixture, $\Delta G < 0$ means that the polymer dissolution in water is spontaneous and the polymer is soluble in water, while $\Delta G > 0$ means that the polymer dissolution is nonspontaneous and the mixture undergoes a phase separation.

In the case of pNIPAm, when the pNIPAm dissolves in the water, ΔH makes a negative contribution due to the hydrogen bonding formation between the water molecules and the amide groups in pNIPAm chains. However, the water molecules interacting with the pNIPAm chains based on hydrogen bonding yield a decreased system entropy ($\Delta S <$ 0) and a positive entropic contribution ($-T\Delta S > 0$). Therefore, ΔG grows, as the elevated temperature leads to an increased positive entropic contribution. When the $T >$ LCST of pNIPAm, the positive entropic contribution dominates over the negative enthalpic contribution, and ΔG becomes positive. Then, a phase separation takes place in the polymer-water mixture, and the conformation of the pNIPAm chains undergoes a transition from random coil to globule.

A schematic depiction of the of pNIPAm phase transition at an elevated temperature is shown in Figure 1-2(A). At a temperature lower than the LCST, the hydrogen bonding between the amide group on the polymer chain and water molecules makes the pNIPAm polymer solvated. Meanwhile, the isopropyl group is surrounded by a "cage-like" conformational arrangement of water molecules.[32-33] Thus, at low temperature, the sum of these two types of polymer-water interactions is stronger than the intramolecular interaction within a polymer chain, resulting in an extended random coil state of pNIPAm. However, at a temperature higher than the LCST, the elevated temperature breaks the hydrogen bonding, yielding an entropically favored expulsion of water molecules from the

polymer network. Consequently, the weakened the polymer-water interactions can no longer maintain the extended conformation of the pNIPAm chain, causing it to collapse into a globule conformation (Figure 1-2(B)).
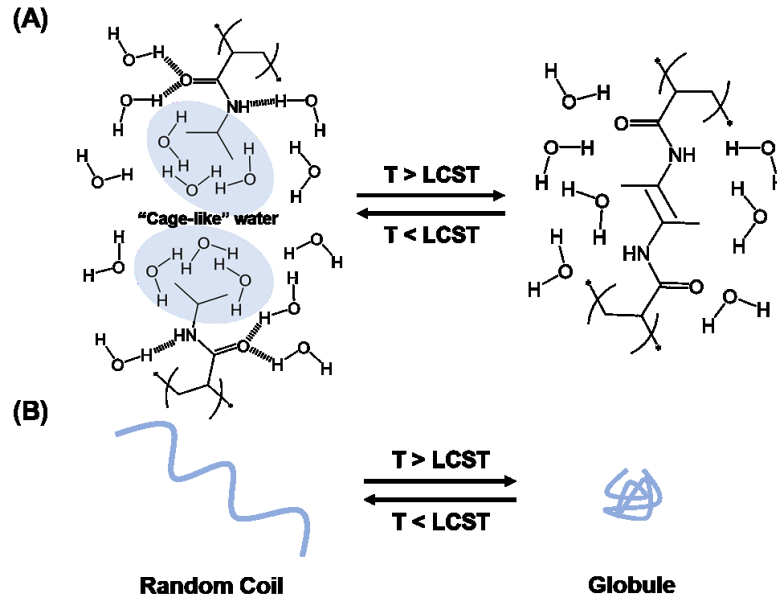
Figure 1-2. (A) Schematic depiction of the phase separation process of the pNIPAm polymer in water. (B) Schematic representation of the temperature-induced conformational change of a pNIPAm polymer chain.

For a particular temperature-responsive polymer, its LCST in pure water can be tuned by changing the hydrophobicity of the polymer. That is, co-polymerizing a hydrophilic co-monomer makes the polymer more hydrophilic and endows it with a higher LCST, while hydrophobic co-monomers will cause its LCST to decrease.[34-35] In addition to the polymers' hydrophilicity, LCST is related to the nature of the co-solvent, ionic strength of the solution, crosslinking density of the polymer network, and molecular weight.[36-38]

1.1.2 pH-Responsive Polymers

pH-Responsive polymers are a group of polymers that can undergo structural/property changes in response to solution pH, such as the conformation of the polymer chains, cross-linking density, solubility, and swellability. pH-responsive polymers can be weak acid/bases that bear ionic moieties at specific solution pH or non-ionic polymers with pH-sensitive covalent bonds that ioniza at specific solution conditions.[39-40] For example, carboxylic acid groups (like those found in acrylic acid (AAc)), with pKa ~ 4.25, deprotonate in water to generate a negatively charged carboxylate group when pH > pKa, while the negative charge can be neutralized when the environmental pH is low (e.g., pH 3). Similarly, phosphoric acid and sulfonic acid groups in polymers also show this kind of protonation–deprotonation behaviour around their pKa, which are 2.15 and 1.92, respectively.[41] A special pH-responsive weak acid functional group is phenylboronic acid, which can accept and release hydroxide ions in response to the solution pH. That is, when the solution pH is greater than its pKa (~8.5), the boron atom would bind to a hydroxide ion and form a negatively charged group.[42] In contrast, amine groups, including primary, secondary, and tertiary amines, as the representatives of weak bases, show the ability of binding protons to form cationic groups as a response to the decrease in the solution pH. A summary of different kinds of pH-responsive ionic moieties is listed in Figure 1-3. The charge status switching behavior of the polymers based on these ionic moieties is also reversible, depending on the solution pH.

(A)

Anionic pH-responsive groups

Carboxylic acid   Phosphoric acid   Sulfonic acid   Phenylboronic acid

Cationic pH-responsive groups

Primary amine   Secondary amine   Pyrrolidine (tertiary amine)   Pyridine

(B)

Linker — Degradation product

Orthoester

Acetal/Ketal

Imine

Hydrazone

cis-aconityl
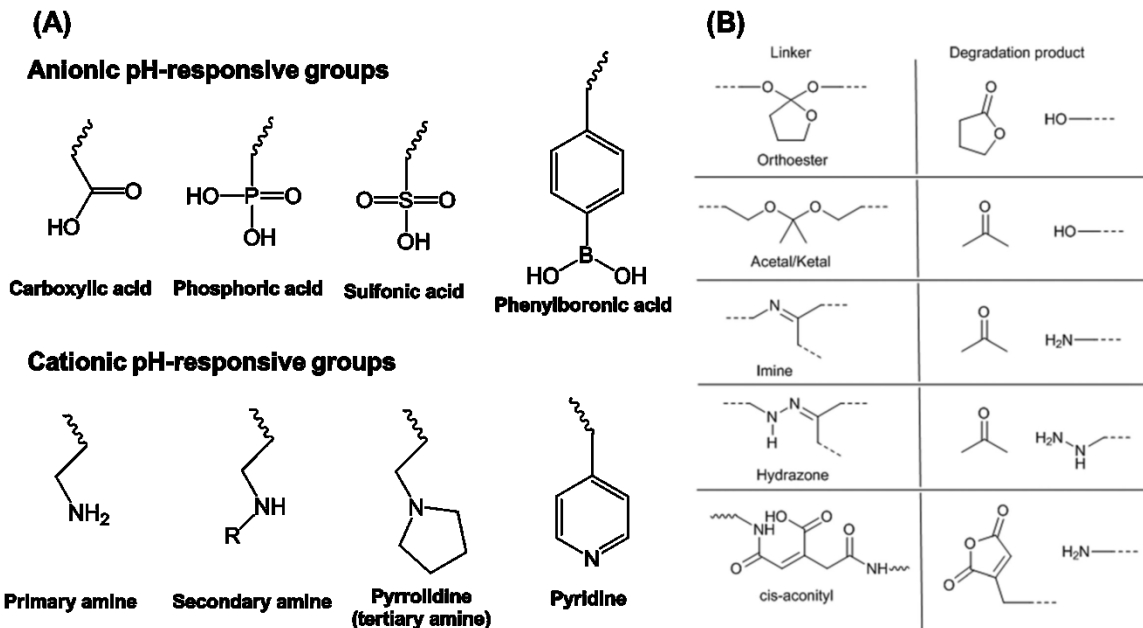
Figure 1-3. (A) List of common ionic pH-responsive groups in pH-responsive polymers. (B) List of some acid-ultrasensitive linkages and groups. [Reproduced with permission from ref. 40, Copyright 2013, RSC Publications]

In an aqueous solution, ionized pH-responsive moieties bind readily to opposite charged agents electrostatically, as such therapeutic agents, making the pH-responsive polymers interesting for biomedical applications, as the pH varies over a large range between different biological environments. For example, gastric juice has a pH < 2, intestinal juice has a pH > 8, the pH range of blood plasma is maintained within the range of 7.35 to 7.45, and the extracellular pH of many tumors is mildly acidic (pH 5.8–7.2). Therefore, pH-responsive nano-carriers could be designed for anti-cancer drug loading and delivery via triggering of pH manipulation.

Although polyelectrolyte-based pH-responsive polymers have been studied extensively and applied in various pH-responsive systems, one of the most obvious drawbacks is their pH-responsivity at relative low pH (<4) or high pH (>9), which limits their more practical biomedical applications. In the past decade, several pH-responsive

polymers have been prepared based on acid-ultrasensitive (or acid-labile) bonds or linkages. These acid-ultrasensitive linkages are degradable in mildly acidic conditions (pH > 5) due to the fast hydrolysis of the chemical bonding in acidic solutions. Among the different kinds of linkages shown in Figure 1-4, the most widely used acid-ultrasensitive linkage is the acetal/ketal, as the acid-sensitivity of this structure is tunable by incorporating different substituents.[43-44] Therefore, an acetal with a different substituent can be hydrolyzed over a large acidic pH range (pH 2–6).[45] This type of linkage is particularly useful in designing implantable polymeric materials for drug delivery applications that do not require the removal of the implanted material by surgery when the drug release is completed.

In this dissertation, we utilized the transition between the charged and the neutral state of pH-responsive polymers at defined pH values to control the release of small ionic molecules under different conditions.

1.1.3 Light-responsive Polymers

Light-responsive polymers can undergo a macroscopic change, like conformation, charge, polarity, and color, upon exposurate the light irradiation on the light-responsive functional groups or moieties on the polymers. Compared to other stimuli-responsive materials, light-responsive polymers possess the advantage of precise "stimulus dosage" for controlled response. That is, light stimuli can be applied accurately, with temporal and spatial control, to achieve the most ideal response, and the strength of the response also is tunable with a variable light intensity. To make polymers light-responsive, specific functional groups or chemical bonds, also known as "chromophores", which can undergo light-induced structural or conformational change, should be incorporated into the polymers, either in the polymer backbones or on the side chains.

8

In general, the light-responsive behaviour of the light-responsive polymers can be either reversible or irreversible, depending on the incorporated chromophore. The reversible response usually is accompanied with isomerisation, polarity change, and/or color change of the chromophore units. There are several chemical compounds, such as azobenzene, spiropyran, salicylideneaniline, etc.,[46] that can undergo these transitions under the irradiation of light. The chemical structures of these compounds and their transformations as a response to light are shown in Figure 1-4. Azobenzene shows its special property to undergo trans to cis photo-isomerization and vice versa upon exposure to a specific irradiation wavelength.[47] Consequently, this isomerisation process is accompanied by a polarity change of the azobenzene, which induces the change in the dipole moment.[48]
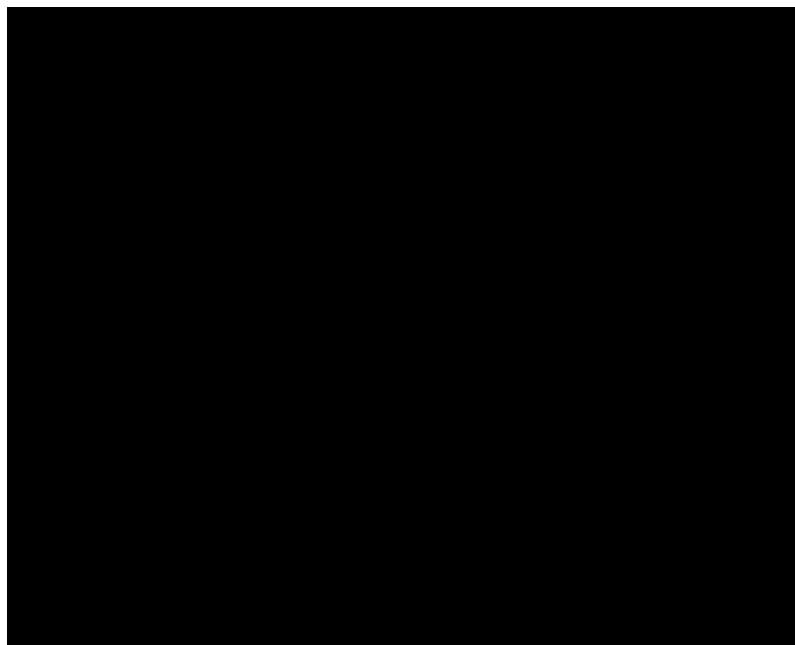
Figure 1-4. Structures and the light-induced reactions of common light-responsive molecules.

On the other hand, an irreversible light-responsive behaviour generally can be observed in photocleavable units. With irradiation, the photocleavable moieties would

decompose into other species via an irreversible process. For example, the *o*-nitrobenzyl ester is one of the most commonly used chromophores featuring an irreversible light-responsive behaviour. A very polar side group can be photocleaved from the *o*-nitrobenzyl ester moiety by UV-light irradiation, which induces a neutral to charged state transition of the material,[49] as shown in Figure 1-4.

Light-responsive groups and/or chemical structures have been utilized to control the formation and dissociation of nanoparticles,[50-51] surface wettability,[52] and molecular recognition.[53]

1.2 Stimuli-responsive Hydrogels and Microgels

Hydrogels are the 3-D networks of hydrophilic polymer chains that are chemically and/or physically crosslinked. With hydrophilic groups and moieties, such as hydroxyl, amide, carboxyl, phosphate, and sulfonate groups, etc., and the crosslinked structure, hydrogels can absorb and retain a large amount of water (80–99% of their weight). Due to the high-water content, hydrogels with similar properties to some biological tissues have outstanding biocompatibility, which are essential for their biomedical applications. By now, research on the biomedical applications of hydrogels is diverse; it includes drug delivery,[54-55] tissue engineering,[56-57] and cell culture.[58-59]

Stimuli-responsive hydrogels can be made by functionalizing normal hydrogels with stimuli-responsive functional groups or moieties or by polymerization of the functional monomers that have responsive properties. For example, functionalizing the hydroxyl groups of the poly vinyl alcohol (PVA) with a photo-responsive molecule, coumarin,

endows PVA-based hydrogel beads with UV-responsivity,[60] and a classic temperature-responsive hydrogel, pNIPAm-based hydrogel, can be made by polymerizing NIPAm monomer.[61]

Hydrogels that are responsive to external stimuli usually undergo a significant change in their swelling ratio, which is defined as the fractional increase in the weight of the hydrogel due to water absorption.[62] The swelling process of hydrogels in water can be described by the Flory and Rehner theory.[63] When a dry hydrogel is soaked in water, the hydration process of the hydrogel material caused by the osmotic pressure would make the polymer network expand. However, the expansion of the flexible polymer network is also restricted by the elastic restoring force due to the crosslinking. Thus, the amount of water that the hydrogel can absorbed, which is defined as the equilibrium swelling ratio, is determined by the balance of these two forces. Therefore, any external stimulus leading to a change in the properties of hydrogel would interrupt the previous balance between the network expansion and the elastic restoring force and induce a change in the water absorption equilibrium of hydrogel. A hydrogel absorbing less water has a smaller size (de-swollen) than when it is absorbing more water (swollen); this is defined as the stimuli-responsivity of the hydrogel. As shown in Figure 1-5, upon exposure to different physical and/or chemical stimuli, the physical properties of hydrogels, such as swellability, mesh size, and refractive index, can undergo a reversible change, which allows them to be used widely in sensors,[64] actuators,[65] and smart surfaces.[66] Many different stimuli-responsive hydrogels have been developed, however, in this dissertation, we will focus mainly on the pNIPAm-based temperature-responsive hydrogels and their applications in controlled drug delivery.
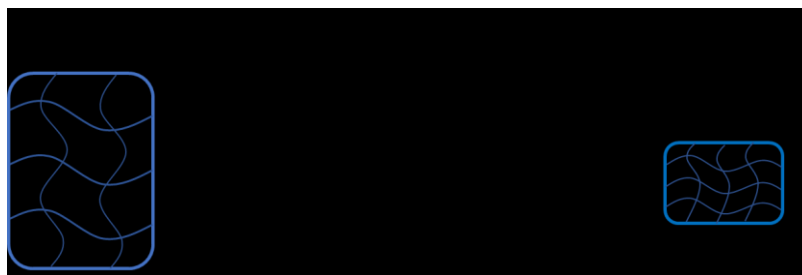
Figure 1-5. The solvation state change of a hydrogel in response to different external stimuli.

1.2.1 Temperature-responsive pNIPAm-based Hydrogels

Temperature-responsive hydrogels are composed of temperature-responsive polymers, such as pNIPAm. Similar to the volume phase transition behavior of the polymers at their LCST, temperature-responsive hydrogels exhibit a swollen–de-swollen volumetric change in a solvent when the solution temperature goes beyond their LCST. The pNIPAm-based hydrogel is the most extensively investigated temperature-responsive hydrogel. A typical pNIPAm hydrogel can be synthesized with free radical polymerization in an aqueous solution containing NIPAm monomers, crosslinkers, and reaction initiators. The most commonly used non-degradable crosslinker is *N,N′*-methylenebis(acrylamide) (BIS).[67] Using the degradable crosslinkers can make the hydrogels partially or fully degradable.[68] Persulfate salts, such as ammonium persulfate (APS) and potassium persulfate (KPS) are typical initiators used in the reaction, as one persulfate ion can decompose into two radical ions at an elevated temperature (>43 °C) to initiate the polymerization reactions. In many cases, APS also is used with an initiation catalyst, *N,N,N′,N′*-tetramethylethylenediamine (TEMED), which reduces the initiation temperature to room temperature or even lower (<0 °C) by the radicals formed by the redox reaction between the APS and TEMED. Furthermore, the chemical/physical properties and/or multi-responsivity of the pNIPAm hydrogel can be tailored by copolymerizing different functional comonomers. For example,

AAc can make the pNIPAm-based hydrogels pH-responsive, and 3-hydroxyethyl methacrylate (HEMA) can make hydrogels more hydrophilic.

1.2.2 Temperature-responsive pNIPAm-based Microgels and Assemblies

1.2.2.1 pNIPAm-based Microgels

pNIPAm-based microgels/nanogels are pNIPAm-based hydrogel micro/nano particles. For example, microgels with a diameter in the range of 100 nm–1000 nm, have similar internal structures as the hydrogels, even though they are physically different. Due to the sub-micron sizes, microgel particles have several orders of magnitude larger surface area-to-volume ratios than hydrogels. In addition, microgels demonstrate a much faster response to the external stimuli. A theory on deswelling kinetics, based on the concept of cooperative diffusion, was proposed by Tanaka and Fillmore[69] and yields the expression shown in Equation 1-2

$$\tau = R^2/\pi^2 D \qquad (1\text{-}2)$$

where τ is the time that the gel needs to complete the volumetric change, R is the radius of the gel, and D is the cooperative diffusion coefficient. This theory concludes that the response time of the gel is proportional to its size. Therefore, because of the significantly decreased size of the microgels, the temperature-responsive microgels de-swell much faster than the bulk hydrogels, and their response times are typically in the millisecond timescale.[70]

pNIPAm-based microgels can be prepared by free radical precipitation polymerization, defined as a polymerization that starts from a homogeneous monomer solution and ends in a polymer dispersion; this is one of the most convenient methods for

the microgel synthesis.[71-72] The following components, NIPAm, crosslinkers, and initiators, are essential to synthesize uniform and stable microgel particles, although Gao and Frisken reported the self-crosslinking of pNIPAm microgels without crosslinkers during the synthesis. The selection of the initiators is important to synthesize the microgels with good monodispersity. Usually, ionic initiators (usually 0.1 mol% to 0.2 mol% of total amount of monomer), such as persulfate salts and 2,2′-azobis *N, N′*-dimethylene iso butyramidine (AIBI), are good options because the ionic initiators impart the surface of the microgel particles with charges and stabilize the particles. Moreover, the charge property of the initiators also should be compatible with the comonomers to achieve a good microgel yield. This means that the selected initiator should have the same type of charge as the comonomers[73] because opposite charges between the initiator and comonomer would result in a reduced zeta-potential of the microgel particles and induce particle aggregation. In this dissertation, free radical precipitation polymerization was used to synthesize all microgels, and APS or AIBI was used for different microgel synthesis. Figure 1-6 shows the mechanism of pNIPAm-based microgel formation in the free radical precipitation polymerization.
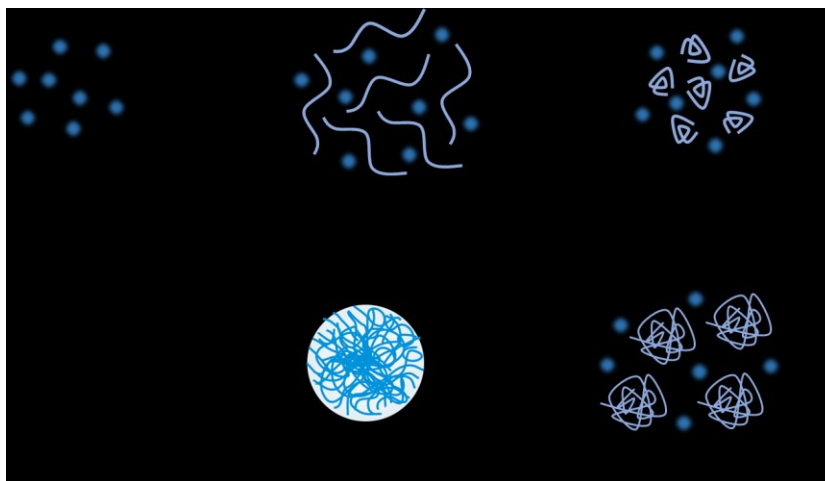
Figure 1-6. Mechanism of microgel formation in free radical precipitation polymerization.

In this reaction, the temperature should be higher than the initiator activation temperature and LCST of the polymers. There are two main reasons for this. First, the polymerization reaction needs to be triggered by the free radicals formed from the initiator decomposition at high temperature. Second, the elevated temperature allows the oligomers to collapse into primary nuclei, which work as seeds for the following particle growth. There are several factors that can affect the size of the resultant microgels, including reaction temperature, ionic strength, and surfactant concentration. At a lower temperature, a smaller fraction of the initiator would be activated at the beginning of the reaction, converting fewer amounts of the monomers into the nuclei. Therefore, more of the remaining monomers are distributed onto fewer nuclei in the particle growth step, and as a result, the final microgels will have an increased size.[70] Inorganic salts and ionic surfactants are a pair of agents that are used to control the size of synthesized microgels. Typically, a higher concentration of salt can increase the particle sizes, while a higher concentration of surfactant would decrease the particle sizes.[74] According to the surface electrical double layer theory,[75] the increased ionic strength decreases the double layer thickness around the microgel particles and can induce the aggregation of small particles to larger particles. In contrast, the surfactants stabilize the small particles and prevent aggregation, thus, resulting in smaller microgels.[76]

Microgels prepared with only the NIPAm monomer are only temperature-responsive, while the multi-responsive microgels, microgels that are responsive to multiple stimuli, can be prepared by incorporating another responsive functional moiety into the microgels. The functional moiety can be either copolymerized with NIPAm as a functional monomer or be modified on the previously prepared pNIPAm microgels to form the multi-responsive

15

microgels. For example, a temperature and pH-responsive microgel can be prepared by copolymerizing a pH-responsive monomer, AAc, with NIPAm.[77] In another example, a temperature and triglyceride-responsive pNIPAm microgel was prepared by modifying the pNIPAm-based microgels with lipase by an EDC/NHS coupling reaction.[78] With these methods, the temperature-responsive pNIPAm-based microgels could be designed to respond to a variety of stimuli, such as UV-light,[79] electric field,[80] and redox agents.[81]

1.2.2.2 pNIPAm-based Microgel Assemblies

Previous research has shown that secondary structures could be established with the self-assembly of microgels as building blocks.[82-84] The secondary structures can be a one dimensional (1D) monolayer,[82, 85] two dimensional (2D) films,[83] or three dimensional (3D) bulk hydrogels.[84, 86] Different applications have been found for these structures, like functional coating, sensing, and biosensing. For example, a microgel monolayer was developed as a nonfouling coating to enhance the biocompatibility of biomedical devices,[87] microgel-based 2D colloidal crystal hydrogels were prepared as a sensing system for different stimuli,[88-89] and a large-scale colloidal photonic crystal demonstrated tunable bandgaps when it was prepared with pNIPAm-based microgels.[90] The Serpe group originally developed a microgel-based device, called an etalon, that has outstanding optical properties.[82] This device, with its excellent stimuli-responsivity, shows great potential in applications of sensing, biosensing, and drug delivery.[78, 91-92]

To prepare the etalon device, a solution of pNIPAm-based microgel was painted on a Cr/Au coated glass substrate. The microgel monolayer was formed by rinsing away excess microgels from the substrate. Then, another layer of Cr/Au was deposited on top of the microgel layer to make a sandwich structure of the etalon device. An illustration of an

etalon device is shown in Figure 1-12(A). It is obvious that the distance between the two metal layers is determined by the thickness of the microgel monolayer. When a light is irradiated on the etalon surface, the transmitted light and the reflected light interfere with each other and generate a visible color due to the thin-film interference (Figure 1-12(B) and Figure A-1).
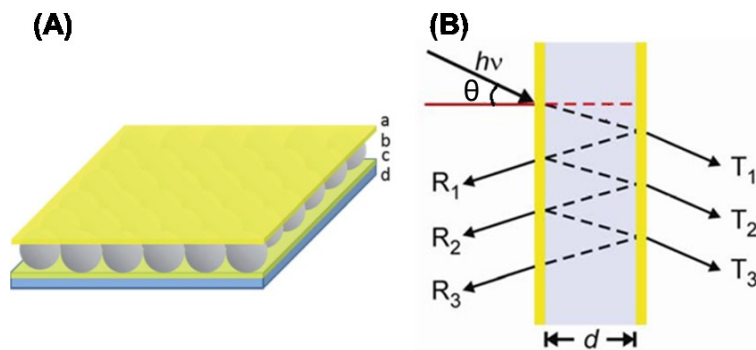
Figure 1-7. (A) Schematic of a pNIPAm microgel-based etalon: (a) 15 nm of Au layer with 2 nm of Cr adhesion layer, (b) Microgel monolayer, (c) 15 nm of Au layer with 2 nm of Cr adhesion layer, and (d) glass substrate.[93] [Reproduced by permission of The Royal Society of Chemistry.] (B) Schematic of the light resonance and interference in an etalon.

A setup of a spectrophotometer probe, shown in Figure 1-13(A), is commonly used for quantitive analysis of the color of the etalon devices. The etalon exhibiting visible colors shows a unique multi-peak reflectance spectra (Figure 1-13(B)) due to the interference of light resonating in the microgel layer between the two Au layers.[82] The position and order of the peaks can be predicted using Equation 1-3

$$m\lambda = 2nd(\cos\theta) \tag{1-3}$$

where n is the refractive index of the dielectric layer (the microgel layer in our case), d is the mirror–mirror distance (distance between the two Au layers), θ is the angle of incident light relative to the normal, and m (an integer) is the order of the reflected peak. The

equation indicates that a shift in reflected light wavelength, λ, is expected as the microgel layer thickness, d, changes. If θ is fixed, λ is dependent only on d. Due to the response of the pNIPAm microgels to the stimuli, etalons have been shown to exhibit responses to many organic/inorganic compounds, ionic strength, and biomolecules.
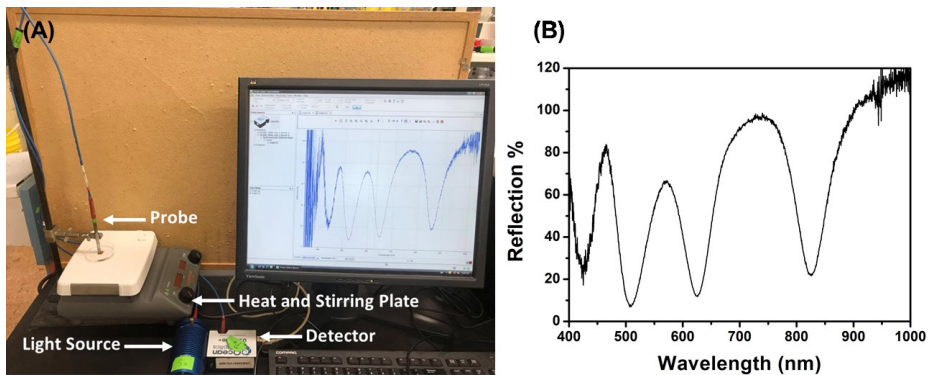
Figure 1-8. (A) An instrumental setup for reflectance spectrum collection. (B) A sample reflectance spectrum of an etalon.

1.2.3 Applications of the Responsive Microgels and Their Assemblies

Due to their high porosity and stimuli-responsive nature, many new applications of the responsive microgels have arisen over the past few decades. These applications can be classified into three main categories: sensing/biosensing, controlled drug delivery, and water remediation. In this section, we will introduce some typical examples for each of the applications briefly.

1.2.3.1 Sensing/Biosensing

Swelling–deswelling is the key mechanism for the responsive microgels in sensing and biosensing applications. An example of this was presented by Hoare et al.,[94] where they used the swelling behaviors of the APBA-modified pNIPAm-based microgels in solution

to illustrate the presence of glucose. Specifically, the phenylboronic acid groups in the microgels can bind to the diol structure of the glucose molecules and form the negatively charged complex,[95] which increases the anionic charge density in the microgels and leads to a swelling response of the microgels due to the stronger charge–charge repulsion. When the etalon-based sensing systems are developed with microgels, the swelling/deswelling of the microgels in response to the analyte is converted to the peak shifts of the reflectance spectrum of the etalons. Our group reported an etalon-based pH sensor based on the partial protonation of the carboxylic acid. Specifically, as a weak organic acid, the carboxylic acid group has a wide pH range that allows it to be protonated/deprotonated partially, and the fraction of the deprotonated carboxylate groups increases as the solution pH increases. This results in a swelling response of the microgel layer in the etalon and a red shift of the reflectance spectrum.[96] Recently, our group synthesized reductant-responsive microgels by using a disulfide bond crosslinker.[97] The disulfide bond can be reduced and dissociated by dithiothreitol (DTT). Thus, the microgels, either suspended in solutions or assembled in etalon devices, show a swelling response to the DTT due to the decreased crosslinking density.

1.2.3.2 Controlled Drug Delivery

Another area of the responsive microgels that is intensively studied is the application of controlled drug delivery. The porous structure of microgels allows the drug molecules to be incorporated onto the microgel interiors, and their significant volumetric transition may be employed to promote the drug release processes.[98] In addition to the pH and temperature changes as the stimuli to trigger the drug release by microgels, some biomolecules, like

glucose and enzymes, also can activate the release of the drugs. Liu and co-workers reported a self-regulated insulin delivery system based on dual-responsive microgels.[98] In this research, the phenylboronic acid group and the disulfide bond were incorporated to make the microgels responsive to both glucose and an intracellular reductant, glutathione tripeptide (GSH), which can release pre-loaded insulin in response to either of these two stimuli. In some cases, using microgels alone does not show the desired target selectivity for the precise drug release. To address this problem, Zhang et al. prepared anti-cancer drug-loaded microgel entrapped microparticles for a targeting drug delivery.[99] Specifically, the anti-cancer drug-loaded microgels are coated with a layer of glycogen that has transferrin receptors grafted on the surface. As the cancer cells have overexpressed transferrin on the cytomembrane, these microparticles demonstrate great selectivity and cytotoxicity to the cancer cells. On the other hand, using the microgel assemblies is also a promising method to control the release of drugs from microgels.

1.2.3.3 Water Remediation

In the process of wastewater treatment, coagulation and flocculation are critical for removing the contaminants. Microgels with porous structures are capable of absorbing a variety of materials, like fine particles, colloids, organic compounds, and heavy metal ions.[100] For example, microgels made with polyelectrolytes can absorb organic dye molecules or heavy metal ions electrostatically from the wastewater samples, and the used microgels could be regenerated simply by changing the solution pH.[101]

1.3 Applications of Stimuli-responsive Polymer Materials in Controlled Drug Delivery

1.3.1 Background of Controlled Drug Delivery

Conventional drug administration, such as oral drug dose, usually requires high and/or repetitive dosage to maintain a sufficient blood drug concentration and stimulate a therapeutic effect. This is because only a small fraction of the dosage can reach the relevant sites, and most of the dosed drug is either degraded or metabolized before arrival at the required site in the gastrointestinal tract and/or the liver. However, a high dosage may cause side effects, and an insufficient blood drug concentration between two dosages lowers the drug efficacy. To maximize the drug efficacy and minimize the potential side effects, scientists continue to develop more advanced controlled drug delivery systems that can release a drug to the required site and maintain a constant local drug concentration.

Starting in the 1950s, controlled drug delivery technology has progressed tremendously from primitive sustained release systems to sophisticated self-regulated release systems. The development of controlled drug delivery was described by Kinam Park as occurring in three generations.[102] The first generation controlled drug delivery technology (1950–1980) focused on the development of sustained release systems by oral and transdermal delivery routes. The second generation (1980–2010) technology was developed based on the self-regulated release systems, long-term release systems, and nanotechnology-based delivery systems. After 2010, the development of the third generation technology started, which includes on-off switching on-demand drug delivery, targeted delivery of an anticancer drug, and extreme long-term drug delivery over six months to one year.

To achieve the desired curative effect for the diseases, an appropriate route of therapeutic drug administration is critical. Scientists have been working on designing new drug delivery systems that can be applied with the alternative drug administration routes in order to increase the patient's compliance, lower the invasiveness to the body, decrease the side effects, and achieve precise medicine delivery to the relevant sites. There are several typical routes of drug administrations, including oral, hypodermic injection, transdermal, and implantable. In the following paragraphs, we will introduce and discuss advantages, drawbacks, and recent development of drug delivery technologies for each drug administration route.

Oral, as a traditional delivery method, is the most popular and desirable administration route due to the convenience of ingestion, pain avoidance, and patient compliance. However, there are some challenges for the oral delivery. The gastrointestinal tract (GIT) of a human has various digestive enzymes with an extremely low-pH environment, thus the oral-intake of drugs may involve their decomposition and/or enzyme degradation in the stomach before they are absorbed by the intestine. This problem is extremely challenging for protein/peptide-based drugs, such as insulin and enfuvirtide; the latter is a peptide-based drug that can be injected only as a salvage therapy in patients with multi-drug resistant HIV.[103] However, there are some strategies that attempt to realize the oral delivery of proteins and peptides. For example, (1) co-admit the protease inhibitors and absorption enhancers to minimize the enzymatic degradation and improve the drug permeability in the GIT;[104] (2) utilize the micro/nano particles and liposomes-based drug delivery systems to protect the drug from the harsh environment and enzymatic degradation

in the GIT;[105-106] and (3) improve the membrane permeability and proteolytic stability of the drugs with modifications on their physicochemical nature.[107-108]

Injection, as an alternative method to deliver drugs that are not compatible with oral delivery, introduces drugs directly into the bloodstream or hypodermic tissues with needles, providing an enhanced therapeutic effect and increased dosage effectiveness. Although the injection method has some disadvantages, such as invasiveness and chances of infection, when it is applied to the novel drug delivery systems, it acquires more advantages, including ease of application, reduced total body drug dosage by localizing the delivery on relevant sites, and decreased patient discomfort by extending drug release periods.[109-110]

A biodegradable polymeric hydrogel that can undergo a sol-gel transition in situ is becoming a competitive candidate in injectable drug delivery systems, as the polymer precursor solutions dissolving the drug molecules can be injected at the target site and convert instantly into a solid hydrogel in situ to form a long term drug delivery material, which prevents significant tissue irritation and damage.[111-112] Recently, most research on injectable hydrogels has focused on hydrogels that are responsive to physiological conditions or are formed under particular physiological conditions in order to reduce the risks involved in the conventional hydrogel implantation surgeries, such as pain, scarring, and infections.[113] On the other hand, polysaccharides such as alginate, chitosan, hyaluronic acid, cellulose, pullulan, etc., are the most commonly used materials in the preparation of injectable hydrogels due to their non-toxicity and excellent biocompatibility. For example, Anderson and co-workers prepared a polysaccharide-based nanoparticle that can be injected into tissues and aggregate to form a hydrogel in situ.[114] Specifically, insulin, glucose oxidase (GOx), and acid-sensitive acetal-modified dextran (m-dextran) are

entrapped in both chitosan nanoparticles and alginate nanoparticles. When the hydrogel precursor solutions containing the nanoparticles are injected into the tissues, the nanoparticles aggregate electrostatically to form the hydrogel. With the presence of glucose in the tissue, the GOx converts the glucose into gluconic acid, which then degrades the m-dextran and releases the insulin. The hydrogel formed by a single injection can release insulin slowly in response to the glucose and maintain the blood glucose level of mice up to 10 days. Beside the design of the materials for injectable hydrogels, the needle for the injection also was studied by Kang and Lee.[115] The needles prepared with partially crosslinked catechol-functionalized chitosan can undergo a solid-to-gel phase transition in situ, which seals the punctured tissues, preventing uncontrollable bleeding and intramuscular infections.

With the transdermal route, therapeutic drugs can be self-administered by patients non-invasively. The most common transdermal drug delivery structure is patch-based, which usually is composed of a drug reservoir and a release control membrane. The drug reservoir works as a holder to load the drug and determine the total amount of dosage, and the release control membrane, made with biocompatible porous materials, works as a barrier to tune the dosage period. However, the patch-based transdermal delivery systems are not compatible with drugs that have a high molecular weight, such as proteins and peptides, due to their low permeability to the stratum corneum barrier above the skin. To overcome this hurdle, a small needle-aid vaccination system was developed, which breaches the stratum corneum barrier and delivers the vaccine to the potent epidermal Langerhans and dermal dendritic cells to generate a stronger immune response with a much lower dosage.[116] Recently, microneedle-based patches have drawn more and more attention,

as these types of devices can deliver a variety of drugs efficiently with the transdermal route. Specifically, drugs can be loaded into microneedles that are made with biocompatible polymers. As soon as the microneedles puncture the skin, the drug is released directly from the needles into the hypodermic tissues. For example, Gu et al. reported a close-loop glucose-responsive microneedle array patch for in vivo insulin delivery.[117] By integrating the H_2O_2-responsive polymeric vesicles containing insulin and GOx with the hyaluronic acid-based microneedle array, the pre-loaded insulin can be released rapidly from the disassembled vesicles due to the enzymatic reaction involved by glucose, GOx, and H_2O_2.

The concept of implantable drug delivery systems (IDDS) was proposed in 1938 by Deansby and Parkes, who investigated the release of the implanted compressed pellets of crystalline estrone in the subcutaneous tissue of castrated male chickens.[118] Since the 1960s, when the silicones were used to prolong the administration period of therapeutic agents by Folkman and Long,[119] research on IDDS focused mainly on improving the systems' stability,[120] biocompatibility,[121] compatibility between drugs and carriers,[122] and patient acceptance. The IDDS have been classified historically into two major types, drug implants and implantable pumps containing drugs. In addition, the drug implants can be classified further into non-degradable and degradable systems.[123] The drug implant systems release the drugs at a controlled rate with the assistance of polymer coating and membranes, while the implantable drug pump systems control the rate and amount of the drug release by utilizing different types of "pumping force" applied to the implanted devices, such as osmotic pressure,[124] peristaltic movement of certain components in the device,[125] and infusion of external solutions.[126] No matter which type, the polymeric materials with good

biocompatibility to the human physiological environments provide a significant contribution for the IDDS and can be used for the preparation of the matrix, scaffold, membrane, coating, and filling.[127] The non-degradable polymers commonly used in IDDS include polyurethane (PU), poly (methyl methacrylate) (PMMA), polyethylene (PE), and poly(ethylene terephthalate) (PET). The degradable polymers include poly(lactide), polyanhydride, and collagen. Compared to the drug delivery systems based on other drug administration routes, IDDS demonstrate their outstanding ability to release therapeutic agents with high efficiency and great controllability in on-demand drug delivery.[128-130] Many of the implantable devices, especially the sustainable release devices, require external power sources, such as lithium-ion batteries, for a sustainable operation. However, the limited energy stored in batteries limits the device lifetime and leads to unwanted surgeries for the device replacement. Recently, more and more research has focused on the development of self-powered IDDS. The IDDS can be powered by the enzymatic biofuel cells,[131] triboelectric nanogenerators,[132] or piezoelectric nanogenerators.[133] For example, Wang and co-workers developed a biofuel cell powered self-regulated acetaminophen release system that can sense the abdominal trauma (ABT) and release acetaminophen on-demand.[131] Specifically, this system contains a lactate dehydrogenase-coated anode and an acetaminophen-loaded, conductive polymer-modified cathode. When the ABT-induced lactic acid is oxidized by the lactate dehydrogenase, the electrons generated by this reaction would trigger the release of the acetaminophen from the cathode to relieve the ABT.

1.3.2 Polymeric Material-based Controlled Drug Delivery Systems and Mathematical Models of the Drug Release Processes

Although there are a number of different types of materials that have diverse applications in controlled drug delivery systems, polymeric materials are by far the most most widely investigated over the past several decades, and it plays a key role in the development of the second generation drug delivery systems. Polymeric materials endow the drug delivery systems with increased efficacy, reduced adverse effects, lower toxicity, and convenience.[17, 134-135] For example, some small-molecule anti-cancer drugs have short half-lives in blood plasma and cytotoxicity to both healthy cells and cancer cells. However, by utilizing polymeric materials, such as surface functionalized block copolymer micelles, the anti-cancer drug can be well-protected from the enzymatic degradations and has significantly enhanced cancer cell selectivity.[136-137]

Polymeric drug delivery systems with a variety of different formations, from macroscale to nanoscale, have been developed over the past 50 years.[138] Most of the systems developed in the early stages were on the macroscale, e.g., silicone rubber-based mucosal inserts, polysaccharide-based oral capsules, and synthetic polymer-based skin patches.[139] Between 1980 and 2000, biodegradable polymers were used widely to prepare the devices and structures on the microscale, e.g., poly (lactic acid) (PLA)-based sutures,[140] polycaprolactone (PCL)-based microparticles,[141] and poly (lactic-*co*-glycolic acid) (PLGA)-based microspheres.[142] Over the last three decades, relying on the development of nanotechnology, nanoscale drug delivery systems have made great progress. The newest formations of nanodrugs include synthetic polymer-based micelles,[143] PEGylated liposomes,[144] and protein-drug conjugate nanoparticles.[145]

Polymeric materials play a critical role in controlled drug release systems by controlling the release of the therapeutic agents at a constant rate over a long period and making the release rate of drugs tunable for various therapeutic treatments. The drug release from a modified release system is controllable with various methods, such as diffusion, dissolution, swelling, osmosis, and erosion.[146] Therefore, analyzing the drug release processes with mathematical models is becoming valuable in the design of the polymeric material-based drug delivery systems. With a proper mathematical model, the drug release behavior of a specific controlled release system can be predicted. In addition, the mathematical models also can help researchers to optimize the drug release systems by comparing the theoretical release profiles with the experimental release profiles. In the following sections, we will discuss the mathematical models of different drug release systems, including classical drug diffusion, polymer degradation, and erosion.

1.3.2.1 Zero-order Model

Some drug release systems are designed to release the active agent at a constant rate over a certain period of time to achieve an equalized administration and elimination of the active agent, resulting in a uniform drug concentration in plasma and/or tissue. In these systems, the polymers act as a uniform membrane surrounding the drug molecules, and the drugs release at a constant rate. Therefore, a drug release process with a constant rate can be described by the zero-order model, whose mathematical expression is given by Equation 1-4

$$Q_t = Q_0 + k_0 t \qquad (1\text{-}4)$$

where Q_t is the amount of drug dissolved at time t, Q_0 is the initial amount of drug in solution, and k_0 is the zero-order release rate constant. This relation can be used to describe the dissolution of the drugs from the release systems that do not disaggregate, such as some transdermal release systems and matrix tablets with low-solubility drugs, coated forms, and osmotic systems, and it is ideal to describe the membrane controlled dosage forms.[147] For example, an oral intake core tablet with a water-permeable coating is a zero-order release system. After swallowing, the active agent dissolves in the hydrated core until the concentration reaches the saturation. Then the active agent diffuses from the saturated reservoir through the membrane and reaches the gastrointestinal fluid. The constant release rate is due to a stationary concentration gradient across the membrane provided by the saturated reservoir in the core.[148]

1.3.2.2 First-order Model

The formation of the controlled release systems that release a drug in the first-order model could be similar to the zero-order model systems. However, the active agents in the first-order model systems usually have a higher solubility in the medium, which provides a concentrated reservoir with fully dissolved active agents. Therefore, when the systems start to release the active agent, the concentration of the reservoir would decrease gradually as a function of time, causing an equivalent concentration gradient across the membrane. In this case, the change in concentration with respect to the change in time is dependent on the concentration, which can be expressed by Equation 1-5

$$dC/dt = -k_1 C \qquad (1\text{-}5)$$

where C is the percentage of the drug remaining in the reservoir at time t, and k_1 is the first-order release rate constant in units of time^{-1}. Assuming that the volume of the medium is constant, therefore, C can be written as (Q_t/Q_0), where Q_t is the amount of the drug remaining in the reservoir at time t, and Q_0 is the initial amount of active agent in the reservoir. By integrating both sides of Equation 1-5, the mathematical expression of the first-order model will be obtained, as shown in Equation 1-6

$$\log Q_t = \log Q_0 - k_1 t/2.303 \tag{1-6}$$

where k_1 is the first-order release rate constant.[148-149]

1.3.2.3 Higuchi Model

In 1961, Higuchi developed a mathematical model, also known as the Higuchi model, to describe the drug release from ointment bases (planar systems).[150] Since then, the Higuchi model has been used widely to describe the drug dissolution from matrix systems. Generally, this model is related to the particles of drug dispersed in a homogeneous matrix exposed into a diffusing medium, which was proposed initially by Higuchi formation by Equation 1-7

$$Q = \sqrt{D(2C - C_s)C_s t} \tag{1-7}$$

where Q is the amount of released drug at time t per area, C is the initial total amount of drug in dosage form, C_s is the solubility of the drug in the matrix medium, and D is the diffusion coefficient of the drug in the matrix medium.

This relationship is valid for most of the cases, except when the liquid medium contained in the matrix is saturated with the dissolved drug. Therefore, Higuchi proposed Equation 1-8 in 1962 for the case of a matrix saturated with a drug

$$Q = \sqrt{2C_0\varepsilon Dt/\tau\pi} \qquad\qquad (1\text{-}8)$$

where C_0 is the concentration of diffusing liquid contained in a porous matrix, ε is the porosity of the matrix, and τ is the capillary tortuosity factor.[151] It is obvious that the amount of released drug is proportional to the square root of time. Therefore, this Higuchi model expression can be simplified as Equation 1-9

$$Q = k_H\sqrt{t} \qquad\qquad (1\text{-}9)$$

where k_H is the Higuchi model release rate constant.

Based on the works of Higuchi,[150-152] many theoretical models, including the Korsmeyer–Peppas model and the Baker–Lonsdale model, were developed for various drug release systems that are different in active agent solubility, material of matrices, and formation of matrices.[153]

1.3.2.4 Hixson–Crowell Model

For dosage forms such as tablets, whose surface is dissolving as long as the drug is released, the total surface area of the dosage form decreases proportionally over time, and the geometry remains constant, Hixson and Crowell proposed a theoretical model to describe the drug release behavior of this type of surface erodible drug delivery system.[154] As the surface area of a group of particles is proportional to the cube root of its volume, the mathematical expression of the model is shown in Equation 1-10

$$\sqrt[3]{W_0} = \sqrt[3]{W_i} + k_{HC}t \qquad\qquad (1\text{-}10)$$

where W_0 is the initial amount of the drug in the system, W_i is the amount of drug remaining in the system at time t, and k_{HC} is the Hixson–Crowell model constant, which relates the surface and volume of the dosage forms. When taking other factors into account,

such as concentration, drug density, drug diffusion, and the number of spherical particles, Equation 1-10 can be written as

$$\sqrt[3]{W_0} = \sqrt[3]{W_i} + (k'\sqrt[3]{N}DC_s/\delta)t \qquad (1\text{-}11)$$

where k' is a constant relating surface, dosage form, and particle density, N is the number of particles, D is the diffusion coefficient, C_s is the solubility of the drug in the medium at the temperature of the process, and δ is the thickness of the diffusion layer.

This model describes the drug release from systems where there are changes in the surface area and size of particles and tablets. Note, in this model, the drug release kinetics is determined by the dissolution speed of the dosage form instead of the speed of the drug diffusion. Therefore, the Hixson–Crowell equation can be applied to erodible pharmaceutical dosage forms, such as orally taken tablets, where there is even dissociation that occurs in planes parallel to the surface, while the geometrical characteristics of the tablets remain constant.

1.3.3 Stimuli-responsive Polymeric Materials for Controlled Drug Delivery

As discussed in previous sections, polymer-based materials play an integral role in the advancement of control drug delivery technology because they are highly porous, biocompatible, soft, and functionalizable. Even though the drug delivery devices and systems made by polymeric materials are therapeutically advantageous over the conventional drug delivery systems, they are not yet sensitive enough for us to control the drug release rate in response to change of metabolic states of the body and/or external stimuli manipulation.

To overcome this limitation, the applications of stimuli-responsive polymers in controlled drug delivery systems have been studied widely, as the responsive systems allow us to define precisely when and how much of the therapeutic agents should be released to obtain best efficacy. The concept of stimuli-responsive drug delivery systems was reported first by Yatvin et al. in 1978 with the use of temperature-sensitive liposomes for the enhanced local drugs release by hyperthermia.[155] To design the new systems for drug delivery purposes, the challenges associated with the administration in the body need to be addressed; these include a simple administration route, an effective delivery, adapted responsive behaviors to the pathological conditions, biocompatibility, biodegradability, and low toxicity. Therefore, to apply stimuli-responsive polymers to drug delivery systems and cause detectable behavioral changes of systems in response to the stimuli, the responsive polymer materials usually are conjugated with other materials or structures to obtain better functionality. For example, the temperature-responsive controlled release system can be either applied directly to the drug release sites on the body to utilize the body temperature to trigger the release of the drugs or combined with other heat generation structures to control the release. T. Hoare et al. presented a magnetite-microgel composite membrane to control the ON and OFF of the drug release from the reservoir.[156] Specifically, temperature-responsive microgels mixed with the magnetite nanoparticles act as a magnetic field-responsive gate to block the release of the drug. When the magnetic triggering is applied, the magnetite nanoparticles generate heat and induce the shrinking of the temperature-responsive microgels, which results in the gate to open and a high flux drug to be released.

1.4 Conclusions

In this chapter, we introduced stimuli-responsive polymers, some concepts and applications of the temperature-responsive hydrogels and microgels, some concepts of the controlled drug release systems, some mathmetical models that are commonly used to describe controlled release kinetics, and typical controlled release systems based on stimuli-responsive polymers. There are different formations and mechanisms that utilize stimuli-responsive polymers in diverse controlled drug delivery systems, and some of them draw much attention, e.g., microgels/nanogels, core-shell particles, self-assembled nanoparticles, polymer-biomolecular conjugates, and polymer-inorganic hybrid systems. However, for a specific controlled release system, tuning the drug release rate precisely and conveniently and controlling the release processes of multiple drugs individually is still a challenge. In addition to this, there are numerous limitations exist in current drug delivery technologies, such as being invasive, and high-cost.[157] In many cases, the limitations come from the properties of the therapeutic drugs that need limited administration routes. By far, most of peptide-based and protein-based drugs requires repetitive clinical injection due to the unstability of the drug in common environment, potential enzymatic degradation in human body, and low permeability of intestinal epithelium, which reduces comfort and compliance of patients and increases the cost of the drug dosage.[158] Therefore, to address these problems, newly developed drug delivery technologies should be able to increase the stability of the drug, prolong the drug delivery period, protect the drug against the extreme conditions during the administration, and reduce the body invasion.

In this dissertation, we will discuss some approaches that can control small-molecule release rates in precise and simple ways, based on the microgel-based etalon device and a pNIPAm-based hydrogel–microgel composite (HMC) material. Specifically, pNIPAm was used to prepare the etalon and HMC, and we used them as controlled drug delivery systems and investigated their controlled release mechanisms.

Although our group has previously developed a controlled release system based on the etalon, in this dissertation, we will discuss a surface modification approach to control the small-molecule release in a simple and precise way, and we will use the zero-order and first-order release models to analyze the controlled release behaviors of this system and investigate the mechanisms of the controlled release.

On the other hand, some previous researches reported the HMC-based materials as drug delivery systems by utilizing the hydrogel as an extra diffusive barrier to prolong the drug release period. In this dissertation, we will discuss the preparation of a stimuli-responsive polymer-based HMC material as a small-molecule controlled release system, and discuss some approaches of tuning the chemistry of HMC's hydrogel matrix to control the release kinetics of small molecules. Moreover, the controlled release mechanisms of the HMC-based materials will also be discussed based on the investigation of the interactions between the small molecules and the polymer materials. In addition to this, the HMC material also demonstrates its ability to be used as a multi-drug controlled release system as a proof-of-concept.

This dissertation will mainly focus on the methodologies of small-molecule controlled release by stimuli-responsive materials and devices, which will provide some new ideas for controlling the release of therapeutic drugs in long-term and low-invasive

35

drug delivery systems, such as implantable devices, transdermal delivery devices, hydrogel-based injectable delivery systems, and orally administrative drug delivery formats.

Chapter 2

Alkanethiol Surface Modification of a pH-Responsive Reservoir Device for Small Hydrophilic Molecules Controlled Release

2.1 Introduction

Materials composed of natural and synthetic polymers are ubiquitous in our daily lives. For example, gelatin, a water-soluble polypeptide, is used to make jelly in the food industry; synthetic rubber, an artificial highly elastic polymeric material, has been used widely in the automotive industry; and poly (lactic acid), a biocompatible polymer, has a variety of medical applications, e.g., stents,[159] sutures,[160] and patches.[161] In the past few decades, stimuli-responsive polymers,[162-164] also known as "smart" materials, have attracted much scientific interest due to their ability to respond to external stimuli, e.g., changes in environmental conditions. Stimuli-responsive polymers have found numerous applications as self-healing materials,[165-166] stimuli-responsive actuators,[164, 167-169] and drug delivery reservoirs.[93, 163, 170] The breadth of the application of stimuli-responsive polymers is a result of the diversity of their chemistry that allows them to respond to specific chemical and/or physical stimuli, such as pH,[7, 39] organic/inorganic molecules,[91, 171] biomolecules,[21, 172-173] temperature,[5, 174] light,[12, 175] and electric field.[14-15]

One of the most extensively studied stimuli-responsive polymers is poly (*N*-isopropylacrylamide) (pNIPAm), which undergoes a transition from a water-soluble state

to a relatively insoluble state when the temperature is increased above its lower critical solution temperature (LCST).[4, 31] The LCST for pNIPAm in pure water is around 32.5 °C, above which the linear polymer chain shrinks from an extended (random coil) to a collapsed (globule) state.[176] PNIPAm also can be crosslinked into network structures to yield hydrogels or hydrogel particles (microgel or nanogel, depending on the diameter); these crosslinked structures also exhibit an LCST where they undergo a transition from water swollen to deswollen.[71] In addition, by copolymerizing functional monomers into the hydrogel structures, they can be made to respond to a variety of stimuli. For example, addition of acrylic acid (AAc) renders the resultant material pH responsive. This is a result of AAc being deprotonated (and becoming negatively charged) at pH > 4.25, which leads to polymer swelling as a result of charge repulsion and osmotic swelling; the polymer returns to its native solvation state when the AAc is protonated (and neutralized) at pH < 4.25. Importantly, the negative charge generation as a result of AAc deprotonation allows positively charged small molecules to adhere electrostatically to the polymer structure and to be released when the charge is neutralized.[177-178]

In 2011, the Serpe Group reported on pNIPAm-microgel-based optical devices, called etalons,[82] which can be fabricated by sandwiching a layer of pNIPAm-based microgels between two semi-transparent 15-nm Au layers on a glass substrate. The structure of a microgel-based etalon is shown in Figure 2-1(A). The etalons exhibit visible color and unique multi-peak reflectance spectra due to interference of light resonating in the microgel layer between the two Au layers.[179] The position and order of the peaks can be predicted using Equation (1-3). Etalons have been shown to exhibit responses to DNA,[180] glucose,[181] organic compounds,[78] and small inorganic compounds.[81, 91, 182]

Etalons are also useful for controlled/triggered drug delivery.[177] This is due to the ability of the microgels to absorb and bind small molecules (via electrostatics and other interactions), which then can be triggered to release via changes in environmental conditions.[35] As reported previously, the ultrathin layer of Au deposited on the etalon devices via thermal evaporation deposition is porous,[82, 179] and the porosity can be tuned easily by changing the Au layer thickness, or via surface modification.[93, 177] Regardless of how the Au layer porosity is varied, it can be used to control the release rate of small molecules out of the microgel layer of the etalons.
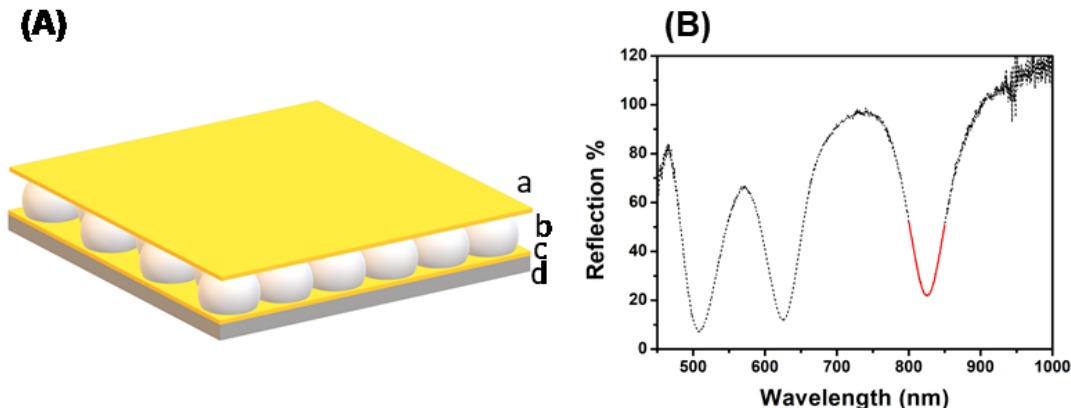
Figure 2-1. (A) Schematic of a pNIPAm-*co*-AAc microgel based etalon: (a) 20 nm of Au layer with 2 nm of Cr adhesion layer, (b) pNIPAm-*co*-AAc microgel monolayer, (c) 15 nm of Au layer with 2 nm of Cr adhesion layer, and (d) glass substrate. (B) Optical reflection spectrum (black dashed curve) of a representative, unmodified etalon. A Gaussian curve was fit (red solid curve) to a portion of the spectrum to identify the wavelength of the trough. (Reprinted with permission from ACS)

In this research, we show that the kinetics of small molecule release from microgels in etalons can be controlled in a more precise and simpler way than has been reported previously by exploiting the ability of alkanethiols to bind to Au surfaces, as a molecular barrier formed with the alkanethiols on the Au blocks the diffusion of the model drug

molecules.[183-185] Specifically, alkanethiol molecules with different functional groups and alkane chain lengths were used to modify the upper Au layer of the model drug loaded etalon device, in order to change the surface hydrophobicity/hydrophilicity. We show that the release rate of the model drug molecule, crystal violet (CV), from the surface modified etalon was slowed by the presence of more hydrophobic alkanethiols and enhanced in the presence of hydrophilic alkanethiols. We went on to investigate the mechanism of release rate control and found that the behavior is a result of the surface-bound thiol blocking the triggering agent from entering the etalon and blocking the release of CV out of the layer. With this surface modification approach, we can envision developing etalon array delivery systems that can release CV (or a drug) quickly and in a sustained fashion, which is always a tradeoff for other triggered delivery systems.

2.2 Experimental Section

2.2.1 Materials

N-isopropylacrylamide (NIPAm) was purchased from TCI (Portland, Oregon) and purified by recrystallization in hexane (Sigma-Aldrich, reagent grade) before use. *N,N′*-methylenebisacrylamide (BIS, 99%), acrylic acid (99%), ammonium persulfate (APS, ≥98%), sodium chloride (≥99.5%), sodium hydroxide (98%), and crystal violet (CV) were purchased from Sigma-Aldrich and used as obtained. Deionized (DI) water with resistivity of 18.2 MΩ•cm was obtained from a Milli-Q system. Hydrochloric acid was purchased from Caledon Chemicals (Georgetown, Ontario). Alkanethiol reagents, including 2-mercapto-1-ethanol (2-OH), 6-mercapto-1-hexanol (6-OH), 11-mercapto-1-undecanol (11-OH), 1-heptanethiol (6-CH_3), 1-dodecanethiol (11-CH_3), and 1-hexadecanethiol (15-CH_3) were purchased from Sigma-Aldrich. The structures and names of each alkanethiol

molecule are shown in Figure 2-2. Cr (flakes, 99.999%) was obtained from ESPI (Ashland, OR) and Au 99.99% purity was purchased from MRCS Canada (Edmonton, Alberta).
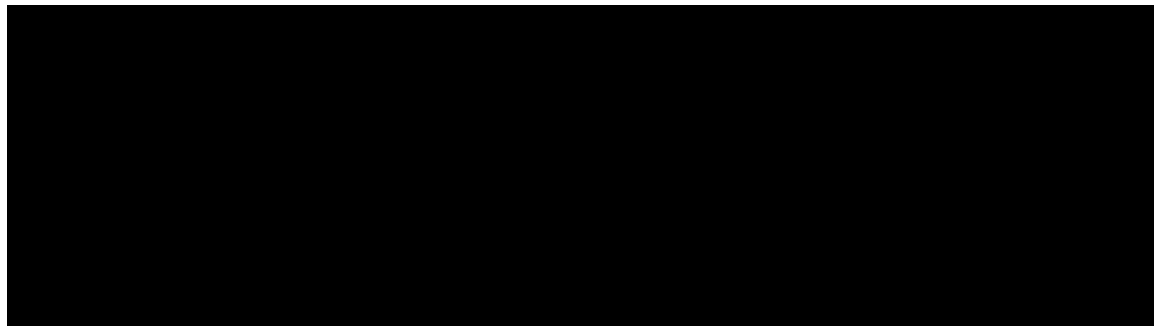
Figure 2-2. Structures, full names, and abbreviations of alkanethiol molecules used in surface modification. (Reprinted with permission from ACS)

2.2.2 Microgel Synthesis

Poly(*N*-isopropylacrylamide)-*co*-acrylic acid (pNIPAm-*co*-AAc) microgels were synthesized via surfactant-free free radical precipitation polymerization, as described previously.[179] Briefly, 10.5 mmol of NIPAm and 0.703 mmol of BIS were dissolved in 99 mL of DI water, and the solution was filtered through a 0.2-μm filter into a 3-neck round-bottom flask fitted with a reflux condenser. The solution was bubbled with N_2 gas for 1 h while heating to 70 °C. Then, 198 μL (2.86 mmol) of AAc were added into the reaction mixture in one aliquot, followed by initiating the polymerization by injection of a solution of APS (0.2 mmol) in 1 mL of DI water. The reaction then proceeded for 4 h at 70 °C under a blanket of nitrogen gas flow. The resultant white microgel suspension was filtered through glass wool after being cooled to room temperature to remove any large aggregates. Next, the microgel solution was purified via a centrifugation-resuspension process with DI water six times. Finally, the microgel pellets formed in the last run of centrifugation were collected, combined, and stored in a glass vial as a concentrated microgel solution.

2.2.3 CV Loaded Etalon Device Fabrication

To prepare etalons, 2 nm of Cr and 15 nm of Au were sequentially thermally deposited using a Torr International Inc. system (Model THEUPG, New Windsor, NY) onto a 25 mm × 25 mm ethanol-rinsed and N_2 gas dried glass microscope coverslip (Fisher's Finest, Ottawa, ON). (Figure 2-3(A)) The Cr/Au substrates were annealed in an oven for 3 h at 250 °C (Thermolyne muffle furnace, Ottawa, ON) and cooled down to room temperature for the microgel layer deposition. To deposit the pNIPAm-based microgel monolayer on the substrate, a previously described painting protocol was used.[186] To accomplish this, a 40-µL aliquot of concentrated microgel solution (from centrifugation) was pipetted onto an ethanol-rinsed, N_2 gas dried substrate and spread out to cover the whole surface. Then, the microgel solution was allowed to dry completely on a hot plate set to 35 °C. The substrates were rinsed copiously with DI water, soaked in DI water overnight at room temperature, and rinsed again, to remove excess microgels not bound to the Au surface. Figure 2-3(B) shows the appearance of the metal-coated glass substrate with a pNIPAm-*co*-AAc microgel layer on it, and the microgel layer is transparent.

To pre-load the CV into the etalon device, microgel-coated substrates were soaked in a 1-mg/mL CV solution for 5 h. The CV solution was prepared by dissolving 200 mg of CV in 200 mL DI water and adjusting the solution pH to 6.5. Excess unbound CV was rinsed off the microgel layer with a solution of pH 6.5 (2 mM NaCl) and incubated in a solution of pH 6.5 (2 mM NaCl) for 1 h. This process was carried out two times to completely remove the unbound CV from the surface without breaking the microgel-CV interaction. The pH of the solutions was maintained at 6.5 to ensure that the AAc groups

were negatively charged so that they could bind the positively charged CV. Then, the CV-loaded microgel layer was dried with N$_2$ gas, and 2 nm of Cr and 20 nm of Au were deposited on the microgel layer. The CV molecules give the substrate a purple color, as shown in Figure 2-3(C), and another metal layer deposition forms a shiny surface on the substrate, as shown in Figure 2-3(D). The non-CV loaded etalon devices were prepared using the same procedure but without the CV loading and rinsing steps.
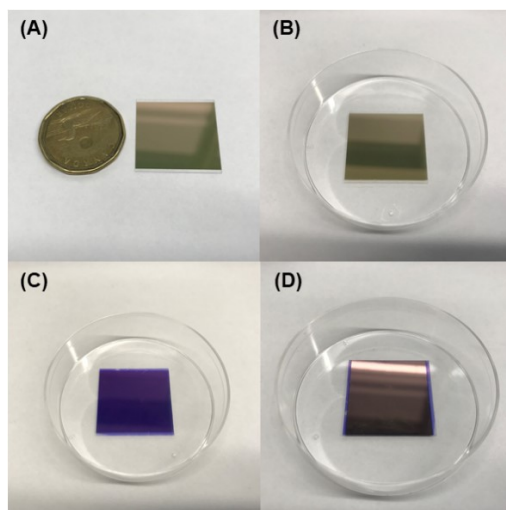
Figure 2-3. (A) 15 nm of Au with 2 nm of Cr adhesion layer deposited on a microscope glass cover slice; (B) metal-coated substrate with a pNIPAm-*co*-AAc microgel layer; (C) A CV-loaded pNIPAm-*co*-AAc microgel monolayer on substrate; (D) a fabricated CV-loaded etalon device with 20 nm of Au and 2 nm of Cr adhesion layer deposited on top of the microgel layer. (Reprinted with permission from ACS)

2.2.4 Etalon Surface Alkanethiol Modification

To accomplish this, the pNIPAm-*co*-AAc microgel-based etalon was fabricated and modified via the protocol shown in Figure 2-4. Specifically, the prepared etalon device was placed in a small beaker, then 3 mL of alkanethiol/diethyl ether solution (20-mM alkanethiol) were added into the beaker to immerse the etalon. The beaker needed to be sealed with two layers of parafilm and one layer of aluminium foil to minimize the solvent

evaporation and peroxide formation due to the environmental light. In this experiment, diethyl ether was used as it can dissolve all the alkanethiols used here without disrupting the CV-microgel interaction. After soaking in the alkanethiol solution for 2 h, the etalons were removed from the beaker and rinsed with diethyl ether. Finally, the surface modified etalons were allowed to dry in air. In our experiments, CV-loaded etalon samples were modified with certain hydrophilic and hydrophobic alkanethiol molecules alone, as described above, or with a mixture of two different alkanethiols.
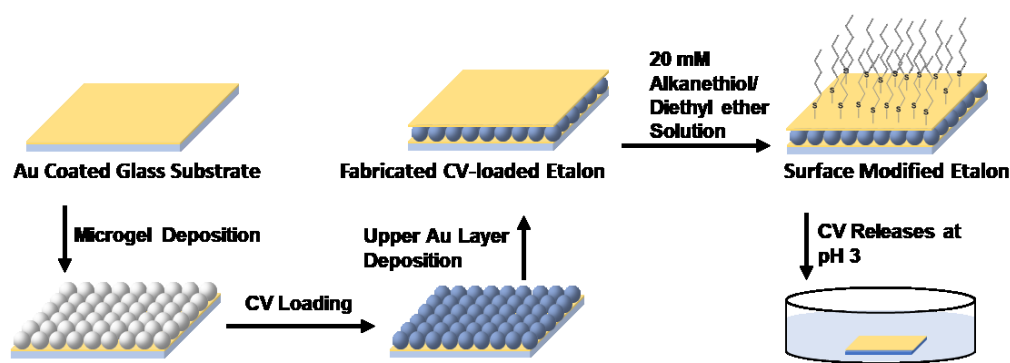
Figure 2-4. Schematic diagram of a CV-loaded surface modified etalon preparation. Note: The orientation of the thiols on the Au layer, and their packing, is drawn in this manner for simplicity, and doesn't represent the real orientation or packing density on the Au. (Reprinted with permission from ACS)

2.2.5 Static Water Contact Angle Measurements

Static water contact angle measurements (rame-hart Model 590 (p/n 590-U1)) were completed by adding 2 μL of DI water on top of the surface of each alkanethiol-modified etalon device and alkanethiol-modified Au surfaces (2 nm of Cr with 20 nm of Au on a glass coverslip).

2.2.6 X-ray Photoelectron Spectroscopy (XPS) Analysis

Alkanethiol modified samples were analyzed with XPS spectrometer (Kratos AXIS Ultra, Al source, source energy: 1486.69 eV). For each sample, survey spectra (pass energy: 160eV, number of scans: 2 , dwell time: 100ms), and high resolution spectrum for elements C (pass energy: 20 eV, number of scans: 12, dwell time: 200 ms), O (pass energy: 20 eV, number of scans: 20, dwell time: 200 ms), and S (pass energy: 20 eV, number of scans: 60, dwell time: 200 ms) were obtained.

2.2.7 CV Release Experiment

A sample etalon device (edges sealed by nail polish) was placed into a glass Petri Dish containing either 20 mL acidic aqueous solution (pH 3, 2 mM NaCl) or a more neutral aqueous solution (pH 6.5, 2 mM NaCl). At the time of addition to the Petri dish, a UV-vis spectrometer (Hewlett-Packard Agilent 8453) coupled with an 89090A temperature controller was used to collect the absorbance spectrum of the solution every 5 min. Sampling the solution from the Petri dish was achieved using a recirculating peristaltic pump with tubing to maintain a continuous solution flow between the quartz cuvette and the Petri dish. The experimental setup is shown in Figure A-3.

2.2.8 Reflectance Spectra

This was done according to previously described protocols.[96-97, 187] Briefly, a reflectance probe was set perpendicular to the surface modified non-CV-loaded etalon soaked in 10 mL of the pH 6.5 solution in a Petri dish. Samples were pre-stabilized in this solution overnight prior to the experiment. As soon as a small amount of concentrated hydrochloric

acid was added into the Petri dish in one aliquot to decrease the solution pH from 6.5 to 3, the reflectance spectrum of the etalon was collected with a spectrophotometer probe (USB2000+ spectrophotometer equipped with HL-2000-FHSA tungsten light source and an R400-7-VISNIR optical fiber reflectance probe, all from Ocean Optics (Dunedin, FL)) every 1 min to monitor the kinetics of the reflectance peak (or trough) shift.

2.3 Results and Discussion

2.3.1 CV Release Study

For these experiments, the positively charged small molecule dye crystal violet (CV) was used as a model drug molecule due to its high absorption coefficient and stability at the experimental conditions used here. The positive charge of CV allows it to bind electrostatically to deprotonated (negatively charged) AAc groups at pH > pKa for AAc (~4.25).[177-178] That is, when microgels are in solution with a pH > 4.25 (e.g., 6.5), their negative charges allow them to bind the positively charged CV electrostatically. Likewise, CV can be triggered to release from the microgels by decreasing the solution pH to 3.0, where the AAc groups in the microgels are neutralized and the electrostatic interactions holding the CV in the microgels are removed. When CV-loaded pNIPAm-*co*-AAc microgels are in an etalon, they can also be triggered to release as a function of solution pH, although the release kinetics are dictated by the porosity of the etalon's upper Au layer.[93, 177]   A typical UV-vis absorbance spectrum of CV in aqueous solution is shown in Figure 2-5(A). As can be seen, a significant absorbance peak can be observed at 590 nm, which is the wavelength we monitored to track CV release. Figure 2-5(B) shows that

etalons composed of microgels loaded with CV can release their CV payload when the microgel charge is neutralized at pH < 4.25, while they do not release significant amounts of CV at pH > 4.25.
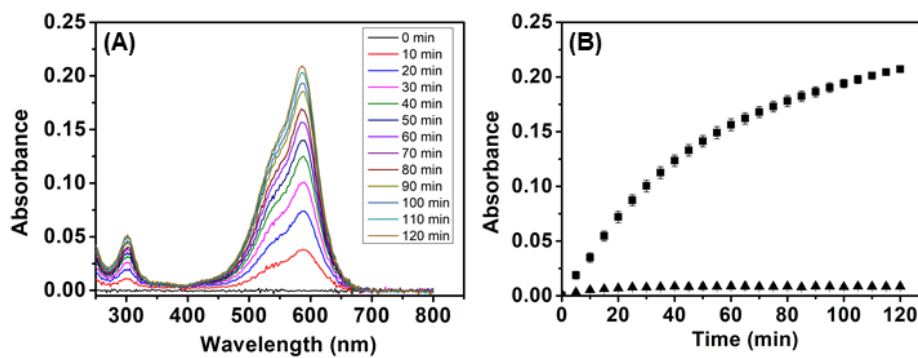
Figure 2-5. (A) UV-vis absorbance spectrum of CV and CV release kinetics of an unmodified etalon sample in a pH 3 solution. (B) Absorbance values at 590 nm as a function of time for an unmodified etalon sample in (■) a pH 3 and (▲) a pH 6.5 solution. (Reprinted with permission from ACS)

In this investigation, we fabricated etalons composed of microgels loaded with CV, followed by the modification of the etalon's top Au layer with three different "hydrophilic" alkanethiols (2-mercaptoethanol (2-OH), 6-mercapto-1-hexanol (6-OH), 11-mercapto-1-undecanol (11-OH)), and three different "hydrophobic" alkanethiols (1-heptanethiol (6-CH_3), 1-dodecanethiol (11-CH_3), 1-hexadecanethiol (15-CH_3)). As mentioned above, the Au porosity can be used to tailor the release kinetics, while here we are probing the ability of the thiol molecule hydrophobicity to control the release rate. We argue that since CV is hydrophilic, its release from the etalon will be hindered by the presence of a hydrophobic thiol, while we expect it to be less hindered by a hydrophilic thiol. We also argue that the release rates are tunable as a result of the different diffusion rates of the acid solution through the various thiol layers that are needed to neutralize the deprotonated AAc in the

microgels. We also investigated the release rates for etalons modified with combinations of the above hydrophobic/hydrophilic alkanethiols.

Initially, we used water contact angle measurements to characterize the modification of the etalon's Au layer with the respective alkanethiols. Figure 2-6 compares the water contact angles of the Au surface of the etalons with and without alkanethiol modification. As can be seen, the water contact angle for the Au layers modified with OH-terminated alkanethiols was ~45°, compared to ~60° for the unmodified Au layers. In contrast, when the Au layers were modified with CH_3-terminated alkanethiols, the water contact angle increases to ~90°. We also showed that a Au layer exposed to a 1:1 mixture of 6-OH and 6-CH_3 (6-O/6-C) yielded a contact angle between that of individual 6-OH and 6-CH_3. These two alkanethiols have the same alkane chain lengths, although 6-OH is terminated with an OH, while 6-CH_3 is terminated with a CH_3 (for a total of 7 C). Therefore, the surface molecular layer thicknesses should be similar for both (although not measured here). In addition, contact angles were measured for alkanethiol-modified Au layers that were deposited directly on glass. As can be seen in Figure 2-6, the alkanethiol modified Au layers on glass consistently show slightly higher water contact angles than those of the Au layers of the etalon. We attribute this to the presence of the microgels underneath the etalon's upper Au layer because the water droplet shows a smaller contact angle when it is absorbed partially by the surface.
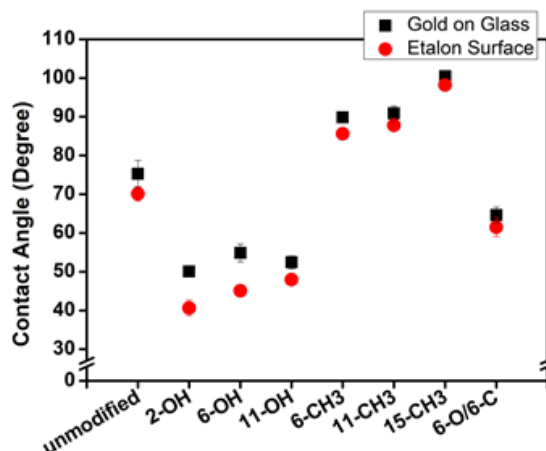
Figure 2-6. Static water contact angles on (■) alkanethiol modified Au layers on glass and the (●) modified top Au layers of etalons. (Reprinted with permission from ACS)

X-ray photoelectron spectroscopy (XPS) also was used to assess the atomic composition of the thiol-modified surfaces to confirm the presence of the expected elements. As can be seen in the O 1s high resolution XPS spectra shown in Figure 2-7(A)-(D), the S 2p high resolution XPS spectra shown in Figure 2-7(E)-(H), and the atomic percentage bar chart in Figure 2-8, the atomic percentage of C, O, and S calculated from the XPS survey spectrum shows that all samples, including the unmodified etalon, show significant amounts of C and O; this is likely due to C and O in the atmosphere and possibly residual diethyl ether. However, the O atomic percentage is higher for the 6-OH sample, compared to 6-CH3, which we attribute to the presence of the terminal OH group. On the other hand, S is seen on all thiol-modified surfaces, which further supports the hypothesis that the surfaces indeed are modified with the thiols (Figure 2-8(E)-(H)). However, Figure 2-7 shows that a lower percentage of S is detected on the 6-O/6-C sample, relative to the others, which could mean that the surface modification was less effective in this case. This

may come from the deficient surface coverage of the alkanethiol molecules with the nonuniform thiol molecules in the modification process.[188]
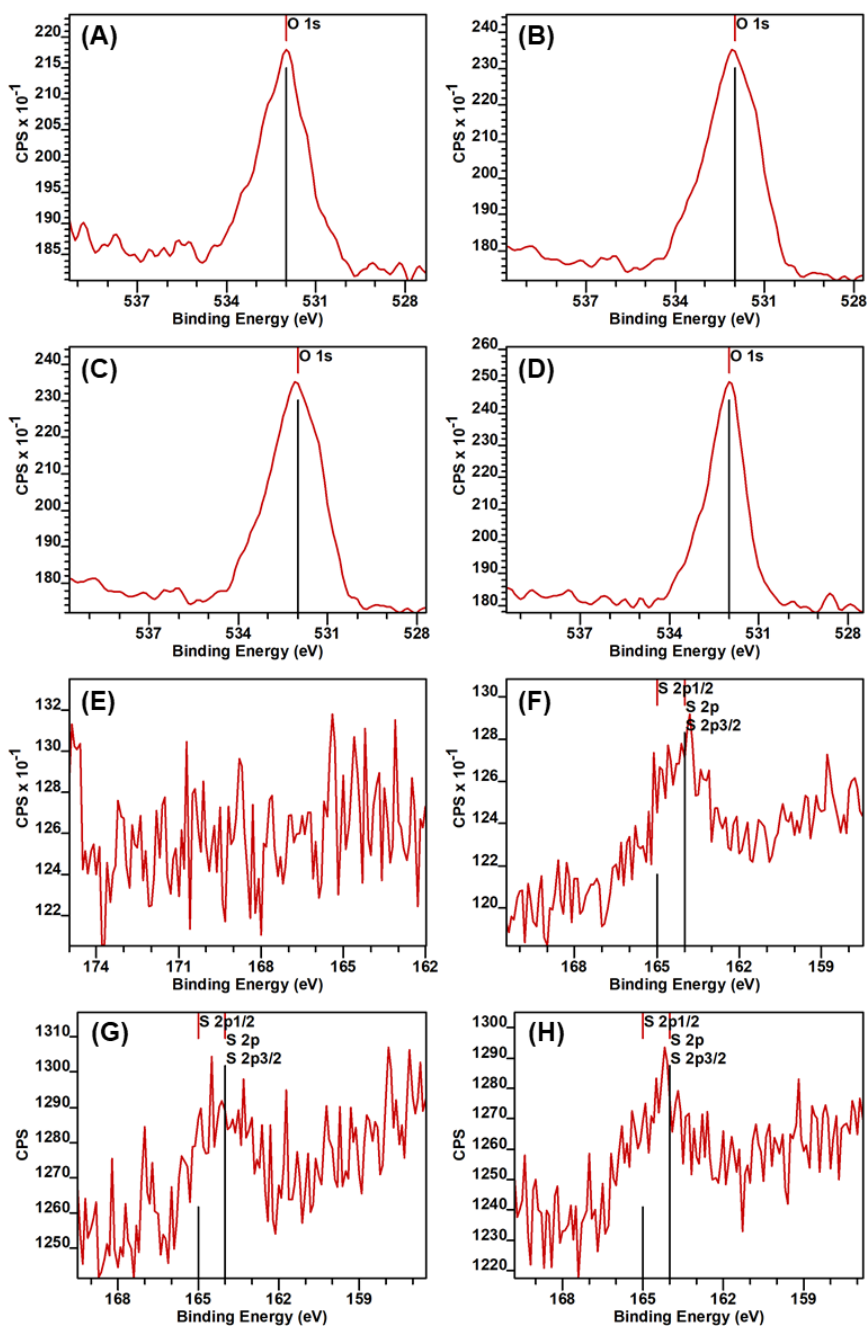
Figure 2-7. High resolution XPS O 1s spectrum of (A) unmodified, (B) 6-OH, (C) 6-CH$_3$, (D) 6-O/6-C etalon samples and high resolution XPS S 2p spectrum of (E) unmodified, (F) 6-OH, (G) 6-CH$_3$, (H) 6-O/6-C etalon samples. (Reprinted with permission from ACS)
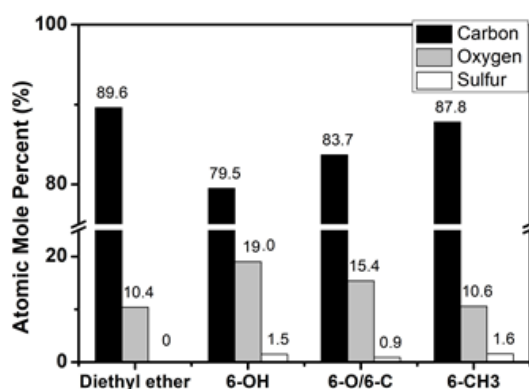
Figure 2-8. Atomic mole percentage of elements C, O, and S on different surface modified etalon samples, calculated from XPS survey scan spectra. (Reprinted with permission from ACS)

PNIPAm microgel-based etalon devices have exhibited the ability to release small molecules (or drugs) with a rate that is dependent on the porosity of the etalon's upper Au layer. Here, we investigate how the presence of thiols immobilized on the etalon's upper Au layer can impact the release kinetics of small molecules loaded in the microgel layer. To study this, we monitored the CV release kinetics from the etalons with their upper Au layer modified with alkanethiols of varying polarities (as indicated above). For these experiments, etalons composed of microgels preloaded with CV were added to glass Petri dishes containing a solution of pH 3 (2 mM NaCl), and the solution's absorbance spectra were collected with a UV-vis spectrometer every 5 min. Since the pNIPAm-*co*-AAc microgels are pH-responsive, the loaded cationic CV molecules could be released from the microgel layer to the external solution in a pH-triggered fashion. Meanwhile, since the CV molecule has the strongest UV-vis absorbance peak at 590 nm, the absorbance at 590 nm was used to quantify the CV concentration in solution. Figure 2-9(A) and (B) show the CV release as a function of time for the etalons modified with the indicated alkanethiols. As can be seen, in each case, the average release rate reaches a maximum at the beginning of

the release, while some, e.g., 2-OH and 6-OH, gradually approach a plateau. The observed release profile is a result of CV diffusing out of the etalon's microgel layer, through the top Au layer, into the solution in a pH triggered fashion. Fick's first law can be used to explain the observed data, which relates the diffusion flux, J, to a concentration gradient, as in Equation 2-2

$$J = D(\mathrm{d}\varphi/\mathrm{d}x) \tag{2-2}$$

where D is the diffusion coefficient, φ is the concentration, and x is the position. In our case, at the beginning of the CV release process, the concentration difference between the inside and outside of the etalon device, $\mathrm{d}\varphi/\mathrm{d}x$, is the highest, and it gradually decreases as CV diffuses out of the etalon and into the solution, causing J to decrease gradually. As the release approaches completion, the inside and outside environments have a very similar concentration, and the CV release kinetics approach a plateau, as shown in the CV release kinetics curve of 2-OH and 6-OH samples in Figure 2-9(A). Therefore, a controlled release process with a gradually decreasing release rate can be described with a first-order release model, which has been used to describe drug release from a reservoir with a release constant that depends on the drug concentration in the reservoir.[189] The generic equation (Equation 2-3) for the first-order release model is

$$\log Q_t = \log Q_0 - k_1 t/2.303 \tag{2-3}$$

where Q_t is the total number of moles of drugs remaining in the reservoir (the CV-loaded etalon device in our case) at time t, Q_0 is the total number of moles of drugs in the reservoir initially, and k_1 is the first order rate constant (time^{-1}). Then, the derivative of Equation 2-3 can be written as Equation 2-4

$$Q_0 - Q_t = Q_0(1 - e^{-k_1 t}) \tag{2-4}$$

where the term $(Q_0 - Q_t)$ can be regarded as the amount of released CV from the sample etalon device at time t, which is directly related to the UV-vis absorbance value, and Q_0 can be regarded as the total amount of released CV, which also is represented by the maximum absorbance value of the release kinetics curves. Beer's law states that the solution absorbance and concentration are proportional, thus the amount of CV released into solution is related directly to the solution absorbance if the solution volume is constant. Therefore, the CV release kinetics curve for each release profile could be fitted with Equation 2-5

$$A_t = A(1 - e^{-k_1 t}) \tag{2-5}$$

where A_t is the solution absorbance at time t, A is the theoretical maximum absorbance value, and k_1 is the first-order release rate constant. Fitting the data in Figure 2-9 to Equation 2-5 allows values for k_1 and A for the CV release kinetics to be obtained for each sample, as tabulated in Table 2-1.
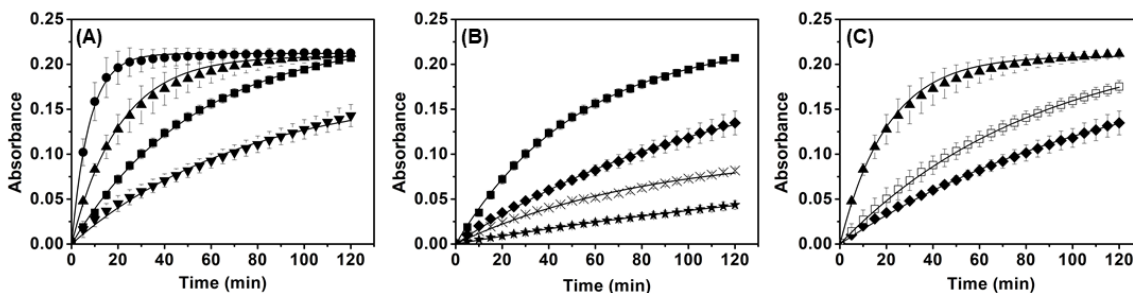
Figure 2-9. (A) Absorbance at 590 nm as a function of time for etalons that are (■) unmodified or modified with (●) 2-OH, (▲) 6-OH, and (▼)11-OH. (B) Absorbance at 590 nm as a function of time for etalons that are (■) unmodified, or modified with (◆) 6-CH₃, (×)11-CH3, and (★)15-CH3. (C) Absorbance at 590 nm as a function of time for etalons that are modified with (▲) 6-OH, (◆) 6-CH3, and (□) 6-O/6-C. Data points are average values for four replicate experiments, error bars are the standard deviation of the four measurements, and solid curves are fit lines to the data using Equation 2-5. (Reprinted with permission from ACS)

Table 2-1. CV Release Rate Constant, k_1, and Theoretical Maximum Absorbance, A, Including their Standard Errors, Obtained from Fitting Equation 2-5 to the Respective Data

Sample	CV Release Rate Constant, k_1* in min^{-1}	Theoretical Max. Absorbance**, A
Unmodified	0.0189 ($\pm$0.0003)	0.229 ($\pm$0.001)
2-OH	0.1357 ($\pm$0.0007)	0.211 ($\pm$0.001)
6-OH	0.0462 ($\pm$0.0009)	0.208 ($\pm$0.001)
11-OH	0.0128 ($\pm$0.0007)	0.197 ($\pm$0.006)
6-CH$_3$	0.0085 ($\pm$0.0003)	0.208 ($\pm$0.006)
11-CH$_3$	0.0051 ($\pm$0.0007)	0.196 ($\pm$0.004)
15-CH$_3$	0.0020 ($\pm$0.0003)	0.205 ($\pm$0.005)
6-O/6-C	0.0124 ($\pm$0.0002)	0.224 ($\pm$0.002)

*, ** Values, including standard errors, predicted by fitting the data with Equation 2-5.

From Figure 2-9(A) and the values in Table 2-1, it can be seen that when the etalon samples were modified with short-chain hydrophilic alkanethiols, such as 2-OH and 6-OH, their CV release rate constants are high relative to the unmodified control samples. We believe that this is due to the hydroxyl group of the alkanethiol molecules making the surface more hydrophilic, which allows the acid to enter the etalon's microgel layer more easily, and also improves the ability of the hydrophilic CV to exit the Au. However, when the long-chain alkanethiol, 11-OH, was used to modify the etalons, the CV release was inhibited partially by the modification, which is likely due to the highly hydrophobic alkane being next to the Au layer, slowing down the CV release. Also, the longer alkane chain length can increase the diffusion path length that the CV needs to traverse in order to enter the solution.

In contrast, when the samples were modified with hydrophobic alkanethiols, such as 6-CH$_3$, 11-CH$_3$, and 15-CH$_3$, they all exhibit significantly slower CV release kinetics, compared to the control sample and the hydrophilic alkanethiol modified samples, and the release rate tends to decrease as the alkyl chain length increases. We believe that this is due to the Au surface becoming increasingly hydrophobic, making the acid entrance into the

microgel layer more difficult. Furthermore, as described above, the long alkane chain next to the Au layer will render the Au hydrophobic and increase the diffusion path length that the CV must traverse to enter the solution. From the rate constants presented in Table 2-1, we can conclude that alkanethiol surface modification can be used to control the CV release rate from etalon devices, and the release rate is related to the chain length of alkanethiol molecules and their functionality (ultimately the whole molecule's polarity). In addition, what needs to be pointed out is that the theoretical maximum absorbance values predicted by the curve fitting are all within a close range, from ~0.19 to ~0.22, which illustrates that our surface modification approach only impacts the CV release rate and has a negligible impact on how much CV actually can be released. Finally, we show that mixtures of alkanethiols on the etalons can be used to tune the release kinetics further. As can be seen in Figure 2-9(C), the etalons modified with a 1:1 mixture of 6-OH with 6-CH$_3$ (6-O/6-C) had release kinetics that were between the etalons modified with just 6-OH and just 6-CH$_3$.

As mentioned previously, we aim to make arrays composed of multiple etalons that each are capable of releasing CV (or a drug) with a predefined rate. If this can be achieved, we will have finer control of the release profiles than can be accomplished with individual etalons alone. Hence, we show here that release rates can be tuned further by simply adding etalons modified with different thiols to the same release solution. In this case, we hypothesize that we will see a release profile that is a combination of the release profiles of the individual etalons that we used. To accomplish this, an unmodified etalon sample was split into two equal halves, and each part was treated with the desired thiols (or could be left unmodified). After that, the two halves were recombined with scotch tape, and the CV release performed. Figure 2-10(A) shows the composite CV release profile for an

etalon modified with 15-CH$_3$ alkanethiol releasing with an unmodified etalon. As can be seen, the resultant CV release profile exhibits a release behavior similar to both the unmodified and the 15-CH$_3$ modified etalons individually. Specifically, it shows a phase of rapid initial release (0–100 min) like the unmodified etalon, followed by a slower and sustainable release region (100 min–1200 min) like the 15-CH$_3$ modified etalon. From this, it was not clear if the release rate of one etalon could impact the release rate of another etalon in the same solution. That is, if an etalon releases fast in the presence of a slow releasing etalon, does the release rate of the slow etalon decrease because of the decrease in concentration gradient that drives the CV out of the etalon? Figure 2-10(B) shows the CV release profiles for the recombined etalons and the sum of the release profiles for each of the halves individually. As can be seen, the actual release profile from the recombined etalons is slightly slower than what is observed by simply summing up the release profiles of the individually releasing etalons.
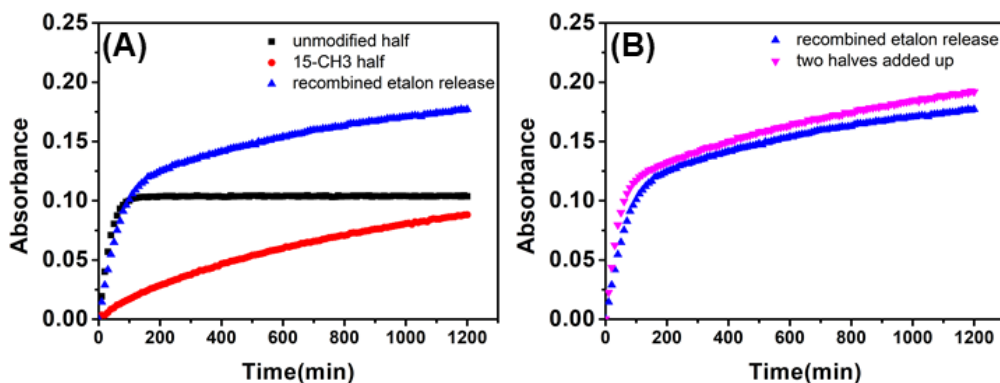
Figure 2-10. CV release profiles from recombined etalons that have different surface modification. (A) Comparison of CV release profile of a (▲) recombined unmodified and 15-CH$_3$ modified etalon sample, and individual (■) unmodified, and (●) 15-CH$_3$ modified etalons. (B) Comparison of a (▲) CV release profile of recombined unmodified and 15-CH$_3$ modified etalons, and the (▼) sum of absorbance values of the individually releasing etalons. (Reprinted with permission from ACS)

In addition, when we split an etalon into four equal quarters, modified three of the quarters with 2-OH, 6-OH, and 15-OH alkanethiols, respectively, and left one of them unmodified, the recombined composite etalon also showed a slightly slower CV release profile than the summed up release profiles of the individual quarters. (Figure 2-11) We believe that this phenomenon is attributed by the decreased CV concentration gradient when some CV is released by fast release etalons before the CV release process of the slow release etalons. Therefore, we conclude that if etalons with drastically different release rates are combined, the release from the fastest one can alter the release profile of the slower one by decreasing the Fickian diffusion.
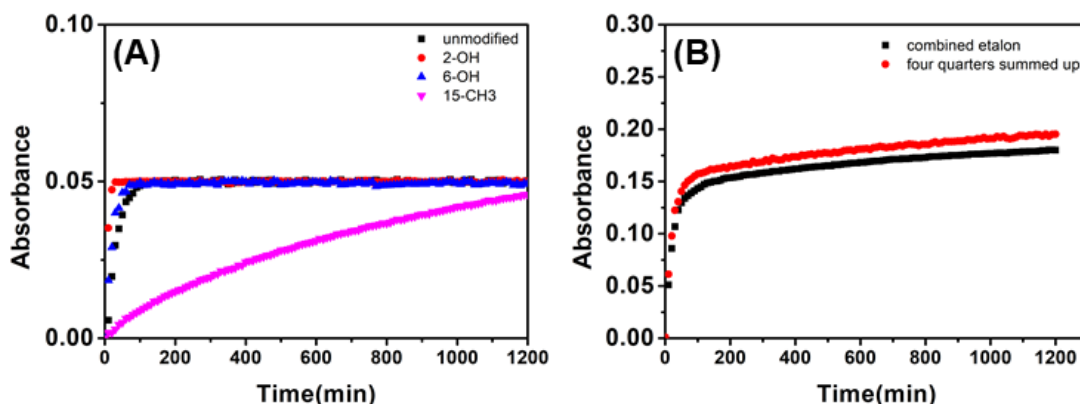
Figure 2-11. CV release profiles from recombined etalons that have different surface modification. (A) CV release profile of (■) unmodified, (●) 2-OH, (▲) 6-OH, and (▼) 15-CH₃ modified etalons. (B) Comparison of (■) CV release profile of recombined unmodified and 15-CH₃ modified etalons, and the (●) sum of absorbance values of the individually releasing etalons. (Reprinted with permission from ACS)

In summary, we found that alkanethiol surface modification allows us to tune the CV release rate from etalons. We found that the release rates depended on the length of the alkane chain of the thiol and its functionality, with shorter, more hydrophilic thiols releasing faster than longer, more hydrophobic thiols. The observed rate is necessarily a

result of the ability of the acid solution to get into the microgel layer of the etalon to trigger

release and the ability of the CV to exit through the Au layer, which are both dependent on

the hydrophobicity of the alkanethiol layer. In the next section, we exploit the pH

responsivity of the microgels and the tunable optical properties of the etalons, in an attempt

to decouple the acid diffusion kinetics into the microgel layer from the CV release kinetics

from the microgel layer.

2.3.2 Acid Response Kinetics of Alkanethiol-Modified Etalons

In order for CV to be released from the microgels in an etalon, the acid solution needs to

enter the microgel layer through the etalon's Au layer and neutralize the microgel's AAc

groups. Therefore, the rate of CV release also will depend on the ability of the acid to enter

the etalon. A more hydrophilic surface coating should result in the acid solution

neutralizing the microgels faster, compared to a hydrophobic surface coating, therefore, it

yields faster CV release rates.

To investigate the kinetics of an acid solution entering the etalon, we utilized their

optical properties and their ability to change color in response to changes in solution

conditions. Specifically, we have shown that etalons exhibit multipeak reflectance spectra,

and the position of the peaks in the spectra depends on the solvation state of the microgels,

which can be impacted by solution conditions. For these investigations, we exploited the

ability of pNIPAm-*co*-AAc microgels to change the diameter in response to the pH of the

solution; they are more swollen in solutions with pH > pKa (compared to solutions with

pH < pKa) due to the charged groups in the microgels repelling one another and osmotic

swelling effects. As can be inferred from Equation 2-1, swollen (large diameter) microgels

in etalons will lead to red-shifted reflectance peaks, while deswollen (small diameter) microgels will exhibit blue-shifted reflectance peaks. To investigate the response kinetics of our etalons to pH, we quickly switched the pH of the solution exposed to the etalons from 6.5 to 3 while monitoring the reflectance spectra over time. An example of this behavior can be seen Figure 2-12. Here we assume that the deswelling of pNIPAm-*co*-AAc microgels is a fast and non-rate-determining step. Thus, how much faster the microgel responds to the acid can represent how much faster the acid enters the Au layer.
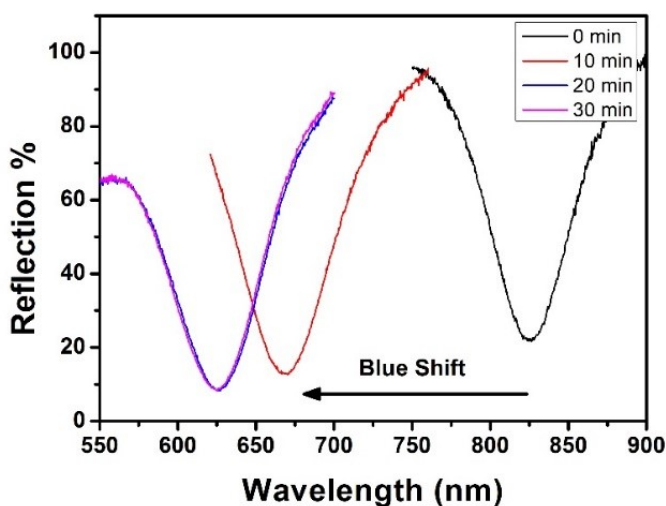
Figure 2-12. Collection of a partial reflectance spectrum of an unmodified etalon sample at different times after the solution pH changed from 6.5 to 3. (Reprinted with permission from ACS)

In our experiments, non-CV-loaded etalons were modified with different types or combinations of alkanethiols, and the reflectance spectra were collected every minute after the solution pH was switched from 6.5 to 3. As can be seen Figure 2-13, in each case, the reflectance peaks blue shift upon decreasing the solution pH from 6.5 to 3.0. This is a result of the AAc groups being protonated and allowing the microgels to decrease in diameter.[190-191] Of note is the shape of the response curves, which have substantial linear pH response

ranges, compared to the CV release curves (Figure 2-9). This can be explained using a zero-order diffusion model.[189] Specifically, different from the diffusion of CV from the microgel reservoir to the external environment, the permeation of an acid solution into the microgel layer does not have a significant effect on its concentration inside and outside the etalon device. We assume this because AAc protonation reduces the acid concentration by a negligible amount and the concentration inside the microgels is likewise low at the early stage of etalon's response to the pH change. Therefore, a constant concentration difference of acid between the two sides of the etalon's upper Au layer would result in a nearly constant diffusive flux, based on the Fick's first law, Equation 2-1. Since the zero-order release model is usually used to describe the drug release through a membrane with a constant concentration gradient between the two sides of the membrane,[192-193] and as mentioned above, there is a constant acid concentration gradient between the two sides of the etalon's Au layer at the beginning of the response, the diffusion kinetics of acid solution in this case could be described with the zero-order release equation shown below

$$C_t = C_0 + k_0 t \qquad (2\text{-}6)$$

where C_t is the cumulative amount of drug released at time t; C_0 is the initial drug concentration in solution; k_0 is the zero-order release rate constant; and t is time. However, as we are using the zero-order release model to describe the diffusion of acid through the etalon surface, the C_t is defined as the cumulative acid concentration in the microgel layer at time t; and C_0 is the initial acid concentration in the microgel layer. On the other hand, since the response kinetics of pNIPAm-*co*-AAc microgels to solution pH changes relates to how quickly the acid solution can reach the microgels, the resulting etalon response kinetics can be related to the permeation rate of the acid solution into the etalon's microgel

layer through its Au layer. Thus, Equation 2-7, having the same format as Equation 2-6, can be used to fit the data and obtain the zero-order rate constant

$$\Delta\lambda_t = \Delta\lambda_0 + k_0 t \tag{2-7}$$

where the $\Delta\lambda_t$ is the total blue shift value at time t, $\Delta\lambda_0$ is the initial blue shift of the reflectance peak, which is zero in our case, and k_0 in nm/min is the response of the etalon, which is related to the permeation of hydronium ions.
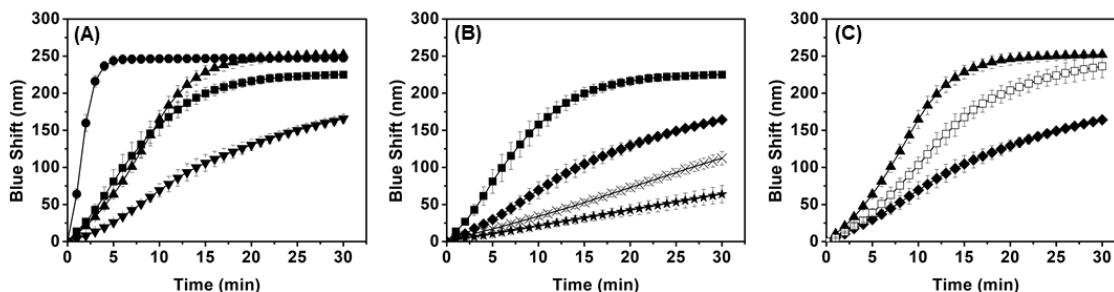
Figure 2-13. Optical reflectance trough shifts versus time of (A) hydrophilic alkanethiol, (B) hydrophobic alkanethiol and (C) mixed alkanethiol modified CV-loaded etalon samples in pH 3. In this figure, (■) for unmodified, (●) for 2-OH, (▲) for 6-OH, (▼) for 11-OH, (◆) for 6-CH3, (×) for 11-CH3, (★) for 15-CH3, and (□) for 6-O/6-C. In all three graphs, data points are average values of three replicate experiments, error bars are the standard deviation of the three measurements, and solid curves are just connections of data points. (Reprinted with permission from ACS)

To compare the ability of the acid solution to enter the microgel layer, we fit the first three minutes' data with Equation 2-7 to obtain k_0. The data fitting graphs are listed in Figure 2-14.
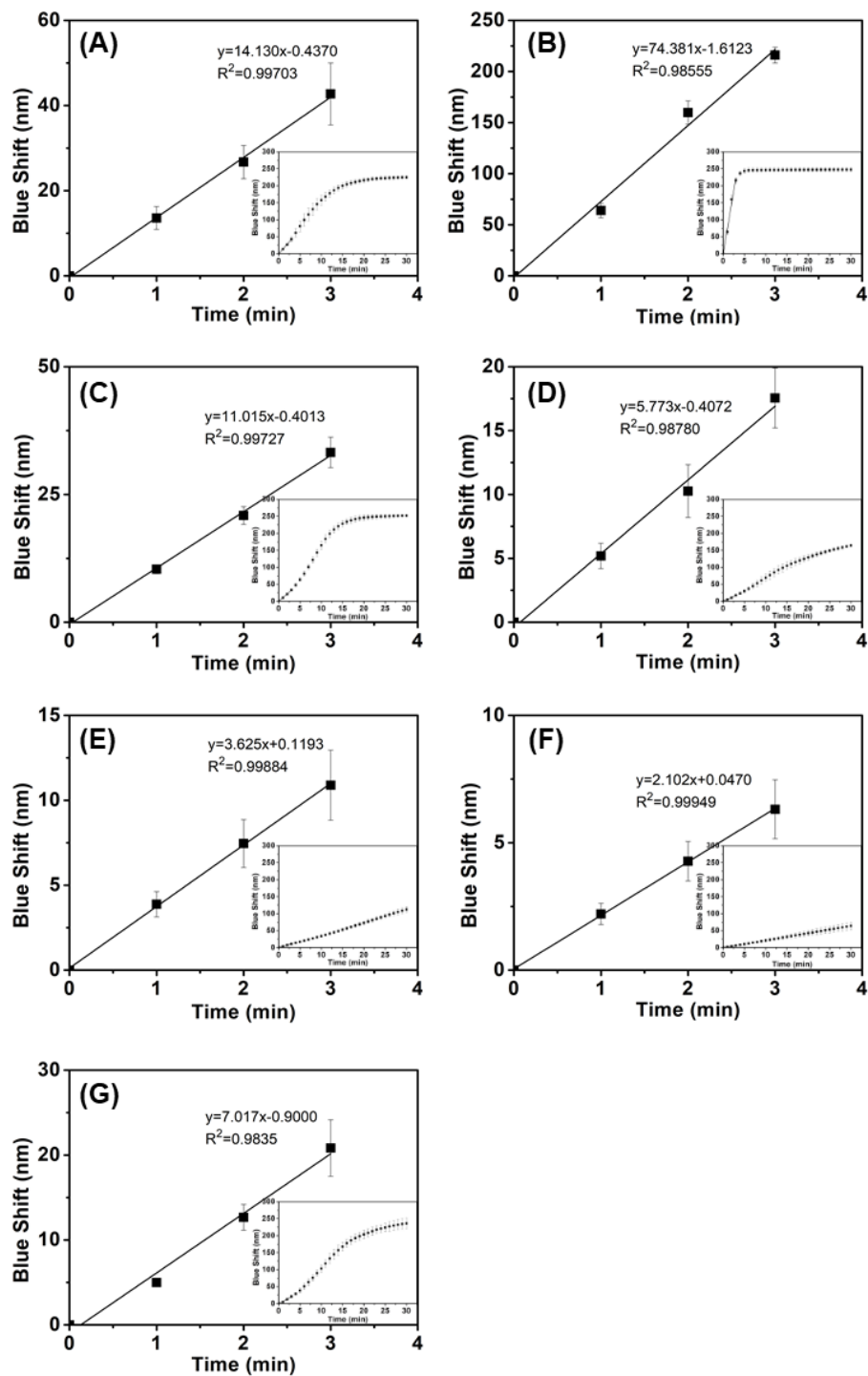
Figure 2-14. Defining initial slope of blue shift kinetics curves of (A) unmodified, (B) 2-OH, (C) 6-OH, (D) 6-CH$_3$, (E) 11-CH$_3$, (F) 15-CH$_3$, and (G) 6-O/6-C etalon samples with linear fitting on the initial four data points. The subfigure is the full blue shift kinetics curve of each modified sample. (Reprinted with permission from ACS)

Higher values of k_0 translate into faster penetration of the acid into the etalon's microgel layer. The data in Table 2-2 shows the k_0 values obtained from Equation 2-7 for the various etalons investigated. By comparing these values, we see that the thiols with longer alkane chain lengths result in slower response kinetics (and hence slower acid penetration into the microgel layer), regardless of the thiol functionality (i.e., hydrophobic/hydrophilic). Furthermore, we note that 2-OH has the highest k_0, which likely is due to it having both a hydrophilic head group and the shortest alkyl chain length. On the other hand, by comparing the blue shift kinetics of the etalon samples modified with 6-OH, 6-CH_3, and 6-O/6-C mixed alkanethiol, we find that the diffusion rate of acid into the microgel layer also is related to the hydrophobicity of the modified surface (Figure 2-9(C) and Table 2-2). When we maintain a constant alkyl chain length to eliminate the different blocking effects from the different lengths of alkyl chains, a hydrophilic surface demonstrates a greater value of calculated zero-order diffusion rate constant than a hydrophobic surface.

Table 2-2. Hydronium Ion Diffusion Rate Constants Approximated with the Initial Slope of the Optical Reflectance Spectrum Trough Blue Shift Kinetics of Each Kind of Surface Modified Etalon Samples

Sample Name	Diffusion Rate Constant, k_0 [*], in nm•min^{-1}
Unmodified	14.13
2-OH	74.38
6-OH	11.02
11-OH	4.456
6-CH_3	5.773
11-CH_3	3.625
15-CH_3	2.102
6-O/6-C	7.017

[*] Values are the slope of the fitted curves based on the Equation 2-7.

Overall, from the optical reflectance shift kinetics data as well as the calculated zero-order diffusion rate constants of the surface modified etalon samples, we find that the diffusion of hydronium ions through the etalons' upper Au layer is related to the selected alkanethiol for surface modification, and both the chain length and the functional group of the alkanethiol molecules have an effect on the permeation of hydronium ions.

2.3.3 Release Mechanism

It is known that the protonation of AAc in the pNIPAm-*co*-AAc microgels is required for CV release from the etalon to be triggered. The above results demonstrate that the ability of the acid to enter the microgel layer and for CV to exit the microgel layer is controlled by the chemical modification of the etalon's Au layer. Therefore, we propose that the observed CV release kinetics are a result of the combined ability of the acid solution to enter the microgel layer and the ability of CV to exit the microgel layer, both being controlled by the nature of the thiol coating on the etalon's Au layer. Specifically, when the acid solution permeation process is fast due to presence of a hydrophilic, short chain alkanethiol on the etalon's Au layer, more CV can detach electrostatically from the microgel's neutralized AAc groups in a shorter period of time (compared to a more hydrophobic, long chain alkanethiol), resulting in a higher concentration of free CV in the microgel layer and a large concentration gradient that promotes CV exiting the microgel layer. Furthermore, the ability of CV to get out of the microgel layer is impacted in the same manner by the chemical nature of the thiol. In order to differentiate the combined effects from these two factors, Figure 2-15 shows both the pH response kinetics and the release kinetics for etalons modified with 2-OH and 6-OH. Similar plots can be seen in

Figure 2-16 for the remaining thiols. From Figure 2-15(A) and (B), we can see that the

time period required by the blue shift to reach its maximum value, t_A, is shorter than the

time it takes for the UV-vis absorbance to reach its maximum, t_{CV},.This means that from

$t = 0$ to $t = t_A$, the CV release rate is controlled by the ability of the acid to enter the

microgel layer, and the ability of CV to exit the microgel layer, all controlled by the thiol

chemistry. Moreover, after t_{CV}, the acid permeation (and microgel neutralization) is

presumably complete, and the observed CV release is related *only* to its ability to exit the

microgel layer, as dictated by the thiol chemistry. Therefore, we can claim that the time

difference, $\Delta t = t_{CV} - t_A$, illustrates the actual effect of surface grafted alkanethiol

molecules on the CV release process.
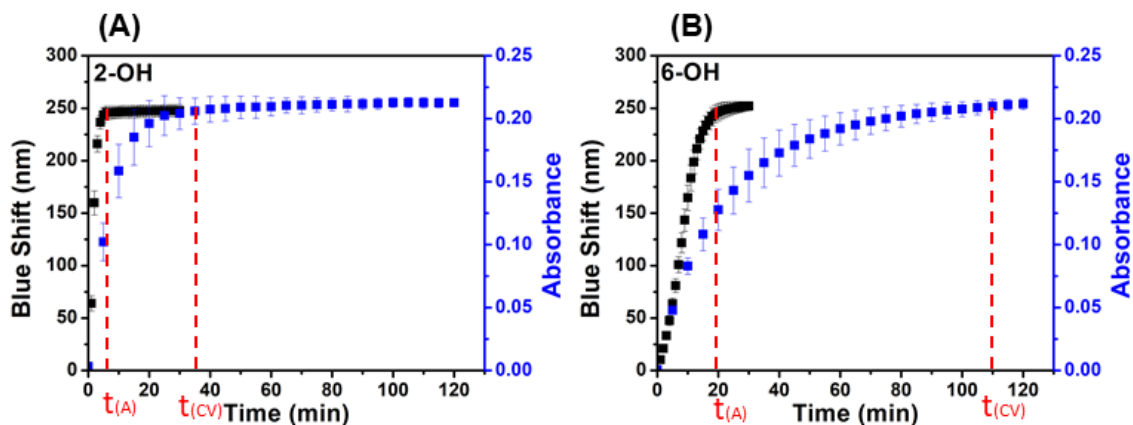
Figure 2-15. (A) Kinetics comparison between the CV release and the reflectance spectrum blue shift of (A) 2-OH and (B) 6-OH modified etalon samples. Black squares: blue shift kinetics (left y-axis, re-drawn from the data in Figure 2-13; blue dots: CV release kinetics (right y-axis, re-drawn from the data in Figure 2-9). The dashed lines are used to determine the time at which each curve reaches its maximum value. (Reprinted with permission from ACS)
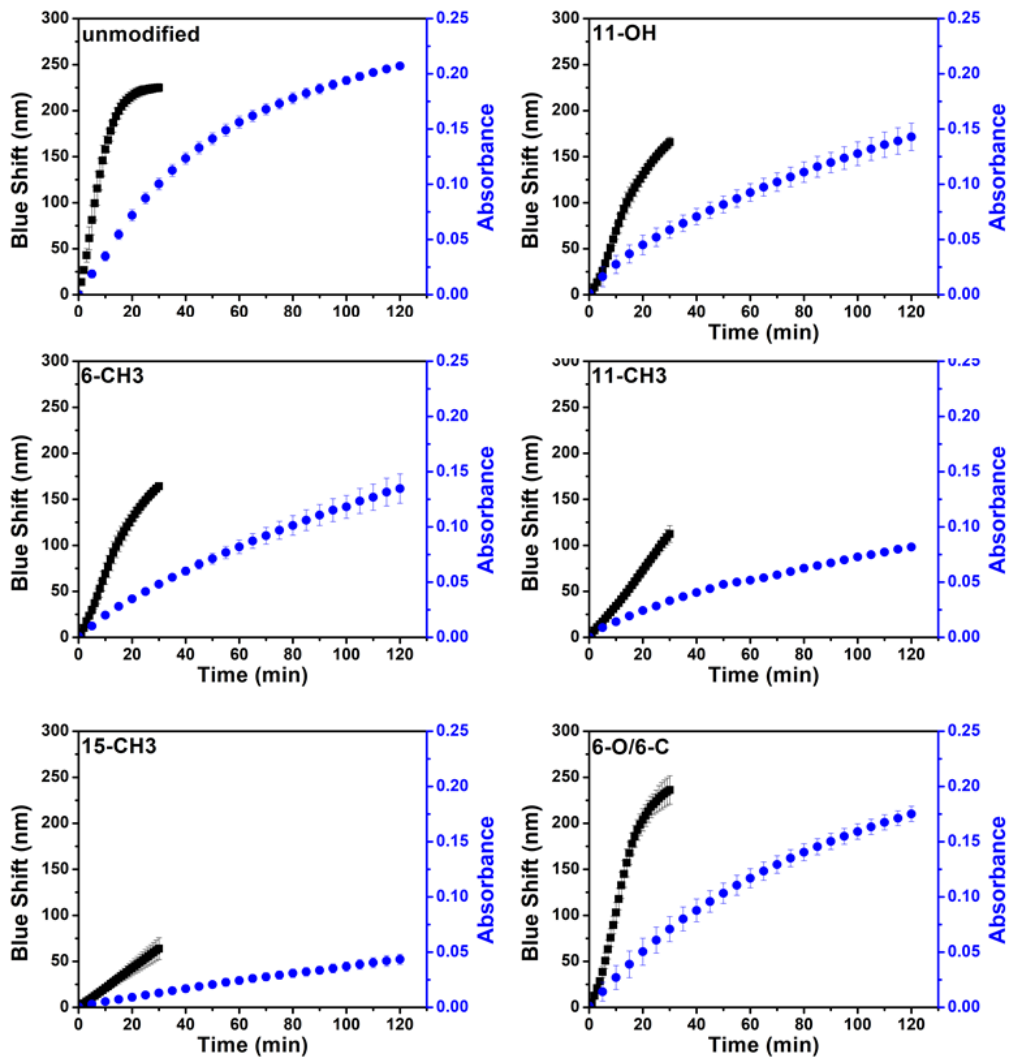
Figure 2-16. Comparison between CV release kinetics and optical reflectance spectrum trough shift kinetics of each kind of modified etalon samples. (Reprinted with permission from ACS)

It can be seen from Figure 2-15 that the 2-OH and 6-OH alkanethiol have different effects on the CV release. Moreover, the effects coming from other alkanethiols also are different from each other. To quantify and compare the effect of different alkanethiols to the CV release process, we need to calculate the Δt values of each alkanethiol, according to their graphs in Figure 2-16. However, there might be some bias in picking the time points where the curves reach the maximum values, as these curves are asymptotic curves.

Therefore, we consider calculating the time difference of the CV release curve and the reflectance spectrum blue shift curves to reach their half maximum value, which is denoted by $\Delta t_{1/2} = t_{1/2CV} - t_{1/2A}$. To determine $t_{1/2CV}$, the CV release rate constants and the theoretical maximum absorbance values in Table 2-1 were used. To determine the $t_{1/2A}$, we use the maximum blue shift of the unmodified sample, which is 224 nm, as a reference maximum blue shift for the various samples, although the 2-OH and 6-OH samples have different maximum blue shifts due to random errors in experiments. This is because the maximum blue shift depends only on the microgel layer thickness and we assume that the surface modification does not affect the swellability of the pNIPAm-based microgel. The determination is made on the basis of the following: if the blue shift kinetics of modified samples go beyond the half of this value (112 nm) within the 30 min of experimental time, we would pick the time point that corresponds to the blue shift around 112 nm; if not, the fitted equations in Figure 2-14 would be used to predict the time point. Therefore, the $\Delta t_{1/2}$ was calculated with $t_{1/2A}$ and $t_{1/2CV}$ and shown in Table 2-3.

Table 2-3. List of Time Periods for Sample Etalons to Reach Their Half Maximum Blue Shift, $t_{1/2A}$, Half Maximum Absorbance, $t_{1/2CV}$; and Time Difference between Them, $\Delta t_{1/2}$

Sample Name	$t_{1/2A}$ (min)	$t_{1/2CV}$ (min)	$\Delta t_{1/2}$ (min)
unmodified	6.5	36.67	30.20
2-OH	1.5	5.11	3.60
6-OH	7.5	15.00	7.50
11-OH	16	54.15	38.15
6-CH$_3$	16.5	81.55	65.10
11-CH$_3$	30	135.91	106.00
15-CH$_3$	53.5*	346.57	311.10
6-O/6-C	10.5	55.90	45.40

[*] value obtained by calculation with fitted equation in Figure 2-14(F)

Surely, the greater the value of $\Delta t_{1/2}$, the more significant is the blocking effect of the alkanethiol molecules on the CV to get out of the etalons. By comparing the $\Delta t_{1/2}$ values of all the alkanethiol modified etalon samples with the unmodified control sample, we find that the short-chain hydrophilic alkanethiols can accelerate the CV release from the surface modified etalon devices, as the hydrophilic surface promotes the permeability of hydrophilic CV molecules. When the alkyl chain length increases to 11-carbon, this positive effect is counteracted by the blocking from a long alkyl chain, which results in a slower CV release process of the 11-OH sample. For the same reason, all the hydrophobic alkanethiol modifications, especially the 15-CH_3 modification, show a strong blocking effect on the CV release, as they make the etalon samples have a greater $\Delta t_{1/2}$ than the unmodified etalon.

Table 2-3 also shows the correlation between the CV release and the etalon's surface hydrophobicity. Among the etalon samples modified with 6-OH, 6-O/6-C, and 6-CH_3 alkanethiols, when the surface hydrophobicity increases as the hydrophobic alkanethiol content increases, the preloaded CV molecules are released by the etalon samples over a longer time period. This can be explained by the reduced permeability of ionic molecules through a hydrophobic layer.

2.4 Conclusions

In this research, the upper Au surface of the etalon device was modified with alkanethiol molecules in different alkyl chain lengths and different hydrophobicity, and this surface modification can change the small cationic molecules release rate from the modified

sample etalon devices. By analyzing the results of CV release kinetics and the reflectance spectrum shifting kinetics, we found that both the CV's diffusion and the acid solution's permeation through the etalon upper Au layer are affected by the surface modification; these two processes can be described by a first-order release model and a zero-order release model, respectively.

In addition, combining two halves of the etalon with different surface modifications could generate a composite etalon device demonstrating a combination of a rapid release with a sustainable release of small molecules. This surface modification approach proposes an efficient and convenient method for precisely tuning the small molecules release process from a pH-responsive reservoir device.

Chapter 3

Controlling and Understanding the Small-Molecule Release Behaviors of Stimuli-responsive Hydrogel–Microgel Composite Materials

3.1 Introduction

Hydrogels have been identified as a promising candidates for the development of drug delivery systems because of their good biocompatibility and physicochemical similarity to the extracellular matrix of cells.[194] Meanwhile, the physical/chemical properties of hydrogels, such as the desired mechanical strength and its affinity to drug molecules, also can be tailored readily by chemical modifications, which broaden the applications in in-vivo drug delivery.[195-197] In the past decade, a number of hydrogel materials have been applied successfully for the controlled release of therapeutic drugs of clinical interest.[198-203]

Some properties that impart hydrogels with compatibility in drug delivery systems, however, limits their performance in practical clinical applications. For example, the use of hydrogels with highly hydrated microstructures that are designed for excellent biocompatibility usually results in rapid release of the entrapped drugs from the hydrogel over a few hours to days. To address this challenge, some approaches, including reduced water content[204], covalent crosslinking,[205] and drug-polymer covalent linkage,[206] were reported to decrease the drug release rate and prolong the release period up to several weeks.

Instead of using hydrogels alone, preparing a hydrogel–microgel composite (HMC), also known as a "plum pudding" hydrogel that has drug-loaded microgel particles embedded in a hydrogel, drew attention to eliminate rapid release and extend the release of the drug due to the additional diffusion barrier to drug release.[194, 207-209] For example, an injectable HMC prepared by Sivakumaran et al. can release bupivacaine sustainably over two months.[209] Such materials were reported also by I. Lynch and co-workers from a drug delivery perspective.[207, 210-212] However, the diffusion behavior of the pre-loaded drug molecules, except for some polymeric molecules (e.g., poly(ethylene) glycol) from the HMC materials, have not been investigated systematically yet under the effect of different components of the hydrogel matrix.

In this study, we prepared a small-molecule-loaded stimuli-responsive-polymer-based HMC and investigated the small-molecule release behavior from the HMC under the effect of different hydrogel matrix compositions. Specifically, poly (*N*-isopropylacrylamide) (pNIPAm)-based microgels were first loaded with cationic crystal violet (CV), and subsequently embedded in a pNIPAm-based hydrogel; we then investigated the pH triggered release from the microgels in the HMC (see Figure 3-1). We also determined that by changing the composition and properties of the pNIPAm-based hydrogel matrix of the HMC, such as crosslinking density, hydrophobicity, and internal charge density, the CV release rate from the HMC can be tuned readily. This study also involved the investigation of the possible mechanisms of controlled release of small cationic molecules in terms of the CV-hydrogel matrix interaction, which provides a potential controlled release modality for drug delivery systems based on the hydrogel–microgel composite materials.

71
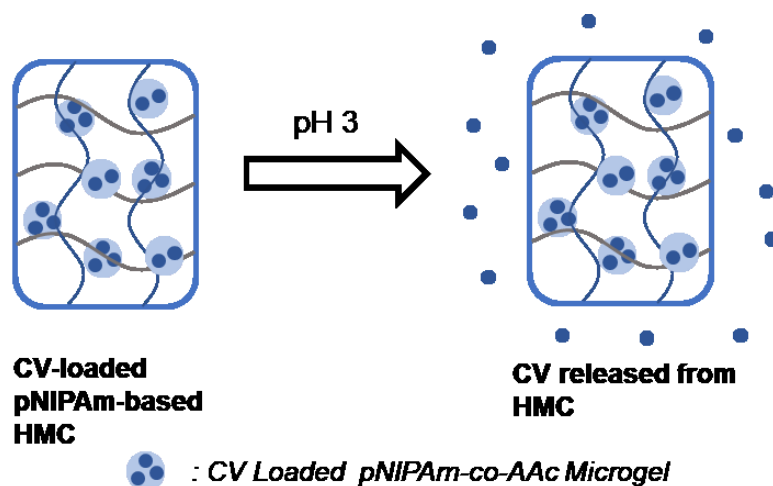
Figure 3-1. Schematic diagram of a pH-responsive CV release process of a CV-loaded pNIPAm-based hydrogel–microgel composite (HMC).

Among several different types of stimuli-responsive hydrogels, the thermally responsive pNIPAm-based hydrogel is one of the most extensively studied hydrogels over the last few decades, as its phase transition temperature, around 32 °C, is close to human body temperature, which encourages researchers to use this material in many physiological applications. pNIPAm-based microgels/nanogels, have drawn much attention as well because they are easily prepared, highly monodispersed, simply functionalized, and non-toxic. In addition to their temperature responsivity, both pNIPAm-based hydrogels and microgels can be tailored to respond to other physical/chemical stimuli, e.g., pH,[213] ionic strength,[214] temperature,[215] light,[216] and electric/magnetic field,[217-218] by copolymerizing with different functional co-monomers. For example, the addition of acrylic acid (AAc) renders the resultant poly (*N*-isopropylacrylamide-*co*-acrylic acid) (pNIPAm-*co*-AAc) microgels pH-responsive. AAc exhibits a pKa of 4.25; therefore, the extent of protonation and deprotonation of the carboxylate group depends on solution pH. Moreover, this protonation–deprotonation process allows the microgel to bind and release cationic

molecules,[177-178] which is the basic mechanism of the pH-responsive small-molecule release in this research.

3.2 Experimental Section

3.2.1 Materials

N-isopropylacrylamide (NIPAm) was purchased from TCI (Portland, Oregon) and purified by recrystallization from hexanes (ACS reagent grade, EMD, Gibbstown, NJ) prior to use. *N,N'*-methylenebisacrylamide (BIS) (99%), acrylic acid (AAc) (99%), ammonium persulfate (APS) (98+%), *N,N,N',N'*-tetramethylethylenediamine (TEMAD) (99%), sodium chloride, sodium hydroxide, crystal violet (CV), *N*-hydroxyethyl acrylamide (HEAm) (97%), 2-acrylamido-2-methyl-1-propanesulfonic acid (AMPS) (99%), benzyl bromide (98%), and vinyl imidazole (99+%) were obtained from Sigma Aldrich (St. Louis, MO) and were used without any treatments. *N*-octyl methacrylate (OMA) was purchased from Polysciences, Inc. Hydrochloric acid was purchased from Caledon Chemicals (Georgetown, Ontario) and was used as received. Water used in the experiments is deionized (DI) water, with a resistivity of 18.2 MΩ cm.

3.2.2 Synthesis of Microgels

pNIPAm-*co*-AAc microgels were prepared via a surfactant-free free radical precipitation polymerization process that was described previously.[219] Briefly, a 3-necked round-bottom flask was fitted with a reflux condenser, nitrogen inlet, and thermometer, and charged with

the monomer solution, a solution of NIPAm (10.5 mmol, 75%mol), and BIS (0.7 mmol, 5%mol) in 99 mL deionized water, previously filtered through a 0.2-μm syringe filter (Thermo Fisher). The solution was bubbled with N_2 gas while stirring and heating to 70 °C over ~1 h. Next, 2.8 mmol of AAc (20%mol) were added to the heated reaction mixture with a micropipette in one aliquot. Then, the reaction was initiated with a solution of APS (0.2 mmol) in 1 mL of DI water. The reaction was allowed to proceed at 70 °C for 4 h under a blanket of N_2 and vigorous stirring. The resulting suspension was filtered through glass wool to remove any large aggregates and distributed into centrifuge tubes for purification. The synthesized microgels were purified via centrifugation at 8000 rpm for about 45 min to form a pellet, followed by removal of the supernatant and re-suspension with DI water. This process was repeated six times to remove any unreacted monomers, and the purified microgel suspensions were re-combined and lyophilized.

3.2.3 Model Drug Loading

To load the model drug, CV, into the pNIPAm-*co*-AAc microgels, 0.5 g of the lyophilized dry pNIPAm-*co*-AAc microgel were suspended into 200 mL of a 2-mg/mL CV solution (pH adjusted to 6.5). The microgels were isolated with centrifugation, and the unbounded CV molecules were washed away by re-suspending the isolated microgels into a solution of pH 6.5 (2 mM NaCl), followed by centrifugation (8000 rpm, 45 min). This centrifugation–resuspension process was carried out six times. Finally, the CV-loaded microgels were collected by removing the supernatant and storing the bottom pellet in a centrifuge tube. The concentration of the CV-loaded microgels, is 0.056 g/mL, and the drug-loading content is 0.0505 mmol per g of dry microgels (2.1 wt%).

3.2.4 Synthesis of 1-Benzyl-3-Vinylimidazolium Bromide

1-Benzyl-3-vinylimidazolium bromide (BVB) was synthesized following a reported process.[220] The liquid benzyl bromide (8.55 g, 50 mmol) was added dropwise into a solution of vinyl imidazole (4.71 g, 50 mmol) in 50 mL of diethyl ether in an ice-water bath, followed by running the reaction for 16 h at room temperature. The crude product was collected with vacuum filtration, yielding a white solid that was washed with diethyl ether. After that, the final product was dried under vacuum overnight to evaporate any remaining solvent. (Yield: 32%) ^{1}H NMR (400 MHz, D_2O, 298 K, δ, ppm): 7.77 (d, 1H, –N^+–**CH**–N–), 7.42–7.56 (m, 7H, aromatics), 7.10 (dd, 1H, –N–**CH**=CH$_2$), 5.78 (dd, 1H, –N–CH=**CH**$_{trans}$), 5.43 (s, 2H, Ph–**CH$_2$**–N^+–), 5.41 (dd, 1H, –N–CH=**CH**$_{cis}$).

3.2.5 Preparation of the CV-loaded Hydrogel–Microgel Composites (HMC)

A 1-mL concentrated CV-loaded microgel solution (0.056 g/mL) or pure microgel solution (0.053 g/mL) was added into a 3-dram vial containing a monomer mixture solution composed of 0.7352 g of NIPAm, 0.0528 g of BIS, 0.01 g of APS, and 3.25 mL of DI water. The mole ratio, monomer composition, and solvent may be varied for the preparation of different HMC samples (Table 3-1). Specifically, 5 mol%, 10 mol%, or 15 mol% of the covalent crosslinker, BIS, was used to prepare the HMCs with different pore sizes; 5 mol% or 10 mol% of OMA or HEAm was used to prepare the HMCs with different hydrophobicity/hydrophilicity; and 1 mol% or 2 mol% of BVB or AMPS was used to prepare the HMCs with different charge density. After degassing with bubbling N_2 for 10

min, the HMC pre-solution was incubated in an ice-water bath for 30 min to pre-cool the reaction solution. To initiate the polymerization reaction, 18.8 µL of TEMED were added into the vial while the solution is stirred vigorously with a magnetic stir bar. The stirring was stopped 30 s after adding TEMED, and the vial was stored in an ice-water bath overnight. The formed HMC material was removed from the vial and cut into the default size, (5, 5, 5) mm, for the following experiments. The cutting of the hydrogels was completed using a razor blade and a small plastic mould that was designed to yield maximal material dimension consistency.

To load CV into those HMCs that were synthesized in an ethanol/water mixture solvent, entrapping the pure microgels, the prepared HMCs should first be soaked in DI water for three days, changing the water twice a day to rinse off all the ethanol. Then, the clean HMCs were cut into (5, 5, 5) mm dimensions and soaked in a 0.5-mg/mL CV solution (pH 6.5) for three days, followed by incubating in a pH 6.5 solution (2 mM NaCl) for another five days, changing the solution every 12 h to rinse off the unbounded CV in the hydrogel matrices.

3.2.6 X-ray Photoelectron Spectroscopy (XPS) Analysis

Lyophilized HMC samples were analyzed with XPS spectrometer (Kratos AXIS Ultra, Al source, source energy: 1486.69 eV). For each sample, survey spectra (pass energy: 160 eV, number of scans: 3, dwell time: 100 ms) and high resolution spectrum for elements C (pass energy: 20 eV, number of scans: 12, dwell time: 200 ms, O (pass energy: 20 eV, number of scans: 12, dwell time: 200 ms), or S (pass energy: 20 eV, number of scans: 80, dwell time: 200 ms)were obtained.

3.2.7 Model Drug Release Experiment

A 25-mL beaker filled with 20 mL of a pH 3 solution (2 mM NaCl) was placed on a hot plate, the solution temperature was maintained at a specific value, and it was stirred continuously at 300 rpm using a magnetic stir bar. The solution was fed through a quartz cuvette into an Agilent 8453 UV-vis spectrophotometer equipped with an 89090A temperature controller and a Peltier heating device, via a peristaltic pump. The experimental setup is shown in Figure A-3. When a HMC sample cube was placed into the solution, the absorbance spectrum of the solution was collected at 3-min intervals.

Table 3-1. List of the Mole Ratios, Monomer Compositions, and Selected Solvents for Different HMC Materials

HMC Samples	NIPAm	BIS	BVB	AMPS	OMA	HEAm	Solvent	Microgels
HMC-5BIS	95%	5%	-	-	-	-	DI water	CV-loaded
HMC-10BIS	90%	10%	-	-	-	-	DI water	CV-loaded
HMC-15BIS	85%	15%	-	-	-	-	DI water	CV-loaded
HMC-1AMPS	94%	5%	-	1%	-	-	DI water	CV-loaded
HMC-2AMPS	93%	5%	-	2%	-	-	DI water	CV-loaded
HMC-1BVB	94%	5%	1%	-	-	-	DI water	CV-loaded
HMC-2BVB	93%	5%	2%	-	-	-	DI water	CV-loaded
HMC-5BISa	95%	5%	-	-	0%	-	Ethanol : Water 7:3 (v/v)	Pure
HMC-5OMA	90%	5%	-	-	5%	-	Ethanol : Water = 7:3 (v/v)	Pure
HMC-10OMA	85%	5%	-	-	10%	-	Ethanol : Water = 7:3 (v/v)	Pure
HMC-5HEAm	90%	5%	-	-	-	5%	Ethanol : Water = 7:3 (v/v)	Pure
HMC-10HEAm	85%	5%	-	-	-	10%	Ethanol : Water = 7:3 (v/v)	Pure

3.2.8 Gel Swelling

The swelling ratios of the HMC samples were determined by calculating the amount of water that the HMC sample absorbs per unit mass of the dry HMC material according to Equation 3-1

$$Swelling\ Ratio = \frac{Wt_{\text{wet}} - Wt_{\text{dry}}}{Wt_{\text{dry}}} \qquad (3\text{-}1)$$

where Wt_{wet} is the mass of the fully swollen gel and Wt_{dry} is the mass of the dry gel.[215]

To determine the swelling ratios of the HMC-5BISa, HMC-5OMA, and HMC-10OMA, three samples of each HMC were used for the mass measurements, and their average swelling ratios with the standard deviations are reported.

3.2.9 CV Diffusion Racing Experiment

Hydrogels (without adding the microgels) with different compositions of co-monomers were prepared in glass tubes in a cylindrical shape. The preparation procedures are the same as the HMC preparation steps. When the hydrogels were formed in the glass tubes, they were immersed in excess DI water for three days to remove the unreacted monomers or ethanol. To run the diffusion racing experiment, the fully swollen hydrogel cylinders were placed in parallel in a plastic Petri dish lid that was filled with 8 mL of 0.5-mg/mL CV solution. Then, CV was allowed to diffuse along the hydrogel cylinders, and the diffusion speed in different hydrogel samples was determined by comparing the height of the colored region from the photographs. Photographs were captured at $t = 0$, $t = 24$ h, and $t = 48$ h. During the whole experiment, the hydrogel samples and the CV solution container are covered by a beaker to minimize water evaporation and possible ambient interference.

3.3 Characterization

In this research, different amounts of crosslinker and different kinds of co-monomers were used to control the small-molecule release rates of the model drug-loaded HMC materials and investigate the relationship between the release rate and the properties of the hydrogel matrix. To characterize the properties and compositions of the resultant HMC materials, a variety of methods and techniques were used, including swelling ratio calculation, Scanning Electron Microscope (SEM), Fourier Transform Infrared Spectroscopy (FT-IR), Differential Scanning Calorimetry (DSC), and X-ray Photoelectron Spectroscopy (XPS).

Figure 3-2 shows the SEM images of the cross sections of the HMCs with different amounts of BIS. The SEM samples were prepared by lyophilizing the HMC gel strips that were peeled off from a bulk gel material by a tweezer followed by soaking in DI water at room temperature until the solvation state equilibrated. The gel strip was ripped off from the bulk gel without cutting to avoid the any change in morphology that can occur from the cutting. To prepare the sample for SEM imaging, the fully hydrated gel samples were frozen with liquid nitrogen to fix their micro structures, and then freeze dried with a lyophilizer. It is obvious that all the HMC samples demonstrate highly porous internal structures and that the pore size decreases as more crosslinker was used in the HMC preparation.
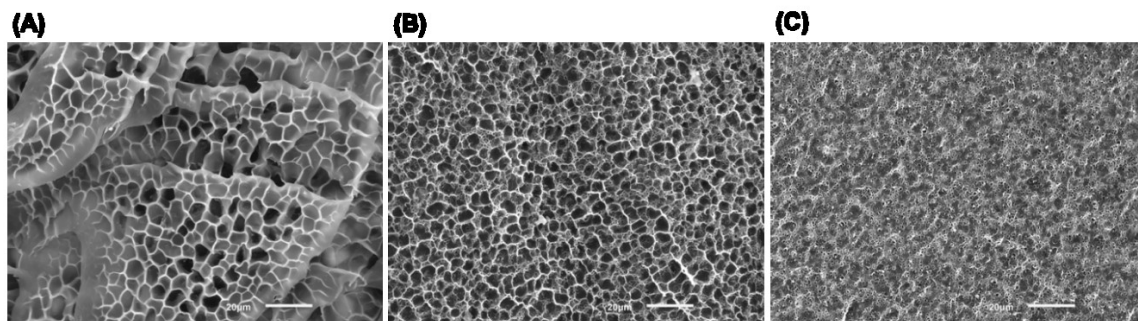
Figure 3-2. Scanning electron microscope (SEM) images of the HMC with different amount of crosslinkers. (A) HMC-5BIS, (B) HMC-10BIS, and (C) HMC-15BIS. (Scale bar = 20 μm.)

The OMA is a co-monomer with a non-polar alkyl chain, therefore, it was incorporated into the hydrogel matrix of the HMC to increase the hydrophobicity of the material. It was reported that the swellability of hydrogel is related to the hydrophobicity of the material.[221] Thus, the swelling ratios of the HMCs with the hydrophobic co-monomers were calculated to quantify their swellability in DI water. Figure 3-3(A) compares the average swelling ratios with the standard deviations of a control HMC sample and OMA-copolymerized HMC samples. The significant difference on their swellability is believed to be attributed to the different hydrophobicity of the polymer materials. In contrast, copolymerizing HEAm that has a hydroxyl group attached in the hydrogel matrix makes the HMCs more hydrophilic. There are studies that show the correlation between the hydrophilicity and LCST of the temperature-responsive polymers. That is, incorporating hydrophilic groups can make the materials more hydrophilic and increases their LCST.[34-35] Thus, we conducted a thermal analysis on the HEAm-copolymerized HMC samples with DSC. Figure 3-3(B) is the graph of the thermal analysis results of the HMC-5BISa, HMC-5HEAm, and HMC-10HEAm samples. It shows that the phase transition temperature of the samples increases from 38.86 °C to 46.71 °C, revealing that the

hydrophobicity of the HMCs increases as the mole percentage of the HEAm in the samples

increases.
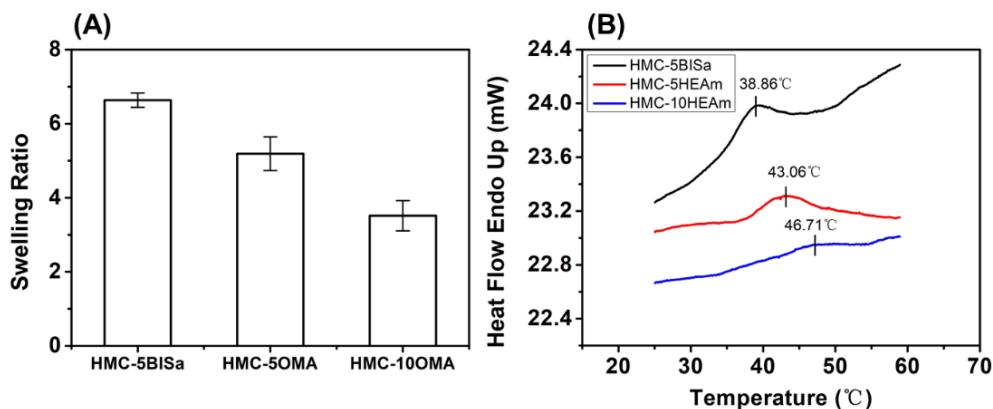
Figure 3-3. (A) A bar chart for the swelling ratios of the OMA-incorporated HMC samples and a control sample. (B) Thermal analysis results obtained with DSC of the HEAm-incorporated HMC samples and a control sample. (The phase transition peaks in the thermal analysis graphs were obtained by Gaussian curve fitting.)

In addition, the presence of OMA and HEAm in the resulting HMCs was illustrated by the XPS analysis. Due to the fact that a C–O bond exists only in the OMA monomer and HEAm monomer and not in the NIPAm or BIS, the high resolution XPS spectrum of the O for the HMC samples were obtained by an XPS imaging spectrometer (Kratos AXIS Ultra). As shown in Figure 3-4, the interpretation of the O 1s XPS spectrum illustrates that when higher mole percentages of OMA or HEAm were added into the hydrogel pre-solutions, the more intensive O 1s peaks corresponding to the C–O bonding environment could be observed in the XPS spectrum.
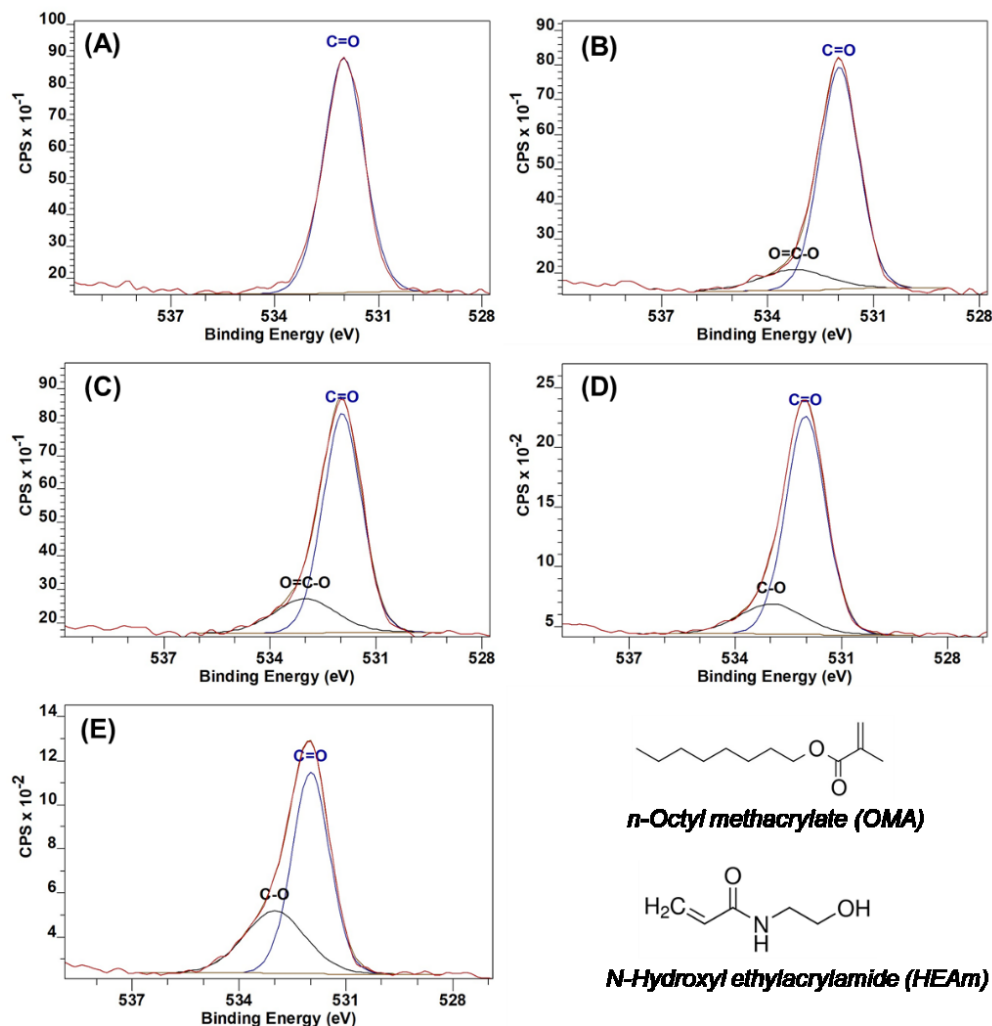
Figure 3-4. O 1s High resolution XPS spectrum and interpretation of (A) HMC-5BISa, (B) HMC-5OMA, (C) HMC-10OMA, (D) HMC-5HEAm, and (E) HMC-10HEAm samples.The O 1s signal peaks in the XPS sprectra were interpreted into multiple peaks representing the O in different bonding environments.

The AMPS monomer was used to introduce negative charges into the HMC, as the sulfonic acid group with pKa ~1.92 can be deprotonated in the solutions with pH > pKa. Since AMPS has S, it makes the HMC-2AMPS show a strong peak on the S 2p high resolution XPS spectrum (Figure 3-5(A)). On the other hand, the BVB monomer, a quaternary ammonium salt, has a permanent positive charge and was used to introduce positive charges into the HMC. In addition, the aromatic rings in the structure of the BVB

molecule generate a weak broad peak around 2100 cm^{-1} in the FTIR spectrum (Figure 3-5(B)), strongly suggesting the presence of BVB in the HMC-2BVB sample.
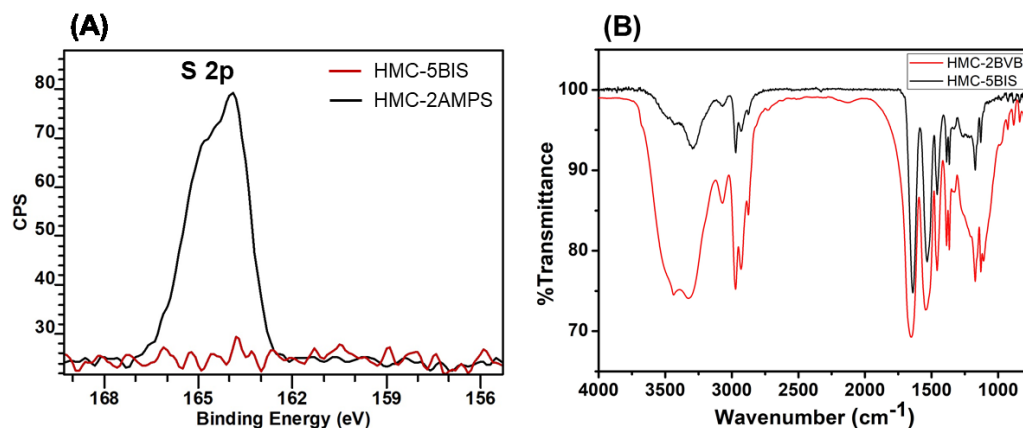
Figure 3-5. (A) S 2p high resolution XPS spectrum of the HMC-5BIS and HMC-2AMPS samples. (B) FTIR spectrum of the HMC-5BIS and HMC-2BVB samples.

3.4 Results and Discussion

3.4.1 Release Mechanism of the CV-loaded HMC

As mentioned above, pNIPAm-*co*-AAc microgels entrapped in HMC are pH-responsive and able to release pre-loaded CV molecules at low pH, and the HMC is believed to release CV in a similar pH-responsive fashion. As shown in previous publications,[93, 177] the UV-vis absorbance spectrum of CV in aqueous solution has a significant absorbance peak at 590 nm, thus, we monitored the solution absorbance value at the wavelength of 590 nm to track the CV release of the HMC samples. In addition, all of the HMC samples prepared for the CV release experiments are cut into (5, 5, 5) mm dimensions to exclude the effect of the sample volume on the CV release kinetics. Figure 3-6(B) shows that when a cubic sample of the HMC-5BIS is exposed in a pH 3 solution (2 mM NaCl), the CV was released much faster than that in a pH 6.5 solution (2 mM NaCl), suggesting that the release of CV

molecules by HMC-5BIS is strongly pH-dependent. Note that the total amount of loaded

CV cannot be released completely within the experimental period, 1 h, which is the reason

for the continuous absorbance increase at the end of the experiments.
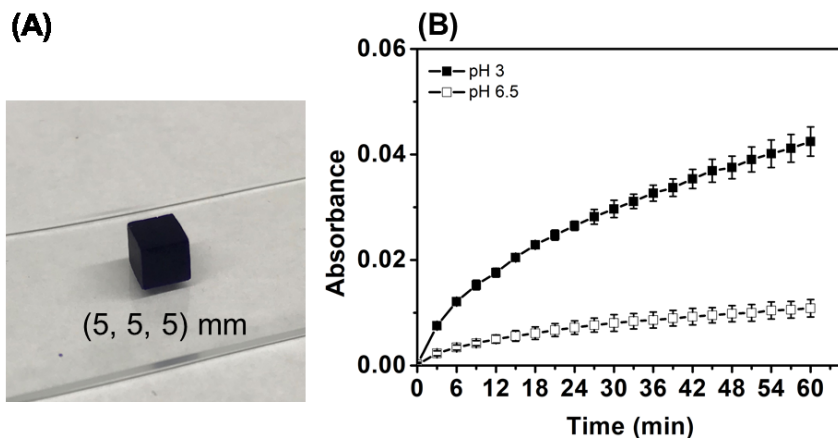
Figure 3-6. (A) A photograph of a HMC-5BIS sample cube with a (5, 5, 5) mm dimension. (B)
Absorbance values at 590 nm as a function of time for the HMC-5BIS sample cubes in a pH 3 and
pH 6.5 solution. (Error bars are the standard deviations of three replicate experiments, and the solid
curve is a connection of data points.)

We also conducted long-term CV release experiments to investigate the CV release

mechanism of the HMC-5BIS for a period of over one hundred hours. Specifically, a HMC-

5BIS sample cube was exposed in a 20-mL pH 3 solution (2 mM NaCl), and its CV release

profile over 73 h was monitored and recorded by a UV-vis spectrometer every 30 min.

Next, the HMC sample cube was removed manually from the solution, and the data

collection was stopped. Then, the sample cube was re-exposed in a fresh pH 3 solution,

allowing the sample to release CV in the new solution and absorbance values to be

collected. After another 30 h, the same process was repeated. Figure 3-7(A) is the CV

release profiles of the HMC sample cube in the three release experiment periods, and its x-

axis indicates the cumulative CV release time. From this figure, we can find that the sample

releases CV at a gradually decreasing rate during the first release period (0–73 h, position a to b), as the slope of the curve is getting smaller as a function of time. Note that the pH value of the final solution after the first 73-h release experiment (position b) is 3.11, which suggests that the decreasing of the CV release rate is unlikely to be caused by the insignificant consumption of the acid in the solution. When the HMC sample cube was re-exposed in a new pH 3 solution, the initial CV release rate (position c) recovered at a faster rate than that at the end of previous release period (position b). According to the nature of the Fickian diffusion, we believe that this release rate recovery is attributed to the increased CV concentration gradient between the inside of the HMC sample and the solution when the sample was transferred from the old high-concentrated solution to the new low-concentrated solution.

In the third release period, t = 114 h to end, the sample was re-exposed in a fresh 20-mL pH 3 solution. As we can see from Figure 3-7(A), at the beginning of this period (position e), the release rate recovery is no longer obvious, as the CV concentration in the HMC sample is very low after the long-term release. Meanwhile, by comparing the HMC sample after the long-term release with a virgin sample, the peripheral section of the used sample shows a more diluted color (Figure 3-7(B)).
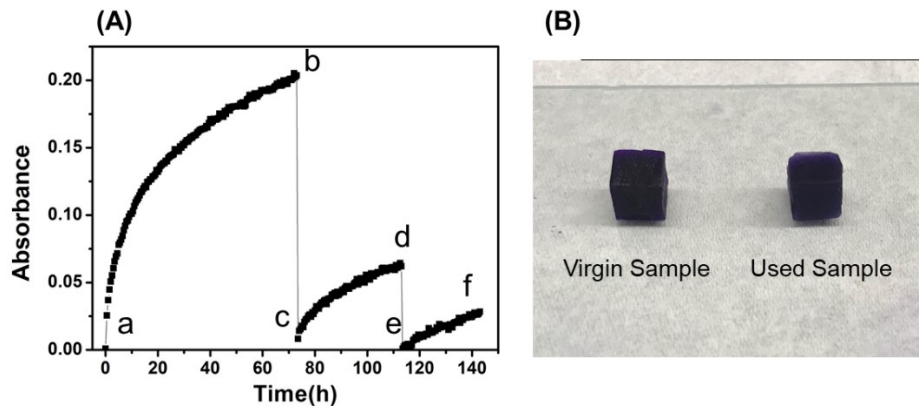
Figure 3-7. (A) Long-term CV release profile of a HMC-5BIS sample. The sample maintained its original shape during the release period of 113 h to 143 h. (The solid curve is a connection of data points.) (B) Comparison between the HMC-5BIS samples before and after a long-term CV release experiment.

To investigate the CV distribution in a used sample, another long-term release experiment was conducted. In this experiment, a HMC sample cube was allowed to release CV in the pH 3 solution (2 mM NaCl) for the first two periods (a' to b' and c' to d') that are same as the previous experiment, and the CV release profile is plotted in Figure 3-8(A). However, before the third release period, the sample was removed from the pH 3 solution and cut into two equal halves to expose the central section of the HMC sample cube. Then, these two halves were put into a fresh pH 3 solution to complete the third CV release experiment (position e' to f'). Figure 3-8(B) shows the magnified CV release profiles over the third release period of the two experiments mentioned above for a comparison of the CV release profiles in the third period of the uncut HMC cube and the HMC cube in two halves. It can be seen that when the HMC sample cube is split in two halves, it can release CV at a faster rate than the sample maintained in its original dimension due to the exposure of the central section. Therefore, we infer that the central section of a used HMC sample

cube has a higher CV concentration than the peripheral section and that the CV release process can cause an inhomogeneous CV distribution in the HMC sample cube.
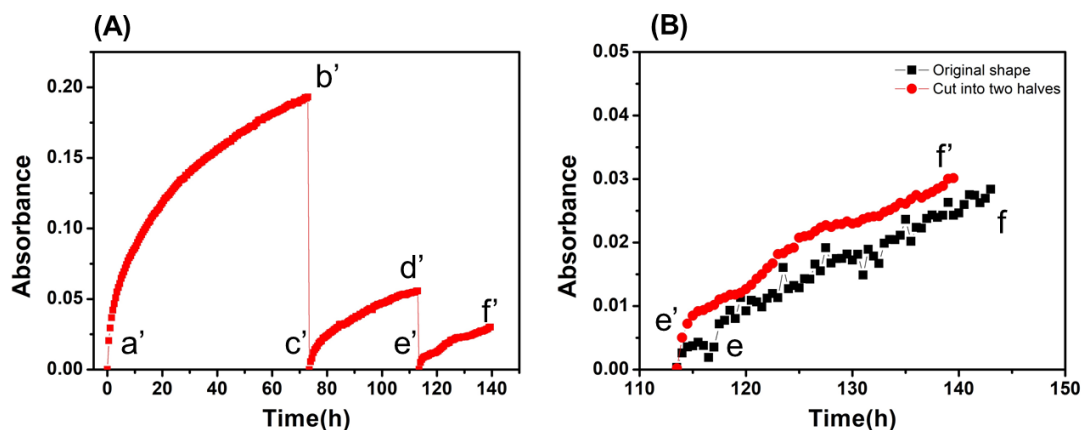
Figure 3-8. (A) Long-term CV release profile of a HMC-5BIS sample. The sample was split into two halves during the release period of 113 h to 143 h. (The solid curve is connection of data points.) (B) Magnified CV release profiles over the third release period of the HMC-5BIS samples between the original cubic shape and the one split in two halves.

Based on this information, we propose that the mechanism of the CV release from the HMC is a Fickian diffusion from the inside to the outside of the HMC. Specifically, when the acid triggers the CV release from the peripheral section, the homogeneous concentration of CV in the material is disrupted, and the positions that are further away from the surface always have a higher CV concentration than the positions that are closer to the surface; this generates a continuous concentration gradient that drives the CV's diffusion.

3.4.2 CV Release Rate Control via Variation in HMC Composition

In previous sections, we discussed the CV release mechanism of the HMC based on the long-term release experiments. Interestingly, the CV release rate from the HMC also was

determined to be related to the composition of the hydrogel matrix of the HMC. In this section, we will discuss the method that can control the CV release rate of the HMC by co-polymerizing different functional monomers, including crosslinkers, hydrophobic/hydrophilic monomers, or ionic monomers, in the hydrogel matrix.

3.4.2.1 CV Release Rate Controlled by Crosslinking Density of the Hydrogel Matrix

CV release was assayed on a series of CV-loaded HMCs with different percentages of crosslinker, BIS, using a pH 3 solution (2 mM NaCl) as the release medium. To determine the effect of the hydrogel matrix crosslinker density on the CV release rate, we monitored the CV release kinetics from the CV-loaded HMC with 5%, 10% and 15% of BIS. Figure 3-9 shows that as the crosslinker density increases, the HMC releases CV at a slower rate, which likely is attributed to the smaller pores in the internal structure of the hydrogel with more crosslinker, as shown in Figure 3-2. This is because the porous structure of hydrogels provides the diffusive pathways to the CV molecules, and a smaller pore size inhibits this diffusion process.
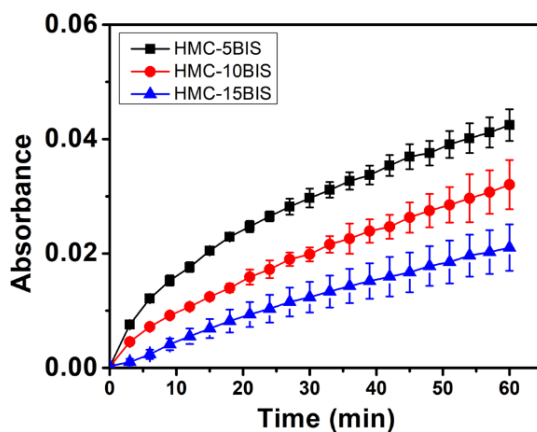
Figure 3-9. CV release profiles of the CV-loaded HMC with different crosslinking densities.

3.4.2.2 CV Release Rate Controlled by the Internal Charge Density of the Hydrogel Matrix

For this study, the internal charge and charge density of the CV-loaded HMC hydrogel matrices were tuned by incorporating a cationic monomer, BVB, and/or an anionic monomer, AMPS. When the HMC samples with different charge properties and densities are exposed in a pH 3 solution (2 mM NaCl), their CV release kinetics demonstrate a strong dependency on the charge properties. As shown in Figure 3-10, a positively charged hydrogel matrix accelerates the CV release, while a negatively charged hydrogel matrix slows down the release of CV. Meanwhile, the CV release rate is related also to the charge density. That is, the HMC containing 2 mol% of positive charges releases CV faster than the one containing 1 mol% of positive charges, and 2 mol% of negative charges in the hydrogel matrix can inhibit the CV release almost completely.
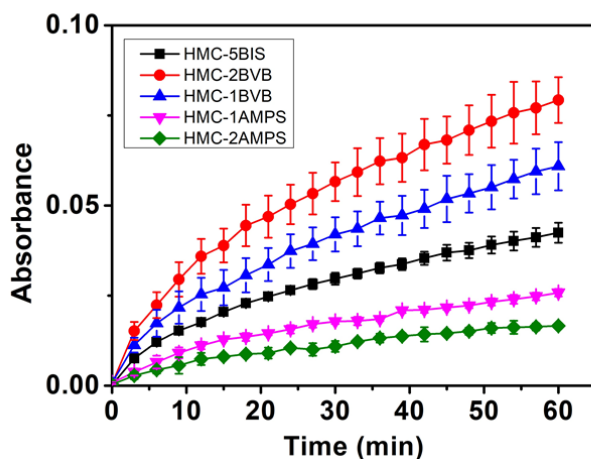
Figure 3-10. CV release profiles of the CV-loaded HMC with different internal charge properties and densities. (Error bars are the standard deviations of three replicate experiments, and the solid curves are connections of data points.)

We believe that this correlation between the internal charge and the CV release behavior of a HMC is attributed to the electrostatic interaction between CV molecules and the polyelectrolyte in the hydrogel matrix.[222] Specifically, when the positively charged CV molecules are released by microgels and diffuse through a hydrogel matrix, a positively charged hydrogel matrix, as shown in Figure 3-11(A), applies a electrostatic repulsion to the CV, which drives CV to move in a faster speed in the matrix. In contrast, when the hydrogel matrix contains negative charges, the electrostatic attraction retains the CV molecules and results in a slow diffusion of CV in the hydrogel matrix (Figure 3-11B).
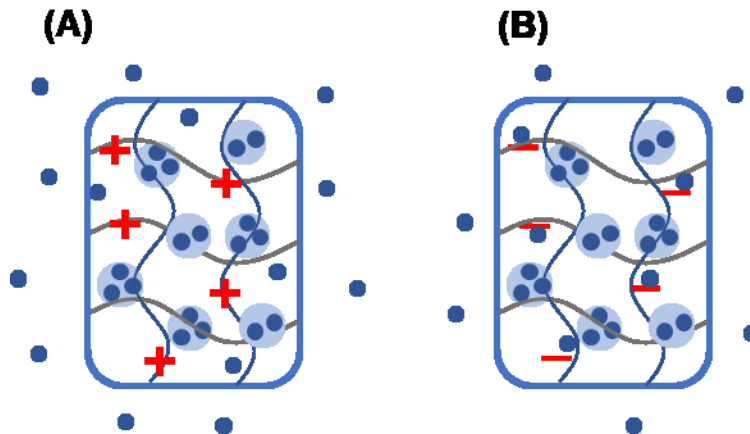
Figure 3-11. Schematic diagram of CV released by HMC with positively charged hydrogel matrix (A) and negatively charged hydrogel matrix.

To compare the CV diffusion speed in the hydrogel matrix with different charge properties and densities, a CV diffusion racing experiment was carried out. Briefly, three pNIPAm-based hydrogels, which contain 2 mol% of BVB, 2 mol% of AMPS, and 5 mol% of BIS, respectively, were prepared in a cylindrical shape. The hydrogel compositions and preparation steps of these three hydrogels are the same as the HMC materials listed in Table 1. The rod-shape hydrogels were put into a Petri dish containing a CV solution perpendicularly, and after a certain amount of time, the height of the violet color showing

on the hydrogels cylinders illustrates the diffusion speed of CV in the materials. As shown in Figure 3-12, CV diffuses in the positively charged hydrogel faster than in the neutral hydrogel, which diffuses faster than in the negatively charged hydrogel due to the electrostatic interaction; this supports our previous explanations.
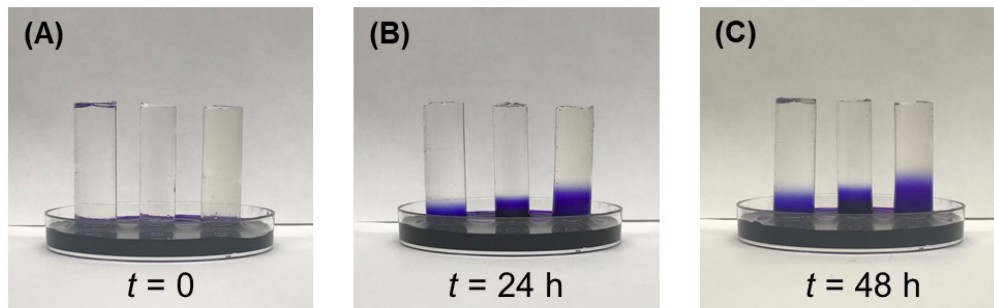
Figure 3-12. Photographs of cylindrical hydrogels in the CV diffusion racing experiment. In each photograph: left, pNIPAm-2%AMPS hydrogel; middle, pNIPAm-5%BIS hydrogel; and right, pNIPAm-5%BVB hydrogel.

3.3.2.3 CV Release Rate Controlled by Hydrophobicity of the Hydrogel Matrix

In this study, HMCs with different hydrogel matrices varying in hydrophobicity were prepared by copolymerizing different mole percentages of OMA or HEAm monomers in an ethanol/water mixture solvent, followed by loading CV into the HMC by immersing HMC sample cubes into a CV solution. Figure 3-13 (A) and (B) show the CV release kinetics from the HMC samples with different hydrophobicity. From these two graphs, we can see that the CV release rate is dependent on the hydrophobicity of the material. That is, more hydrophobic HMCs release CV faster than more hydrophilic HMCs.
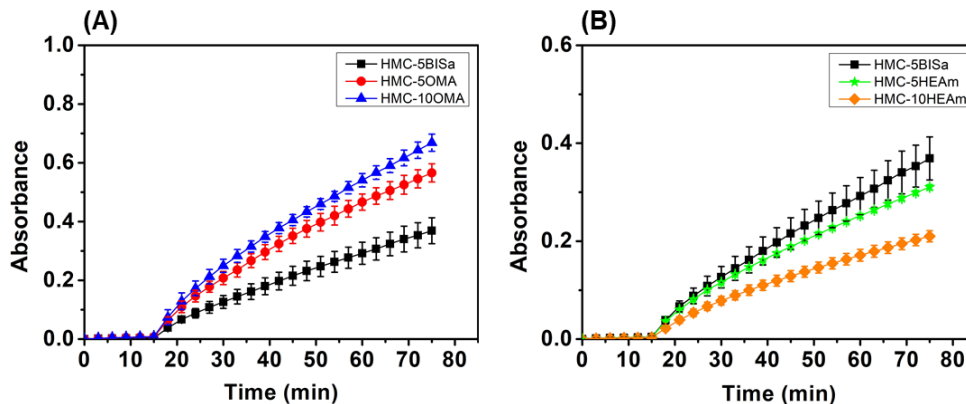
Figure 3-13. CV release profiles of CV-loaded HMCs with different hydrophobicity. The initial solution pH was 6.5, and the solution pH was changed to 3 at t = 15 min by adding one aliquot of concentrated hydrochloric acid. (Error bars are the standard deviations of three replicate experiments, and the solid curves are connections of data points.)

To investigate the effect of the hydrogel matrix on the CV release, another CV diffusion racing experiment was conducted. Briefly, three pNIPAm-based hydrogels, which contain 10 mol% of OMA, 10 mol% of HEAm, and 5 mol% of BIS, respectively, were prepared in a cylindrical shape and put into a Petri dish containing a CV solution perpendicularly. After a certain amount of time, the height of the violet color showing on the cylindrical hydrogels illustrates the diffusion speed of CV in the materials. Figure 3-14 shows that CV diffuses fastest in the most hydrophilic hydrogel and slowest in the most hydrophobic hydrogel, while the diffusion speed is intermediate in the pNIPAm hydrogel containing none of the other monomers. Interestingly, by comparing the CV diffusion racing experiment results and the CV release experiment results, we find that the slowest CV diffusion speed in the most hydrophobic hydrogel cannot explain the fastest release of CV by the most hydrophobic HMC. A possible mechanism that can explain these two incompatible phenomena is that the hydrophilic molecule, CV, has a higher affinity for a more hydrophilic environment than for a more hydrophobic environment. In the CV release

experiments, CV has a higher affinity for the HMC-HEAm materials; thus, the materials have a stronger retention to the diffusion of CV and result in slower release rates. On the other hand, in the CV diffusion racing experiment, due to the lower affinity between the CV and the pNIPAm-10%OMA hydrogel, CV molecules would not like to diffuse from a hydrophilic aqueous environment into a relatively hydrophobic hydrogel material. Thus, it demonstrates a slower diffusion speed.
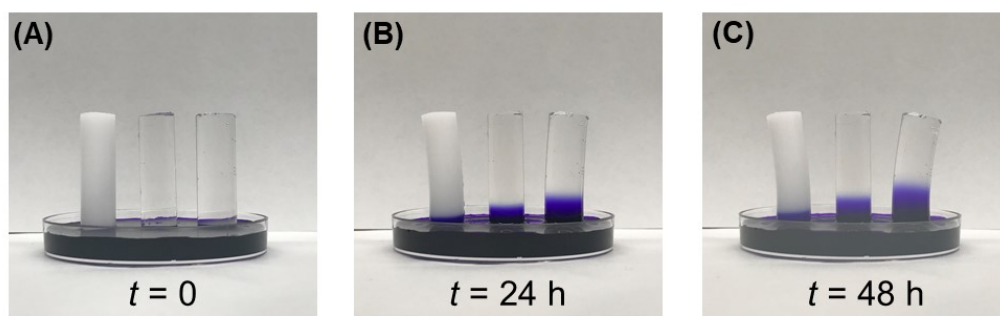
Figure 3-14. Photographs of the pNIPAm-based hydrogels with different hydrophobicity in the CV diffusion racing experiment captured at $t = 0$, $t = 24$ h, and $t = 48$ h. In each photograph: left, pNIPAm-10%OMA hydrogel; middle, pNIPAm-5%BIS hydrogel; and right, pNIPAm-10%HEAm hydrogel.

3.4 Conclusions

In this study, a CV-loaded pNIPAm-based HMC was prepared by entrapping CV-loaded pNIPAm-*co*-AAc microgels in a pNIPAm-based hydrogel. The CV release rate of the HMC material can be controlled by tuning the composition of the hydrogel matrix, which results in the property change of the material, including crosslinking density, internal charge density, and hydrophobicity. By investigating the mechanisms of the CV controlled release in each kind of HMC material, experimental results show that the CV release rate is dependent on the interactions between CV molecules and the polymeric hydrogel material.

Chapter 4

Multi-Drug Controlled Release by Stimuli-responsive Hydrogel–Microgel Composite Materials

4.1 Introduction

In 1965, Frei et al. reported that the treatment of children's acute leukemia is therapeutically more efficient if a combined therapy consisting of two cytotoxic agents was applied, rather than a monotherapy.[223-224] Since then, to improve the clinical efficiency of oncology treatment, developing of the clinical drug combination therapy has been pursued widely. For example, one of the most effective treatment strategies for metastatic breast cancer is a drug combination of doxorubicin, taxane, and platinum-derivatives.[225] In addition, combination therapy for cancer treatment has been reported to reduce the toxicity of individual drugs and suppress drug resistance.[226] For this reason, developing dual/multi-drug delivery systems with potential applications in combination therapy for treatment of diseases has drawn much attention in the past decades.

Although many multi-drug delivery systems based on a variety of materials have been reported, including micro/nano particle-based,[227-228] vesicle-based,[229-230] hydrogel-based,[231-233] and micro-needle-based,[234] the individually controlled release of each drug component is still challenging for many reported multi-drug delivery systems. In this paper, we report a stimuli-responsive hydrogel–microgel composite (HMC) material that can control the release of each preloaded model drug component individually. More

importantly, the combination of released drug molecules can be varied simply by incorporating different drug-loaded microgels; this demonstrates the outstanding flexibility of this type of drug delivery system in the design of combined therapy.

Hydrogels refer to a group of hydrophilic polymeric networks containing a large amount of water (typically 80 to 99%). Over the past decades, they have been investigated as a versatile material in various applications, such as drug delivery,[235-237] tissue engineering,[56-57] self-healable material,[238-239] water remediation,[240-241] bio-sensing,[242-243] etc. In particular, due to the high-water content, hydrogels have structures homologous to biological tissues, outstanding biocompatibility, as well as the capability of entrapping hydrophilic drug molecules, essentially making it an appealing type of drug delivery platform.

Stimuli-responsive hydrogels, also named "smart" hydrogels, whose physical and chemical properties can undergo significant changes in response to the external stimuli, such as pH,[7, 39] ionic strength,[10] temperature,[5, 174] light,[12, 175] and electric/magnetic field[14-15, 244], draw much attention due to their tremendous applications in on-demand drug release[5, 245], smart coating,[246] bio-sensing,[187] artificial muscles,[247] and actuators.[168]

Among a number of different types of stimuli-responsive hydrogels, the temperature- responsive poly *N*-isopropylacrylamide (pNIPAm) based hydrogel has been one of the most extensively studied hydrogels during the last few decades. Its phase transition temperature, also known as the lower critical solution temperature (LCST), around 32.5 °C, is close to the human physiological temperature, encouraging researchers to apply this material onto many physiological applications. The pNIPAm-based hydrogel micro/nano particles, called microgel/nanogels depending on their size, also draw much

attention because they are easily-prepared, highly-monodispersed, simply-functionalized, and non-cytotoxic. In addition to its temperature-responsivity, the pNIPAm-based hydrogel and/or microgel can be tailored to respond to other physical/chemical stimuli, like those mentioned above, by copolymerizing the co-monomers with different functional groups. For example, a well-known pH-responsive pNIPAm-based microgel is pNIPAm-*co*-acrylic acid (pNIPAm-*co*-AAc) microgel, which is prepared by copolymerizing acrylic acid (AAc) with the NIPAm monomer. AAc exhibits a pKa of 4.25, therefore, pNIPAm-*co*-AAc microgels have negative charges at pH > 4.25, with deprotonated AAc groups, while the negative charges can be neutralized at pH < 4.25.

In a similar manner, another two kinds of pNIPAm-based microgels, pNIPAm-*co*-(3-aminopropyl methylacryamide hydrochloride) (pNIPAm-*co*-APMAH) microgels and pNIPAm-*co*-(3-(acrylamido) phenylboronic acid) (pNIPAM-*co*-APBA) microgels, demonstrate their pH-responsivity over different pH ranges due to the pKa of the primary amine group and the phenylboronic acid group, 10.6 and 8.5, respectively. Specifically, the primary amine group is positively charged when the pH < 10.6, while this charge could be neutralized in more basic conditions, such as pH >10.6. On the other hand, the non-charged phenylboronic acid group tends to bind with a hydroxide ion and is negatively charged when the pH > 8.5, but this charge could be diminished when the pH < 8.5 (Scheme 4-1). Therefore, the ionization-neutralization process of these pH-responsive pNIPAm-based microgels allow them to bind and release charged molecules with the variation of solution pH.
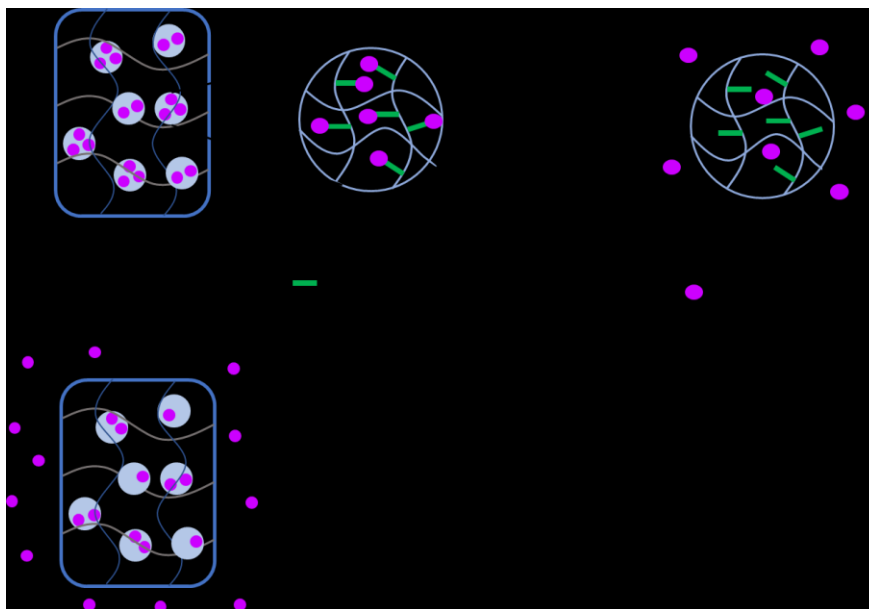
Scheme 4-1. Schematic demonstration of the releasing process of pre-loaded model drug molecules, CV, AY, and RhB, from the model drug-loaded microgel and HMC due to the pH responsivity.

In this research, model drug-loaded pH-responsive pNIPAm-based microgels were entrapped in the pNIPAm-based hydrogel to form the HMC material that can release the pre-loaded drug molecules in a pH-triggered fashion. Briefly, three different charged model drug molecules, crystal violet (CV), acid yellow 17 (AY), and rhodamine B (RhB), are loaded electrostatically into the pNIPAm-*co*-AAc microgels, pNIPAm-*co*-APMAH microgels, and pNIPAm-*co*-APBA microgels, respectively. Then, one or a combination of two drug-loaded microgels are suspended in a NIPAm monomer solution before the initiation of the polymerization reaction, which results in HMC that has drug-loaded microgels in a pNIPAm-based hydrogel. We investigated the drug release behaviors of the HMC under different conditions and determined its ability to control the release of multiple drug molecules individually when different drug-loaded microgels are entrapped in a single HMC.

4.2 Experimental Section

4.2.1 Materials

N-isopropylacrylamide (NIPAm) was purchased from TCI (Portland, Oregon) and purified by recrystallization from hexanes (ACS reagent grade, EMD, Gibbstown, NJ) prior to use. *N,N'*-methylenebisacrylamide (BIS) (99%), acrylic acid (AAc) (99%), 3-aminopropyl methylacryamide hydrochloride (APMAH), 3-(acrylamido) phenylboronic acid (APBA) ammonium persulfate (APS) (98+%), *N,N,N',N'*-tetramethylethylenediamine (TEMED) (99%), sodium chloride, sodium hydroxide, crystal violet, acid yellow 17 (60%+) and rhodamine B (95%+) were obtained from Sigma Aldrich (St. Louis, MO) and were used without any treatments. Hydrochloric acid was purchased from Caledon Chemicals (Georgetown, Ontario) and was used as received. Water used in the experiments is deionized (DI) water with a resistivity of 18.2 MΩ•cm.

4.2.2 Synthesis of Microgels

The pNIPAm-*co*-AAc microgel was prepared with a surfactant-free free radical precipitation polymerization process that was described previously.[92, 219] Briefly, a 3-necked round-bottom flask was fitted with a reflux condenser, nitrogen inlet, and thermometer, and charged with the monomer solution, a solution of NIPAm (10.5 mmol, 75 %mol), and BIS (0.7 mmol, 5 %mol) in 99 mL of deionized water, previously filtered through a 0.2-μm syringe filter (Thermo Fisher). The solution was bubbled with N_2 while stirring and allowed to heat to 70 °C over ~1 h. Next, 2.8 mmol of AAc (20 %mol) were added to the heated reaction mixture with a micropipette in one aliquot. Then, the reaction

was initiated with a solution of APS (0.2 mmol) in 1 mL of DI water. The reaction was allowed to proceed at 70 °C for 4 h under a blanket of N_2 and vigorous stirring. The resulting suspension was filtered through glass wool to remove any large aggregates and distributed into centrifuge tubes for purification. The synthesized microgels were purified via centrifugation at 8000 rpm for about 45 min to form a pellet, followed by removal of the supernatant and re-suspension with DI water. This process was repeated six times to remove any unreacted monomers, and the purified microgel suspensions were re-combined and lyophilized.

The synthesis and purification procedures of pNIPAm-*co*-APMAH microgels are basically similar to the above description, except for the monomer feeding ratio, which is NIPAm (12.6 mmol, 90 %mol) BIS (0.7 mmol, 5 %mol), and APMAH (0.7 mmol, 5 %mol).

To synthesize the pNIPAm-*co*-APBA microgel, 12.6 mmol of NIPAm monomer (90 %mol), 0.7 mmol of BIS (5 %mol), and 0.7 mmol of APBA monomer (5 %mol) were dissolved into 99 mL of 10-mM PBS (pH 8.5). Then, the pH of the PBS monomer solution was adjusted to 8.5, the solution was filtered with a 0.2-μm syringe filter, and transferred into a 3-neck round-bottom flask fitted with a reflux condenser, thermometer, and nitrogen inlet. In this step, 10-mM PBS (pH 8.5) is used to ionize the phenylboronic acid group to promote the dissolution of the APBA monomer. The polymerization reaction ran under a N_2 blanket for 4 h at 70°C after its initiation with 0.2 mmol of APS in 1 mL of 10-mM PBS (pH 8.5). Next, the synthesized pNIPAm-*co*-APBA microgels were filtered with glass wool and purified with the centrifugation-resuspension process six times, followed by lyophilization for the following model drug loading.

4.2.3 Model Drug Loading

To load the model drug, CV, into the pNIPAm-*co*-AAc microgels, 0.5 g of the lyophilized dry pNIPAm-*co*-AAc microgel were suspended into 200 mL of a 2-mg/mL CV solution (pH adjusted to 6.5). The microgels were isolated with centrifugation, and the unbounded CV molecules were washed away by re-suspending the isolated microgels into a solution of pH 6.5 (2 mM NaCl), followed by centrifugation (8000 rpm, 45 min). This centrifugation-resuspension process was carried out six times. Finally, the CV-loaded microgels were collected by removing the supernatant and storing the bottom pellet in a centrifuge tube. In a similar procedure, the model drug, AY, was loaded into the pNIPAm-*co*-APMAH microgels.

To load RhB into the pNIPAm-*co*-APBA microgels, similar precedures with minor modifications were carried out. Specifically, the pH of a 2 mg/mL RhB solution was adjusted to 10.5 to maintain the negative charges on the microgels for drug loading. Meanwhile, the pH of the 2-mM NaCl solution for the microgel rinsing step also was adjusted to 10.5 prior to the use.

The concentration of the CV-loaded microgels, AY-loaded microgels, and RhB-loaded microgels are 0.056 g/mL, 0.082 g/mL, and 0.074 g/mL, respectively. The loaded drug content in the CV-loaded microgels was 0.021 g (0.0505 mmol) per gram of dry microgels (2.1 wt%); the AY-loaded microgels was 0.010 g (0.0184 mmol) per gram of dry microgels (1 wt%); and the RhB-loaded microgels was 0.010 g (0.0211 mmol) per gram of dry microgels (1 wt%).

4.2.4 Preparation of a Model Drug-loaded Hydrogel–Microgel Composite (HMC)

A 1 mL of concentrated CV-loaded microgel solution was added into a 3-dram vial contaning a monomer mixture solution composed of 0.7352 g of NIPAm, 0.0528 g of BIS, 0.01 g of APS, and 3.25 mL of DI water. It was followed by degassing with bubbling N_2 for 10 min and keeping the beaker in an ice-water bath for 30 min to pre-cool the reaction solution. To initiate the polymerization reaction, 18.8 µL of TEMED were added into the vial while the solution is stirred vigorously with a magnetic stir bar. The stirring was stopped 30 sec after adding TEMED, and the vial was stored in an ice-water bath overnight. The formed HMC material was removed from the container and cut into the default size, (5, 5, 5) mm, for further usage. In some cases, different dimensions of the HMC were prepared for specific experiments. The cutting of the hydrogels was completed using a razor blade and a small plastic mould that was designed to yield maximal material dimension consistency.

4.2.5 Preparation of Multi-drug Loaded HMC

To load multiple model drug molecules into the HMC material, two different drug-loaded microgels were added into the HMC pre-solution simultaneously. Specifically, CV-loaded pNIPAm-*co*-AAc and AY-loaded pNIPAm-*co*-APMAH microgel solutions were added into the HMC pre-solution (pH adjusted to 6.5) to form the multi-drug-loaded HMC-AAc-APMAH. Similarly, the HMC-AAc-APBA, was prepared by adding the CV-loaded pNIPAm-*co*-AAc and RhB-loaded pNIPAm-*co*-APBA microgel solutions into the HMC

pre-solution (pH adjusted to 10.5). The polymerization reaction steps are the same as the HMC preparation procedures mentioned above.

4.2.6 Model Drug Release Experiment

A 25-mL beaker filled with 20 mL of a pH 3 solution (2-mM NaCl) was placed on a hot plate, the solution temperature was maintained at a specific value, and it was stirred continuously at 400 rpm using a magnetic stir bar. The solution was fed through a quartz cuvette into an Agilent 8453 UV-Vis spectrophotometer equipped with an 89090A temperature controller and Peltier heating device, via a peristaltic pump. When a HMC sample cube was placed into the solution, the absorbance spectrum of the solution was collected at certain time intervals.

4.3 Results and Discussion

A typical pNIPAm-based hydrogel prepared at low temperature (e.g., in an ice-water bath) has a colorless clear appearance, while the HMC-AAc that has a CV-loaded microgel entrapped in the hydrogel has a deep blue color (Figure 4-1A and B).

To investigate the temperature-responsivity of the HMC-AAc, a differential scanning calorimetry (DSC) study was conducted. On the graph of Figure 4-2A, a broad peak at 33.2 °C illustrates that the LCST of the HMC-AAc is very close to the LCST of the pNIPAm material at ~32.5 °C, which means that the doping of the drug-loaded pNIPAm-based microgel into the pNIPAm-based hydrogel does not change the temperature-responsivity of the material much. In addition, SEM images of the HMC-AAc at different temperatures show the shrinking of pores at elevated temperatures (Figure 4-

1D, E, and F). The SEM samples were prepared by lyophilizing the HMC gel strips that were peeled off from a bulk gel material by a tweezer followed by soaking in DI water at room temperature until the solvation state equilibrated. The gel strip was ripped off from the bulk gel without cutting to avoid the any change in morphology that can occur from the cutting. To prepare the sample for SEM imaging, the fully hydrated gel samples were frozen with liquid nitrogen to fix their micro structures, and then freeze dried with a lyophilizer. It is reported that pNIPAm and/or pNIPAm-based materials undergo a phase transition from a water-soluble state to a relatively water-insoluble state when the environmental temperature increases from below to above their LCST.[4, 31] Therefore, the MHC material is in its swelling state at a temperature below LCST (e.g., 20 °C) and in its deswelling state at a temperature above LCST (e.g., 40 °C).
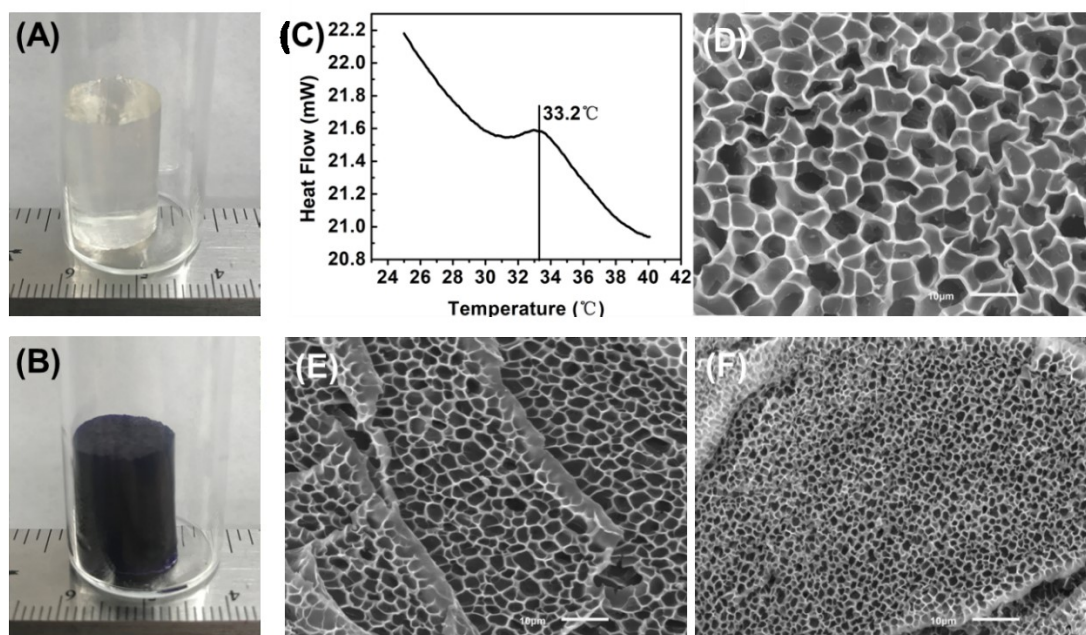
Figure 4-1. (A) A photograph of a pNIPAm-based hydrogel. (B) A photograph of HMC-AAc. (C) Thermal analysis results of a HMC-AAc sample with DSC. SEM images of HMC-AAc samples prepared at (D) 20 °C, (E) 30 °C, and (F) 40 °C, respectively (scale bar = 10 μm).

Based upon the composite structure of the HMC material, we believe that the pH-responsivity of the pNIPAm-*co*-AAc microgel endows the HMC with the ability to release the CV in a pH-responsive fashion. To verify this hypothesis, the HMC-AAc sample cubes were exposed in a pH 3 and a pH 6.5 solution (2-mM NaCl), and the absorbance value at a wavelength of 590 nm, chosen because it is the strongest absorbance peak of CV, of each solution is obtained by the UV-Vis spectrometer (Figure 4-2A). The CV release kinetics of HMC-AAc at low and neutral pH, shown in Figure 4-2B, illustrate that the release of CV molecules from the HMC is strongly pH-dependent. Compared to the release at pH 3, the release of CV at pH 6.5 is inconspicuous, and the small amount of released CV is thought to be the residual of non-specific-bounded CV molecules in the microgel. On the other hand, a continuous increasing of the CV release kinetics shown at the end of the experiment (at 60 min) reveals that the total amount of loaded CV cannot be released completely within the experimental period of 1 h.
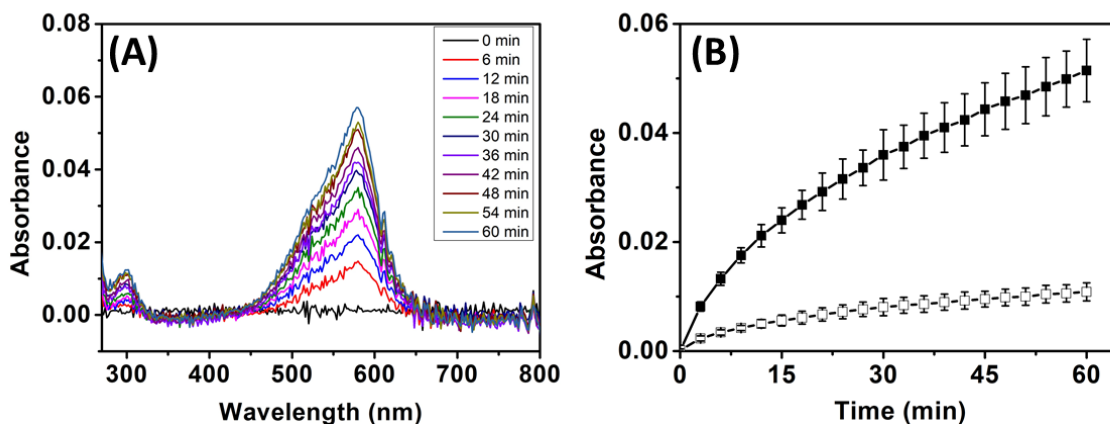
Figure 4-2. (A) UV-vis absorbance spectrum of CV and CV release kinetics of the HMC-AAc sample in a pH 3 solution. (B) Absorbance values at 590 nm as a function of time for the HMC-AAc sample cubes in a (■) pH 3 and (□) pH 6.5 solution. (Error bars are the standard deviations of three replicate experiments, and the solid curve is a connection of data points.)

As shown by the temperature-responsivity of the HMC-AAc, the change in CV release kinetics in response to the environmental temperature change should be investigated. In this experiment, The HMC-AAc sample cubes were exposed in pH 3 solutions at temperature of 20 °C, 30 °C, and 40 °C. This temperature range was selected to cover the LCST range of the material fully. Figure 4-3A shows the CV release kinetics of the HMC-AAc at different solution temperatures; it can be seen that the HMC releases CV faster at lower temperature and slower at higher temperature. In addition, the CV release rate of a HMC-AAc sample cube in a pH 3 solution can be tuned periodically by changing the solution temperature (Figure 4-3(B)). These phenomena can be explained by the different pore size of the HMC material at different solution temperatures, which affects the CV diffusion rate from within the material to the solution. As shown above, the pore size of the HMC material decreases as the temperature increases due to the temperature-responsive deswelling property of the pNIPAm-based hydrogels. Therefore, when the HMC-AAc samples are exposed in a higher-temperature solution, the shrunken pores of the pNIPAm hydrogel block the CV diffusion pathway and result in a slower CV release rate.
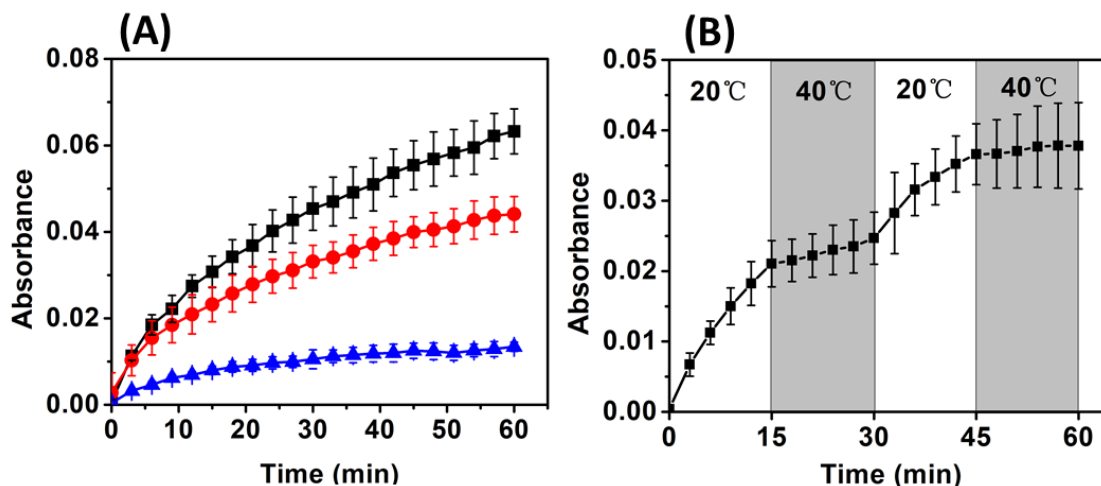
Figure 4-3. (A) Absorbance values at 590 nm as a function of time for the HMC-AAc sample cubes at (■) 20 °C, (●) 30 °C and (▲) 40 °C. (D) CV release profile of the HMC-AAc sample in a pH 3 solution with solution temperature switching between 20 °C and 40 °C. (Error bar is the standard deviation of three replicate experiments, and the solid curves are connections of data points.)

Interestingly, we found that the change of temperature also has an effect on the pH-responsivity of the HMC material. To investigate the relation between the pH-responsivity and the temperature, we tested how fast the HMC-AAc responds to the pH change at different temperatures. In this experiment, a sample cube of HMC-AAc was exposed in 20 mL of a pH 6.5 solution (2-mM NaCl) whose temperature was preset to 20 °C or 40 °C. At the time of putting the HMC-AAc sample into the solution, a UV-Vis spectrometer was used to monitor the solution absorbance every 30 sec. Then, a certain volume of concentrated hydrochloric acid was added into the solution in one aliquot to switch the pH of the solution to 3. Figure 4-4 shows the CV release profiles of the HMC-AAc samples at different temperatures when the solution pH underwent a transition from 6.5 to 3 at time 15 min. We can see that a significant increase in the CV release rate can be observed at both 20 °C and 40 °C when the concentrated acid has been added into the solution.

However, there is a delay between the acid added point and the CV release rate change point in both release profiles, and this delay can be regarded as the time that the material takes to respond to the environmental pH change. In Figure 4-4, the pH response time of the HMC-AAc at 20 °C is approximately 1.5 min, which is shorter than that at 40 °C, 3 min. This is likely due to the shrunken pores of HMC-AAc at 40 °C that inhibit the diffusion of both the hydronium ions and the CV molecules between the inside and the outside of the HMC material. As mentioned above, the protonation of the carboxylic acid group causes the release of CV molecules from the pNIPAm-*co*-AAc microgels. Thus, when the hydronium ions diffuse slower due to the limited diffusion pathway, smaller pores in this case, it takes more time for the entrapped microgels to interact with the penetrated hydronium ions.
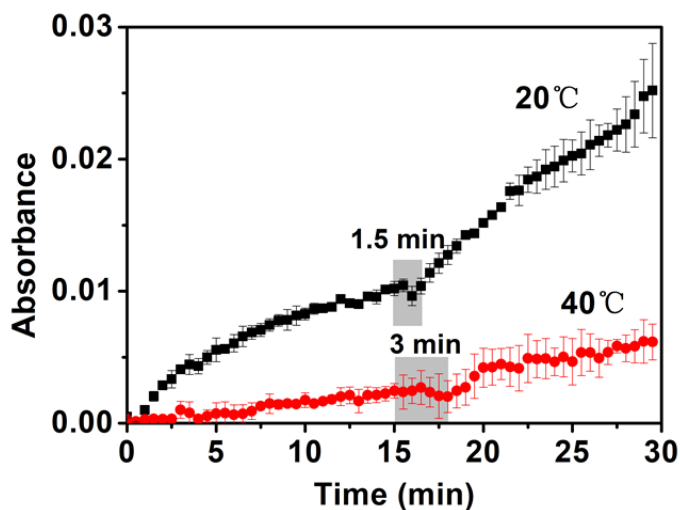
Figure 4-4. CV release profiles of the HMC-AAc sample in a solution with changes in pH from 6.5 to 3 at time 15 min at 20 °C and 40 °C. (Error bars are the standard deviations of three replicate experiments.)

Together, the features of size, shape, and structure that determine the physical properties of hydrogels indicate how the hydrogel can be used in various drug delivery

applications.[248-250] For example, the aspect ratio was reported to correlate with the drug release rate of the bulky hydrogel[251], and tuning of the particle size can improve the biocompatibility of the spherical implanted alginate capsules.[249]

To investigate the effect of the HMC dimensions on the CV release kinetics, we carried out two experiments to compare the CV release rate of the HMC with a different volume and a different surface area (SA), respectively. In the first experiment, we kept the HMC sample volume constant, and analyzed the relation between the CV release rate and surface area of the samples. Briefly, the HMC-AAc was cut into three different dimensions, (5, 5, 5) mm, (5, 10, 2.5) mm, and (10, 10, 1.25) mm, respectively (Scheme 4-2). Therefore, these three samples had the same volume, 125 mm^3, but different surface areas of 150, 175, and 250 mm^2, respectively. Their CV release profiles were monitored by the CV release experiment, as mentioned above. In the second experiment, we kept the HMC sample total surface area constant, and analyzed the relation between the CV release rate and the volume of the samples. Briefly, the HMC-AAc samples prepared were 1 cube with a (5, 5, 5) mm dimension, 4 cubes with a (2.5, 2.5, 2.5) mm dimension, and 16 cubes with a (1.25, 1.25, 1.25) mm dimension (Scheme 4-2). Thus, these three series of samples have the same total surface areas but different volumes, 125, 62.5, and 31.25 mm^3, respectively. The samples were allowed to release CV molecules at pH 3 conditions, and their CV release kinetics were recorded.
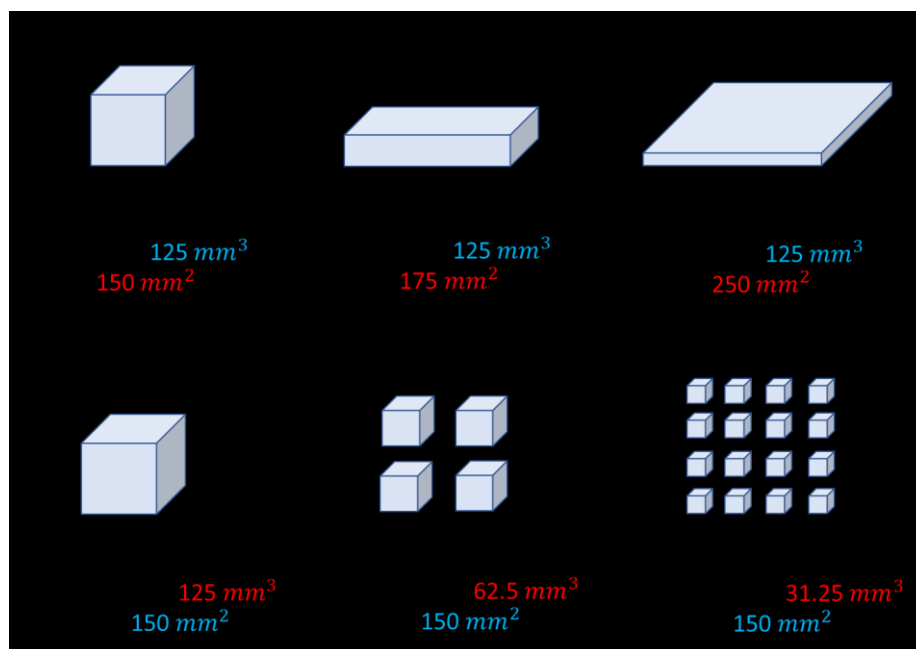
Scheme 4-2. Schematic demonstrations of HMC-AAc samples with different dimensions

Figure 4-5A shows that samples with a larger surface area release CV at a higher rate than samples with a smaller surface area, although they all have the same volume. However, Figure 4-5B shows that samples having the same total surface area release CV at a similar rate, which is independent of the sample volume. We believe that this is because the CV release rate of the HMC sample cube relies on the number of release pathways which depends on the area that the material is in contact with water. Therefore, a greater surface area provides more diffusion routes to the CV molecules, which results in faster release kinetics. The larger volume of the material, however, is not the criterion for the faster release rate if the same surface area of sample is maintained. Overall, from these results, we can conclude that only the surface area and not the volume would affect the CV release rate of the HMC materials.
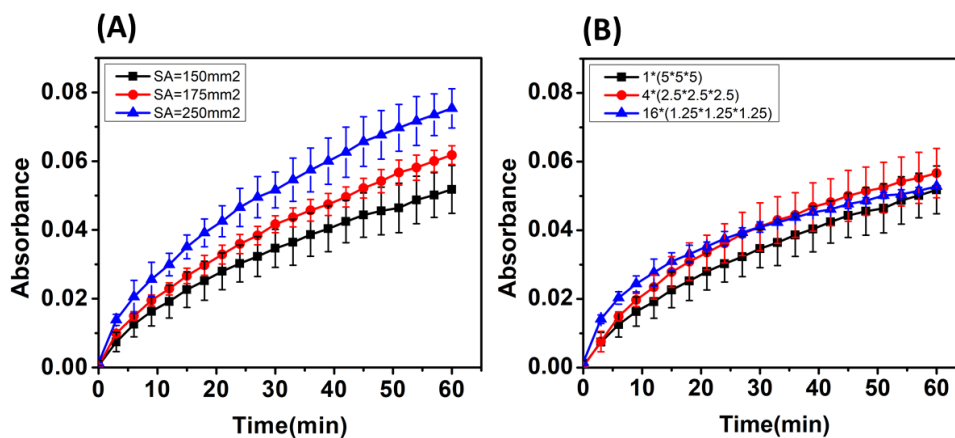
Figure 4-5. (A) CV release profiles of the HMC-AAc samples that have same volume but different surface area. (B) CV release profiles of the HMC-AAc samples that have same total surface area but different volume. (Error bars are the standard deviations of three replicate experiments, and the solid curves are connections of data points.)

The incorporation of pH-responsive monomers, APMAH and APBA, makes the synthesized pNIPAm-based microgels pH-responsive, which is demonstrated by the reversible ionization–neutralization of the microgels. Previous research showed that the increase in charge density inside microgels leads to microgel size increase due to the electrostatic repulsion.[96, 252] This phenomenon was observed also in the microgel hydrodynamic size measurement with dynamic light scattering (DLS). As shown in Figure 4-6A, all three different microgels have a larger size when the solution pH endows them with charges.

110
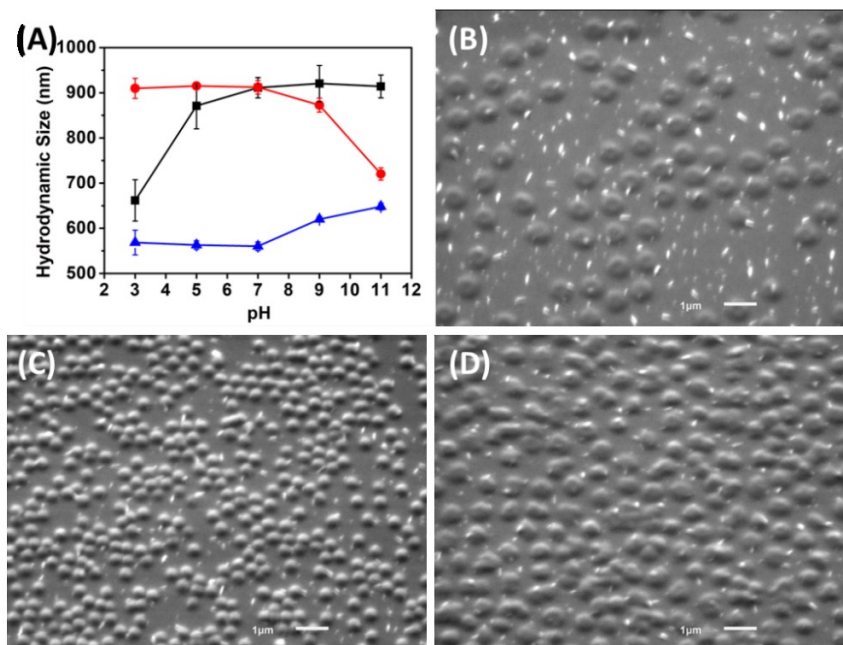
Figure 4-6. (A) Hydrodynamic size of microgels at different pH, (■) pNIPAm-*co*-AAc microgel, (●) pNIPAm-*co*-APMAH microgel, (▲) pNIPAm-*co*-APBA microgel. (Error bars represent the standard deviations of three measurements.) (B), (C) and (D) are the SEM images of pNIPAm-*co*-AAc, pNIPAm-*co*-APBA, and pNIPAm-*co*-APMAH microgels, respectively (scale bar = 1 μm).

Thus, the negatively charged model drug molecule, AY, can be loaded into the pNIPAm-*co*-APMAH microgels at pH 6.5, and the positively charged model drug molecule, RhB, can be loaded into the pNIPAm-*co*-APBA microgels at pH 10.5. For the same reason, when these two microgels were used to prepare the HMC, the AY-loaded HMC-APMAH can release the AY when the solution pH > 10.6 due to the deprotonation of the positively charged primary amine group, but the RhB-loaded HMC-APBA can release the RhB when the solution pH < 8.5 due to the neutralization of negatively charged phenylboronic acid group (Figure 4-7A and B). The release profiles of the AY and RhB were recorded by collecting the UV-Vis absorbance values of the solutions at the wavelength of 400 nm and 550 nm, respectively due to their strongest absorbance peaks at these wavelengths. (Figure 4-7C and D) The model drug-loaded HMC prepared in the 1-

dram vials are shown in Figure 4-8, and the colors of the materials come from the color of the model drug molecules.
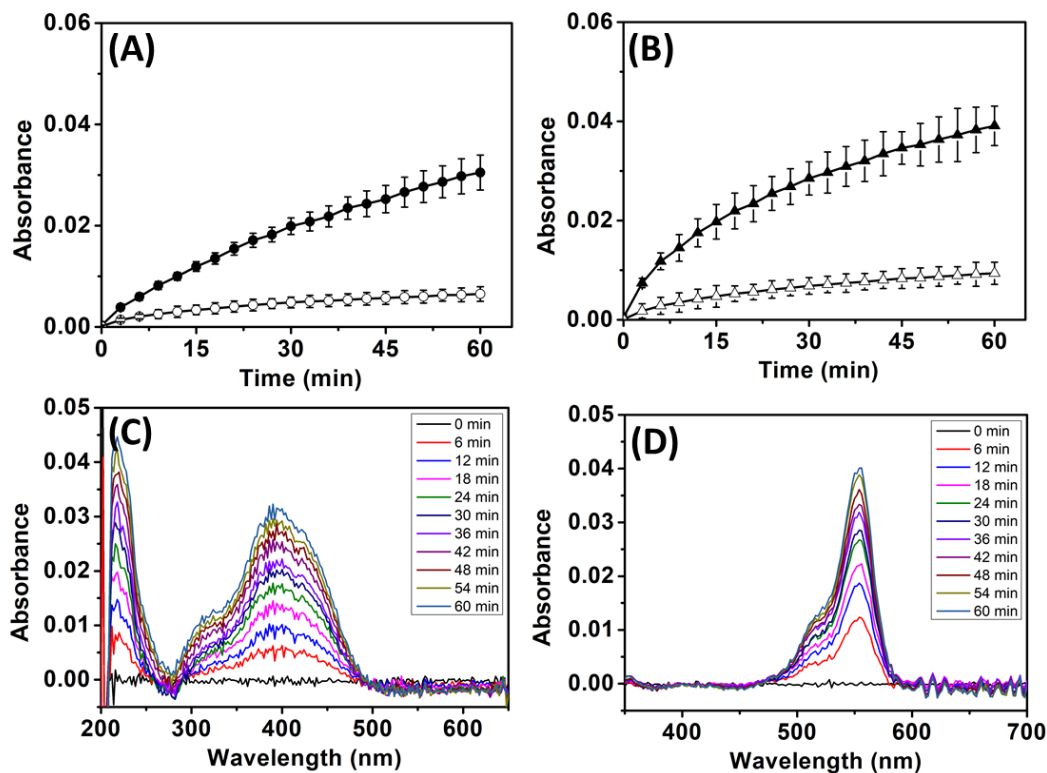
Figure 4-7. (A) Absorbance value at 400 nm as a function of time for the HMC-APMAH sample cubes in a (●) pH 11 and (○) pH 6.5 solution. (Error bars are the standard deviations of three replicate experiments.) (B) Absorbance value at 550 nm as a function of time for the HMC-APBA sample cubes in a (▲) pH 6.5 and (△) pH 10.5 solution. (Error bars are the standard deviations of three replicate experiments.) (C) UV-vis absorbance spectrum of AY and AY release kinetics of the HMC-APMAH sample in a pH 11 solution. (D) UV-vis absorbance spectrum of RhB and RhB release kinetics of the HMC-APBA sample in a pH 6.5 solution.
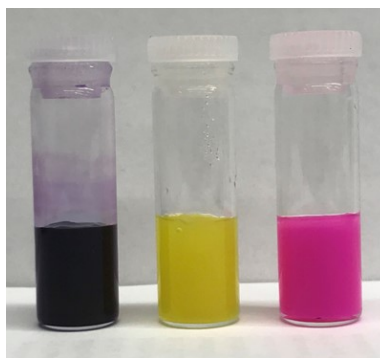
Figure 4-8. The appearance of three different model drug-loaded HMC materials. Left: HMC-AAc, middle: HMC-APMAH, and right: HMC-APBA.

Interestingly, if two different model drug-loaded microgels are incorporated into one HMC material, e.g., the HMC-AAc-APMAH and HMC-AAc-APBA, we can control the release process of each model drug individually. As we know, CV can be released by the pNIPAm-*co*-AAc microgels when pH < 4.25, but AY can be released by the pNIPAm-*co*-APMAH microgel when pH > 10.6. Therefore, the dual-drug controlled release can be achieved by changing solution pH between acidic and basic values. Figure 4-9A shows the CV and AY individual release profile of the HMC-AAc-APMAH when the pH of the solution was switched periodically between 3 and 11 by adding a concentrated hydrochloric acid or sodium hydroxide solution. It is clear that the CV was only released by the HMC at a significant rate at pH 3, but this release is prohibited when the pH was raised to 11. Interestingly, the CV absorbance value has a slight decrease when the solution pH is changed to 11. This is because of the decolorization of CV at basic conditions.[253] On the other hand, as shown in Figure 4-9B, when the HMC-AAc-APBA sample cube was exposed in a pH 10.5 solution, neither the CV nor the RhB were released because both the carboxylic acid group and the phenylboronic acid group are negatively charged at this pH and strongly bind to the model drug molecules. However, the HMC-AAc-APBA started to

release the RhB only when the pH decreased to 6.5 due to the neutralization of the phenylboronic acid group only. Moreover, when the solution pH changed to 3, all the microgels in the HMC-AAc-APBA were neutralized and started to release both the CV and the RhB.
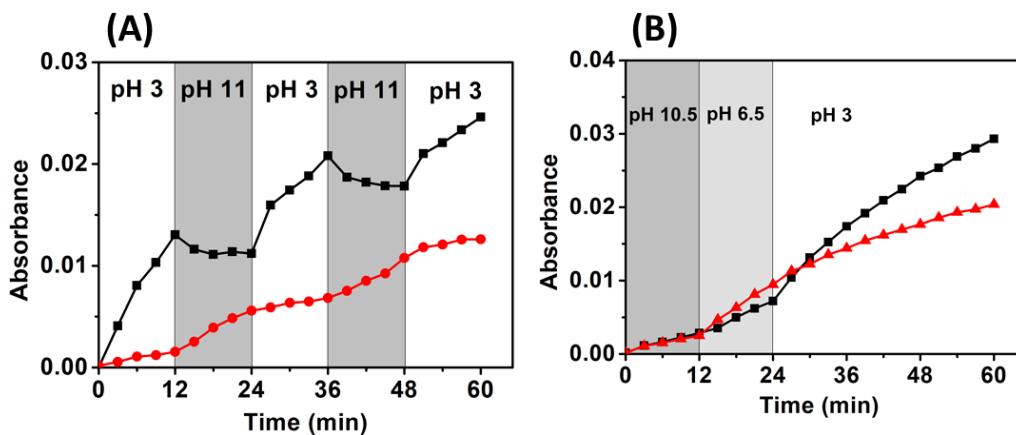
Figure 4-9. (A) (■) CV and (●) AY release profile in a pH switch solution. (B) (■) CV and (▲) RhB release profile in a pH switch solution. (Solid curves are connections of data points.)

4.4 Conclusions

In conclusion, we have prepared pNIPAm-based HMC by doping pNIPAm-based pH-responsive microgels in a pNIPAm-based hydrogel. The HMC material demonstrates its ability to release pre-loaded model drug molecules depending on the pH responsivity of the entrapped pNIPAm-based microgels, and the model drug release behavior is related to the solution temperature, the pH, and the dimension of the HMC material. Meanwhile, by incorporating multiple model drug-loaded microgels, the resultant HMC is capable of controlling the release of multiple model drug molecules individually by changing the solution pH. Moreover, the combination of released model drug molecules can be varied simply by selecting different drug-loaded microgels. This demonstrates the potential of this type of material in applications of multi-drug controlled release.

Chapter 5

Conclusions and Future Outlook

5.1 Conclusions and Future Outlook of an Etalon-based Controlled Release System

In Chapter 2, a stimuli-responsive etalon-based controlled release system was developed by modifying the model-drug-loaded etalon devices with alkanethiols. A layer of pNIPAm-*co*-20%AAc microgel in the etalon device can be loaded with ionic small molecules, such as crystal violet, CV. The CV can be released also by the microgel layer in a pH-responsive fashion and diffuse through the Au upper layer of etalons to the external environment. It was shown that the small-molecule release kinetics is related to both the polarity and length of the chain of alkanethiols and, by utilizing this surface modification approach, the small-molecule release rate can be tuned precisely and easily. Moreover, by combining two etalons that have different surface modification, a composite release profile, such as a rapid and sustainable release, can be achieved.

In this chapter, we also investigated the mechanism of the CV controlled release by the surface modified etalons by comparing the CV release kinetics data and the etalon's response kinetics to the change in solution pH. It was shown that the alkanethiol molecules on the etalon's surface have a blocking effect on the diffusion of both the acidic solution and the CV molecules.

Compared to other polymer film-based drug delivery systems, the etalons can determine the amount of the released drug precisely by taking advantages of the self-assembled microgel monolayer that controls the amount of drug loaded. On the other hand, with surface modifications, the upper Au layer of an etalon acts as a diffusion barrier that allows us to control the release process of the loaded drug.

In future, the etalon-based controlled release system can be utilized to develop implantable and/or patch-based drug delivery devices, and more biocompatible molecules can be used to modify the devices to increase biocompatibility and prolong the drug release period. Furthermore, since it is possible to load different drugs in different parts of an etalon device and control the drug release of each part independently, a drug delivery system with a combined release of multiple drugs from an etalon-based device can be realized. Moreover, self-assembled monolayer (SAM) on Au surface was reported as a promising means to provide chemically well-defined substrates that can be tailored for specific cell culture applications.[254] Therefore, the surface modified etalon-based device could be applied in cell culture applications to control the growth and/or differentiation of the cells by controlling the release of cell growth and/or differentiation factors. By taking advantages of the stimuli-responsivity of the material, the cell culture process can be controlled and manipulated with external stimuli.

5.2 Conclusions and Future Outlooks of HMC-based Controlled Release System

In Chapter 3, a controlled release system based on a hydrogel–microgel composite (HMC) material was developed. The HMC was prepared by embedding pNIPAm-based microgels in a pNIPAm-based hydrogel. When the HMC is loaded with small hydrophilic molecules, the small hydrophilic molecules can be triggered to release in a pH-responsive fashion, and the release rate is related to various factors, such as the temperature of solution, dimension of the material, and composition of the hydrogel matrix. More specifically, the experimental results shown that the small-molecule release rate is tunable by changing the crosslinking density, internal charge density, and hydrophobicity of the hydrogel matrix.

In Chapter 4, the HMC demonstrated its potential as a multi-drug controlled release system. In this study, multiple pNIPAm-based microgels loaded with different model drugs were embedded in a HMC, and the resultant multi-drug-loaded HMC was able to control the release of each model drug individually.

From a drug delivery perspective, the HMC-based controlled release system is particularly interesting, as the limitations of both microgels and hydrogels in drug delivery can be mitigated by this composite material. For example, any biocompatibility issue of microgels could be eliminated by hiding the microgels in biocompatible hydrogels; and the burst drug release can be prolonged by using the hydrogel matrix as a diffusion barrier. Therefore, for further investigation, degradable crosslinkers could be incorporated into the HMC to develop injectable drug delivery systems. As mentioned in Chapter 3, since the HMC-based controlled release systems can prolong the release peiord up to 2 months,[209] and the hydrogel-based materials contains large amount of water, this type of system can

potentially be used for plant grafting. A successful plant grafting usually takes few weeks and requires the protection from excessive water loss and tissue corruption caused by pathogenic bacteria.[255-257] Therefore, applying a hydrated HMC-based material that are loaded with some plant cell differentiation factors and antibiotics onto the joint site could shorten the grafting period and increase the successful rate.

References

1.   Stuart, M. A. C.; Huck, W. T.; Genzer, J.; Müller, M.; Ober, C.; Stamm, M.; Sukhorukov, G. B.; Szleifer, I.; Tsukruk, V. V.; Urban, M., *Nature Materials* **2010,** *9* (2), 101.

2.   Urban, M. W., *Handbook of Stimuli-Responsive Materials*. John Wiley & Sons: 2011.

3.   Roy, I.; Gupta, M. N., *Chemistry & Biology* **2003,** *10* (12), 1161-1171.

4.   Schild, H. G., *Progress in Polymer Science* **1992,** *17* (2), 163-249.

5.   Ma, C.; Shi, Y.; Pena, D. A.; Peng, L.; Yu, G., *Angewandte Chemie International Edition* **2015,** *54* (25), 7376-7380.

6.   Karg, M.; Pastoriza-Santos, I.; Rodriguez-Gonzalez, B.; von Klitzing, R.; Wellert, S.; Hellweg, T., *Langmuir* **2008,** *24* (12), 6300-6306.

7.   Dai, S.; Ravi, P.; Tam, K. C., *Soft Matter* **2008,** *4* (3), 435-449.

8.   Debord, J. D.; Lyon, L. A., *Langmuir* **2003,** *19* (18), 7662-7664.

9.   Lynn, D. M.; Amiji, M. M.; Langer, R., *Angewandte Chemie International Edition* **2001,** *40* (9), 1707-1710.

10.   Snowden, M. J.; Chowdhry, B. Z.; Vincent, B.; Morris, G. E., *Journal of the Chemical Society, Faraday Transactions* **1996,** *92* (24), 5013-5016.

11.   Zhou, J.; Wang, G.; Hu, J.; Lu, X.; Li, J., *Chemical Communications* **2006,** (46), 4820-4822.

12.   Narayan, K.; Kumar, N., *Applied Physics Letters* **2001,** *79* (12), 1891-1893.

13.   Zhao, Y.; Ikeda, T., *Smart light-Responsive Materials: Azobenzene-Containing Polymers and Liquid Crystals*. John Wiley & Sons: 2009.

14.   Murdan, S., *Journal of Controlled Release* **2003,** *92* (1-2), 1-17.

15.   Xu, W.; Gao, Y.; Serpe, M. J., *Journal of Materials Chemistry C* **2014,** *2* (20), 3873-3878.

16.   Filipcsei, G.; Feher, J.; Zrınyi, M., *Journal of Molecular Structure* **2000,** *554* (1), 109-117.

17.   Kamaly, N.; Yameen, B.; Wu, J.; Farokhzad, O. C., *Chemical Reviews* **2016,** *116* (4), 2602-2663.

18.   Ma, N.; Li, Y.; Xu, H.; Wang, Z.; Zhang, X., *Journal of the American Chemical Society* **2009,** *132* (2), 442-443.

19.   Napoli, A.; Valentini, M.; Tirelli, N.; Müller, M.; Hubbell, J. A., *Nature Materials* **2004,** *3* (3), 183.

20.   Nuyken, O.; Burkhardt, V.; Pöhlmann, T.; Herberhold, M. In *Ferrocene containing polymers*, Makromolekulare Chemie. Macromolecular Symposia, Wiley Online Library: 1991; pp 195-206.

21.   Hu, J.; Zhang, G.; Liu, S., *Chemical Society Reviews* **2012,** *41* (18), 5933-5949.

22.   Zelzer, M.; Todd, S. J.; Hirst, A. R.; McDonald, T. O.; Ulijn, R. V., *Biomaterials Science* **2013,** *1* (1), 11-39.

23.   Hoffman, A. S.; Stayton, P. S., *Progress in Polymer Science* **2007,** *32* (8-9), 922-932.

24.   Cobo, I.; Li, M.; Sumerlin, B. S.; Perrier, S., *Nature Materials* **2015,** *14* (2), 143.

25.   Okano, T., Molecular Design of Temperature-Responsive Polymers as Intelligent Materials. In *Responsive Gels: Volume Transitions II*, Springer: 1993; pp 179-197.

26.   Meeussen, F.; Nies, E.; Berghmans, H.; Verbrugghe, S.; Goethals, E.; Du Prez, F., *Polymer* **2000,** *41* (24), 8597-8602.

27.   Hu, Z.; Cai, T.; Chi, C., *Soft Matter* **2010,** *6* (10), 2115-2123.

28.   Idziak, I.; Avoce, D.; Lessard, D.; Gravel, D.; Zhu, X., *Macromolecules* **1999,** *32* (4), 1260-1263.

29.   Ward, M. A.; Georgiou, T. K., *Soft Matter* **2012,** *8* (9), 2737-2745.

30.   Sanchez, I.; Stone, M., *Polymer Blends* **2000,** *1*, 15-53.

31.   Heskins, M.; Guillet, J. E., *Journal of Macromolecular Science—Chemistry* **1968,** *2* (8), 1441-1455.

32.   Tanford, C., *The Hydrophobic Effect: Formation of Micelles and Biological Membranes 2d ed*. J. Wiley.: 1980.

33.   Otake, K.; Inomata, H.; Konno, M.; Saito, S., *Macromolecules* **1990,** *23* (1), 283-289.

34.   Feil, H.; Bae, Y. H.; Feijen, J.; Kim, S. W., *Macromolecules* **1993,** *26* (10), 2496-2500.

35.   Liu, H.; Zhu, X., *Polymer* **1999,** *40* (25), 6985-6990.

36.   Furyk, S.; Zhang, Y.; Ortiz-Acosta, D.; Cremer, P. S.; Bergbreiter, D. E., *Journal of Polymer Science Part A: Polymer Chemistry* **2006,** *44* (4), 1492-1501.

37.   Dalkas, G.; Pagonis, K.; Bokias, G., *Polymer* **2006,** *47* (1), 243-248.

38.   Costa, R. O.; Freitas, R. F., *Polymer* **2002,** *43* (22), 5879-5885.

39.   Kocak, G.; Tuncer, C.; Bütün, V., *Polymer Chemistry* **2017,** *8* (1), 144-176.

40.   Binauld, S.; Stenzel, M. H., *Chemical Communications* **2013,** *49* (21), 2082-2102.

41.   Rumble, J. R., *CRC Handbook of Chemistry and Physics, 100th Edition*. 100th ed.; 2019.

42.   Yan, J.; Springsteen, G.; Deeter, S.; Wang, B., *Tetrahedron* **2004,** *60* (49), 11205-11209.

43.   Fife, T. H.; Jao, L., *The Journal of Organic Chemistry* **1965,** *30* (5), 1492-1495.

44.   Gillies, E. R.; Goodwin, A. P.; Fréchet, J. M., *Bioconjugate Chemistry* **2004,** *15* (6), 1254-1263.

45.   Liu, B.; Thayumanavan, S., *Journal of the American Chemical Society* **2017,** *139* (6), 2306-2317.

46.　Jochum, F. D.; Theato, P., *Chemical Society Reviews* **2013,** *42* (17), 7468-7483.

47.　Yager, K. G.; Barrett, C. J., *Journal of Photochemistry and Photobiology A: Chemistry* **2006,** *182* (3), 250-261.

48.　Kumar, G. S.; Neckers, D., *Chemical Reviews* **1989,** *89* (8), 1915-1925.

49.　Zhao, H.; Sterner, E. S.; Coughlin, E. B.; Theato, P., *Macromolecules* **2012,** *45* (4), 1723-1736.

50.　Huang, Y.; Dong, R.; Zhu, X.; Yan, D., *Soft Matter* **2014,** *10* (33), 6121-6138.

51.　Yan, B.; Boyer, J.-C.; Branda, N. R.; Zhao, Y., *Journal of the American Chemical Society* **2011,** *133* (49), 19714-19717.

52.　Wang, S.; Song, Y.; Jiang, L., *Journal of Photochemistry and Photobiology C: Photochemistry Reviews* **2007,** *8* (1), 18-29.

53.　Nicolas, H.; Yuan, B.; Zhang, X.; Schönhoff, M., *Langmuir* **2016,** *32* (10), 2410-2418.

54.　Hoffman, A. S., *Advanced Drug Delivery Reviews* **2012,** *64*, 18-23.

55.　Bhattarai, N.; Gunn, J.; Zhang, M., *Advanced Drug Delivery Reviews* **2010,** *62* (1), 83-99.

56.　Liu, M.; Zeng, X.; Ma, C.; Yi, H.; Ali, Z.; Mou, X.; Li, S.; Deng, Y.; He, N., *Bone Research* **2017,** *5*, 17014.

57.　Naahidi, S.; Jafari, M.; Logan, M.; Wang, Y.; Yuan, Y.; Bae, H.; Dixon, B.; Chen, P., *Biotechnology Advances* **2017,** *35* (5), 530-544.

58.　Tibbitt, M. W.; Anseth, K. S., *Biotechnology and Bioengineering* **2009,** *103* (4), 655-663.

59.　Caliari, S. R.; Burdick, J. A., *Nature Methods* **2016,** *13* (5), 405.

60.　Seo, S. R.; Kim, J.-C., *Drug Development and Industrial Pharmacy* **2013,** *39* (12), 1921-1927.

61.　Afrassiabi, A.; Hoffman, A. S.; Cadwell, L. A., *Journal of Membrane Science* **1987,** *33* (2), 191-200.

62.　Roy, D.; Cambre, J. N.; Sumerlin, B. S., *Progress in Polymer Science* **2010,** *35* (1-2), 278-301.

63.　Tokarev, I.; Minko, S., *Soft Matter* **2009,** *5* (3), 511-524.

64.　Holtz, J. H.; Asher, S. A., *Nature* **1997,** *389* (6653), 829.

65.　Ionov, L., *Materials Today* **2014,** *17* (10), 494-503.

66.　Schmidt, S.; Zeiser, M.; Hellweg, T.; Duschl, C.; Fery, A.; Möhwald, H., *Advanced Functional Materials* **2010,** *20* (19), 3235-3243.

67.　Huang, G.; Gao, J.; Hu, Z.; John, J. V. S.; Ponder, B. C.; Moro, D., *Journal of Controlled Release* **2004,** *94* (2-3), 303-311.

68.　Burek, M.; Czuba, Z. P.; Waskiewicz, S., *Polymer* **2014,** *55* (25), 6460-6470.

69.   Tanaka, T.; Fillmore, D. J., *The Journal of Chemical Physics* **1979,** *70* (3), 1214-1218.

70.   Wu, X.; Pelton, R.; Hamielec, A.; Woods, D.; McPhee, W., *Colloid and Polymer Science* **1994,** *272* (4), 467-477.

71.   Pelton, R.; Chibante, P., *Colloids and Surfaces* **1986,** *20* (3), 247-256.

72.   Kawaguchi, H., *Polymer International* **2014,** *63* (6), 925-932.

73.   Hu, X.; Tong, Z.; Lyon, L. A., *Colloid and Polymer Science* **2011,** *289* (3), 333-339.

74.   Goodwin, J. W.; Ottewill, R. H.; Pelton, R.; Vianello, G.; Yates, D. E., *British Polymer Journal* **1978,** *10* (3), 173-180.

75.   Grahame, D. C., *Chemical Reviews* **1947,** *41* (3), 441-501.

76.   McPhee, W.; Tam, K. C.; Pelton, R., *Journal of Colloid and Interface Science* **1993,** *156* (1), 24-30.

77.   Lyon, L. A.; Meng, Z.; Singh, N.; Sorrell, C. D.; John, A. S., *Chemical Society Reviews* **2009,** *38* (4), 865-874.

78.   Zhang, Q. M.; Berg, D.; Mugo, S. M.; Serpe, M. J., *Chemical Communications* **2015,** *51* (47), 9726-9728.

79.   Zhang, Q. M.; Xu, W.; Serpe, M. J., *Angewandte Chemie International Edition* **2014,** *53* (19), 4827-4831.

80.   Mohanty, P. S.; Bagheri, P.; Nöjd, S.; Yethiraj, A.; Schurtenberger, P., *Physical Review X* **2015,** *5* (1), 011030.

81.   Zhang, Q. M.; Berg, D.; Duan, J.; Mugo, S. M.; Serpe, M. J., *ACS Applied Materials & Interfaces* **2016,** *8* (40), 27264-27269.

82.   Sorrell, C. D.; Carter, M. C.; Serpe, M. J., *Advanced Functional Materials* **2011,** *21* (3), 425-433.

83.   Serpe, M. J.; Lyon, L. A., *Chemistry of Materials* **2004,** *16* (22), 4373-4380.

84.   Asher, S. A.; Holtz, J.; Liu, L.; Wu, Z., *Journal of the American Chemical Society* **1994,** *116* (11), 4997-4998.

85.   Schmidt, S.; Hellweg, T.; von Klitzing, R., *Langmuir* **2008,** *24* (21), 12595-12602.

86.   Iyer, A. S. J.; Lyon, L. A., *Angewandte Chemie International Edition* **2009,** *48* (25), 4562-4566.

87.   Bridges, A. W.; Singh, N.; Burns, K. L.; Babensee, J. E.; Lyon, L. A.; García, A. J., *Biomaterials* **2008,** *29* (35), 4605-4615.

88.   Li, X.; Weng, J.; Guan, Y.; Zhang, Y., *Langmuir* **2016,** *32* (16), 3977-3982.

89.   Hendrickson, G. R.; Lyon, L. A., *Soft Matter* **2009,** *5* (1), 29-35.

90.   Suzuki, D.; McGrath, J. G.; Kawaguchi, H.; Lyon, L. A., *The Journal of Physical Chemistry C* **2007,** *111* (15), 5667-5672.

91.   Zhang, Q. M.; Ahiabu, A.; Gao, Y.; Serpe, M. J., *Journal of Materials Chemistry C* **2015,** *3* (3), 495-498.

92.   Gao, Y.; Wong, K. Y.; Ahiabu, A.; Serpe, M. J., *Journal of Materials Chemistry B* **2016,** *4* (30), 5144-5150.

93.   Guo, S.; Gao, Y.; Wei, M.; Zhang, Q. M.; Serpe, M. J., *Journal of Materials Chemistry B* **2015,** *3* (12), 2516-2521.

94.   Hoare, T.; Pelton, R., *Macromolecules* **2007,** *40* (3), 670-678.

95.   Springsteen, G.; Wang, B., *Tetrahedron* **2002,** *58* (26), 5291-5300.

96.   Ahiabu, A.; Serpe, M. J., *ACS Omega* **2017,** *2* (5), 1769-1777.

97.   Li, X.; Gao, Y.; Serpe, M. J., *Canadian Journal of Chemistry* **2015,** *93* (7), 685-689.

98.   Li, W.; Guo, Q.; Zhao, H.; Zhang, L.; Li, J.; Gao, J.; Qian, W.; Li, B.; Chen, H.; Wang, H., *Nanomedicine* **2012,** *7* (3), 383-392.

99.   Zhang, Q.; Colazo, J.; Berg, D.; Mugo, S. M.; Serpe, M. J., *Molecular Pharmaceutics* **2017,** *14* (8), 2624-2628.

100.   Pelton, R., *Advances in Colloid and Interface Science* **2000,** *85* (1), 1-33.

101.   Parasuraman, D.; Serpe, M. J., *ACS Applied Materials & Interfaces* **2011,** *3* (12), 4714-4721.

102.   Park, K., *Journal of Controlled Release* **2014,** *190*, 3-8.

103.   Poveda, E.; Briz, V.; Soriano, V., *AIDS Reviews* **2005,** *7* (3), 139-147.

104.   Aungst, B. J., *The AAPS Journal* **2012,** *14* (1), 10-18.

105.   Ichikawa, H.; Peppas, N. A., *Journal of Biomedical Materials Research Part A: An Official Journal of The Society for Biomaterials, The Japanese Society for Biomaterials, and The Australian Society for Biomaterials and the Korean Society for Biomaterials* **2003,** *67* (2), 609-617.

106.   Yun, Y.; Cho, Y. W.; Park, K., *Advanced Drug Delivery Reviews* **2013,** *65* (6), 822-832.

107.   Pauletti, G. M.; Gangwar, S.; Siahaan, T. J.; Aubé, J.; Borchardt, R. T., *Advanced Drug Delivery Reviews* **1997,** *27* (2-3), 235-256.

108.   Choonara, B. F.; Choonara, Y. E.; Kumar, P.; Bijukumar, D.; du Toit, L. C.; Pillay, V., *Biotechnology Advances* **2014,** *32* (7), 1269-1282.

109.   Levy, R. J.; Labhasetwar, V.; Strickberger, S. A.; Underwood, T.; Davis, J., *Drug Delivery* **1996,** *3* (3), 137-142.

110.   Hatefi, A.; Amsden, B., *Journal of Controlled Release* **2002,** *80* (1-3), 9-28.

111.   Jeong, B.; Bae, Y. H.; Lee, D. S.; Kim, S. W., *Nature* **1997,** *388* (6645), 860.

112. Paul, A.; Hasan, A.; Kindi, H. A.; Gaharwar, A. K.; Rao, V. T.; Nikkhah, M.; Shin, S. R.; Krafft, D.; Dokmeci, M. R.; Shum-Tim, D., *ACS Nano* **2014,** *8* (8), 8050-8062.

113. Mathew, A. P.; Uthaman, S.; Cho, K.-H.; Cho, C.-S.; Park, I.-K., *International Journal of Biological Macromolecules* **2018,** *110*, 17-29.

114. Gu, Z.; Aimetti, A. A.; Wang, Q.; Dang, T. T.; Zhang, Y.; Veiseh, O.; Cheng, H.; Langer, R. S.; Anderson, D. G., *ACS Nano* **2013,** *7* (5), 4194-4201.

115. Shin, M.; Park, S.-G.; Oh, B.-C.; Kim, K.; Jo, S.; Lee, M. S.; Oh, S. S.; Hong, S.-H.; Shin, E.-C.; Kim, K.-S., *Nature Materials* **2017,** *16* (1), 147.

116. Prausnitz, M. R.; Langer, R., *Nature Biotechnology* **2008,** *26* (11), 1261.

117. Hu, X.; Yu, J.; Qian, C.; Lu, Y.; Kahkoska, A. R.; Xie, Z.; Jing, X.; Buse, J. B.; Gu, Z., *ACS Nano* **2017,** *11* (1), 613-620.

118. Huber, C. P., *American Journal of Obstetrics & Gynecology* **1940,** *39* (5), 917.

119. Folkman, J.; Long, D. M., *Journal of Surgical Research* **1964,** *4* (3), 139-42.

120. Dash, A.; Cudworth II, G., *Journal of Pharmacological and Toxicological Methods* **1998,** *40* (1), 1-12.

121. Lewis, D. H., *Biodegradable Polymers as Drug Delivery Systems.* **1990**, 1-41.

122. Pizzi, M.; De Martiis, O.; Grasso, V., *Biomedical Microdevices* **2004,** *6* (2), 155-158.

123. Freed, L. E.; Vunjak-Novakovic, G.; Biron, R. J.; Eagles, D. B.; Lesnoy, D. C.; Barlow, S. K.; Langer, R., *Bio/technology* **1994,** *12* (7), 689.

124. Wright, J. C.; Leonard, S. T.; Stevenson, C. L.; Beck, J. C.; Chen, G.; Jao, R. M.; Johnson, P. A.; Leonard, J.; Skowronski, R. J., *Journal of Controlled Release* **2001,** *75* (1-2), 1-10.

125. Ranade, V. V., *The Journal of Clinical Pharmacology* **1990,** *30* (10), 871-889.

126. Buchwald, H.; Grage, T. B.; Vassilopoulos, P. P.; Rohde, T. D.; Varco, R. L.; Blackshear, P. J., *Cancer* **1980,** *45* (5), 866-869.

127. Lyu, S.; Untereker, D., *International Journal of Molecular Sciences* **2009,** *10* (9), 4033-4065.

128. Liu, Y.; Song, P.; Liu, J.; Tng, D. J. H.; Hu, R.; Chen, H.; Hu, Y.; Tan, C. H.; Wang, J.; Liu, J., *Biomedical Microdevices* **2015,** *17* (1), 6.

129. Li, P.-Y.; Shih, J.; Lo, R.; Saati, S.; Agrawal, R.; Humayun, M. S.; Tai, Y.-C.; Meng, E., *Sensors and Actuators A: Physical* **2008,** *143* (1), 41-48.

130. Farra, R.; Sheppard, N. F.; McCabe, L.; Neer, R. M.; Anderson, J. M.; Santini, J. T.; Cima, M. J.; Langer, R., *Science Translational Medicine* **2012,** *4* (122), 122ra21-122ra21.

131. Zhou, M.; Zhou, N.; Kuralay, F.; Windmiller, J. R.; Parkhomovsky, S.; Valdés-Ramírez, G.; Katz, E.; Wang, J., *Angewandte Chemie International Edition* **2012,** *51* (11), 2686-2689.

132. Song, P.; Kuang, S.; Panwar, N.; Yang, G.; Tng, D. J. H.; Tjin, S. C.; Ng, W. J.; Majid, M. B. A.; Zhu, G.; Yong, K. T., *Advanced Materials* **2017,** *29* (11), 1605668.

133. Lu, B.; Chen, Y.; Ou, D.; Chen, H.; Diao, L.; Zhang, W.; Zheng, J.; Ma, W.; Sun, L.; Feng, X., *Scientific Reports* **2015,** *5*, 16065.

134. Uhrich, K. E.; Cannizzaro, S. M.; Langer, R. S.; Shakesheff, K. M., *Chemical Reviews* **1999,** *99* (11), 3181-3198.

135. Bajpai, A. K.; Shukla, S. K.; Bhanu, S.; Kankane, S., *Progress in Polymer Science* **2008,** *33* (11), 1088-1118.

136. Licciardi, M.; Craparo, E. F.; Giammona, G.; Armes, S. P.; Tang, Y.; Lewis, A. L., *Macromolecular Bioscience* **2008,** *8* (7), 615-626.

137. Duncan, R., *Nature Reviews Cancer* **2006,** *6* (9), 688.

138. Hoffman, A. S., *Journal of Controlled Release* **2008,** *132* (3), 153-163.

139. Zaffaroni, A., Bandage for the Administration of Drug by Controlled Metering Through Microporous Materials. Google Patents: 1974.

140. Emil, S. E.; Albert, P. R., Surgical Sutures. Google Patents: 1967.

141. Benoit, M.-A.; Baras, B.; Gillard, J., *International Journal of Pharmaceutics* **1999,** *184* (1), 73-84.

142. Li, J. K.; Wang, N.; Wu, X. S., *Journal of Pharmaceutical Sciences* **1997,** *86* (8), 891-895.

143. Masayuki, Y.; Mizue, M.; Noriko, Y.; Teruo, O.; Yasuhisa, S.; Kazunori, K.; Shohei, I., *Journal of Controlled Release* **1990,** *11* (1-3), 269-278.

144. Gabizon, A.; Martin, F., *Drugs* **1997,** *54* (4), 15-21.

145. Kratz, F., *Journal of Controlled Release* **2008,** *132* (3), 171-183.

146. Langer, R.; Peppas, N., *Journal of Macromolecular Science-Reviews in Macromolecular Chemistry and Physics* **1983,** *23* (1), 61-126.

147. Freitas, M.; Marchetti, J., *International Journal of Pharmaceutics* **2005,** *295* (1-2), 201-211.

148. Bruschi, M. L., *Strategies to Modify the Drug Release from Pharmaceutical Systems*. Woodhead Publishing: 2015.

149. Gouda, R.; Baishya, H.; Qing, Z., *J. Dev. Drugs* **2017,** *6* (02).

150. Higuchi, T., *Journal of Pharmaceutical Sciences* **1961,** *50* (10), 874-875.

151. Higuchi, W. I., *Journal of Pharmaceutical Sciences* **1962,** *51* (8), 802-804.

152. Higuchi, T., *Journal of Pharmaceutical Sciences* **1963,** *52* (12), 1145-1149.

153. Peppas, N. A.; Narasimhan, B., *Journal of Controlled Release* **2014,** *190*, 75-81.

154. AW, H., *Ind Eng Chem* **1931,** *23*, 923-31.

155. Yatvin, M. B.; Weinstein, J. N.; Dennis, W. H.; Blumenthal, R., *Science* **1978,** *202* (4374), 1290-1293.

156. Hoare, T.; Santamaria, J.; Goya, G. F.; Irusta, S.; Lin, D.; Lau, S.; Padera, R.; Langer, R.; Kohane, D. S., *Nano Letters* **2009,** *9* (10), 3651-3657.

157. Wen, H.; Jung, H.; Li, X., *The AAPS Journal* **2015,** *17* (6), 1327-1340.

158. Liu, L.; Yao, W.; Rao, Y.; Lu, X.; Gao, J., *Drug Delivery* **2017,** *24* (1), 569-581.

159. Saito, Y.; Tanaka, T.; Andoh, A.; Minematsu, H.; Hata, K.; Tsujikawa, T.; Nitta, N.; Murata, K.; Fujiyama, Y., *World Journal of Gastroenterology: WJG* **2007,** *13* (29), 3977.

160. da Silva, D.; Kaduri, M.; Poley, M.; Adir, O.; Krinsky, N.; Shainsky-Roitman, J.; Schroeder, A., *Chemical Engineering Journal* **2018,** *340*, 9-14.

161. Lee, M. S.; La, W. G.; Park, E.; Yang, H. S., *Journal of Biomedical Materials Research Part B: Applied Biomaterials* **2017,** *105* (3), 594-604.

162. De las Heras Alarcón, C.; Pennadam, S.; Alexander, C., *Chemical Society Reviews* **2005,** *34* (3), 276-285.

163. Bawa, P.; Pillay, V.; Choonara, Y. E.; Du Toit, L. C., *Biomedical Materials* **2009,** *4* (2), 022001.

164. Gracias, D. H., *Current Opinion in Chemical Engineering* **2013,** *2* (1), 112-119.

165. Cho, S. H.; White, S. R.; Braun, P. V., *Advanced Materials* **2009,** *21* (6), 645-649.

166. Amamoto, Y.; Kamada, J.; Otsuka, H.; Takahara, A.; Matyjaszewski, K., *Angewandte Chemie International Edition* **2011,** *50* (7), 1660-1663.

167. Rajagopalan, M.; Jeon, J.-H.; Oh, I.-K., *Sensors and Actuators B: Chemical* **2010,** *151* (1), 198-204.

168. Li, X.; Cai, X.; Gao, Y.; Serpe, M. J., *Journal of Materials Chemistry B* **2017,** *5* (15), 2804-2812.

169. Li, X.; Serpe, M. J., *Advanced Functional Materials* **2016,** *26* (19), 3282-3290.

170. Li, R.; Feng, F.; Wang, Y.; Yang, X.; Yang, X.; Yang, V. C., *Journal of Colloid and Interface Science* **2014,** *429*, 34-44.

171. Li, J.; Wu, Y.; Song, F.; Wei, G.; Cheng, Y.; Zhu, C., *Journal of Materials Chemistry* **2012,** *22* (2), 478-482.

172. Kahn, J. S.; Hu, Y.; Willner, I., *Accounts of Chemical Research* **2017,** *50* (4), 680-690.

173. Dong, Y.; Wang, W.; Veiseh, O.; Appel, E. A.; Xue, K.; Webber, M. J.; Tang, B. C.; Yang, X.-W.; Weir, G. C.; Langer, R., *Langmuir* **2016,** *32* (34), 8743-8747.

174. Shen, Y.; Dong, L.; Liang, Y.; Liu, Z.; Dai, R.; Meng, W.; Deng, Y., *Journal of Separation Science* **2017,** *40* (2), 524-531.

175.   Cheng, Z.; Wang, T.; Li, X.; Zhang, Y.; Yu, H., *ACS Applied Materials & Interfaces* **2015,** *7* (49), 27494-27501.

176.   Eliassaf, J., *Journal of Applied Polymer Science* **1978,** *22* (3), 873-874.

177.   Gao, Y.; Zago, G. P.; Jia, Z.; Serpe, M. J., *ACS Applied Materials & Interfaces* **2013,** *5* (19), 9803-9808.

178.   Gao, Y.; Ahiabu, A.; Serpe, M. J., *ACS Applied Materials & Interfaces* **2014,** *6* (16), 13749-13756.

179.   Sorrell, C. D.; Serpe, M. J., *Advanced Materials* **2011,** *23* (35), 4088-4092.

180.   Islam, M. R.; Serpe, M. J., *Analytical and Bioanalytical Chemistry* **2014,** *406* (19), 4777-4783.

181.   Sorrell, C. D.; Serpe, M. J., *Analytical and Bioanalytical Chemistry* **2012,** *402* (7), 2385-2393.

182.   Shu, T.; Shen, Q.; Wan, Y.; Zhang, W.; Su, L.; Zhang, X.; Serpe, M. J., *RSC Advances* **2018,** *8* (28), 15567-15574.

183.   Schoenbaum, C. A.; Schwartz, D. K.; Medlin, J. W., *Accounts of Chemical Research* **2014,** *47* (4), 1438-1445.

184.   Tian, Z.; Marconnet, A.; Chen, G., *Applied Physics Letters* **2015,** *106* (21), 211602.

185.   Jiang, L.; Yuan, L.; Cao, L.; Nijhuis, C. A., *Journal of the American Chemical Society* **2014,** *136* (5), 1982-1991.

186.   Sorrell, C. D.; Carter, M. C.; Serpe, M. J., *ACS Applied Materials & Interfaces* **2011,** *3* (4), 1140-1147.

187.   Zhang, W.; Wei, M.; Carvalho, W. S.; Serpe, M. J., *Analytica Chimica Acta* **2018,** *999*, 139-143.

188.   Zhang, L.; Lu, T.; Gokel, G. W.; Kaifer, A. E., *Langmuir* **1993,** *9* (3), 786-791.

189.   Dash, S.; Murthy, P. N.; Nath, L.; Chowdhury, P., *Acta Pol Pharm* **2010,** *67* (3), 217-23.

190.   Dalmont, H.; Pinprayoon, O.; Saunders, B. R., *Langmuir* **2008,** *24* (6), 2834-2840.

191.   Das, M.; Mardyani, S.; Chan, W. C.; Kumacheva, E., *Advanced Materials* **2006,** *18* (1), 80-83.

192.   Gokhale, A., *Pharmaceutical Technology* **2014,** *38* (5).

193.   Ramteke, K.; Dighe, P.; Kharat, A.; Patil, S., *Sch. Acad. J. Pharm* **2014,** *3* (5), 388-396.

194.   Hoare, T. R.; Kohane, D. S., *Polymer* **2008,** *49* (8), 1993-2007.

195.   Qiu, Y.; Park, K., *Advanced Drug Delivery Reviews* **2001,** *53* (3), 321-339.

196.   Kamath, K. R.; Park, K., *Advanced Drug Delivery Reviews* **1993,** *11* (1-2), 59-84.

197.   Oun, R.; Plumb, J. A.; Wheate, N. J., *Journal of Inorganic Biochemistry* **2014,** *134*, 100-105.

198.   Zhang, S.; Ermann, J.; Succi, M. D.; Zhou, A.; Hamilton, M. J.; Cao, B.; Korzenik, J. R.; Glickman, J. N.; Vemula, P. K.; Glimcher, L. H., *Science Translational Medicine* **2015,** *7* (300), 300ra128-300ra128.

199.   Altunbas, A.; Lee, S. J.; Rajasekaran, S. A.; Schneider, J. P.; Pochan, D. J., *Biomaterials* **2011,** *32* (25), 5906-5914.

200.   Singh, N. K.; Lee, D. S., *Journal of Controlled Release* **2014,** *193*, 214-227.

201.   Donnelly, R. F.; McCrudden, M. T.; Alkilani, A. Z.; Larrañeta, E.; McAlister, E.; Courtenay, A. J.; Kearney, M.-C.; Singh, T. R. R.; McCarthy, H. O.; Kett, V. L., *PLoS One* **2014,** *9* (10), e111547.

202.   Liu, J.; Qi, C.; Tao, K.; Zhang, J.; Zhang, J.; Xu, L.; Jiang, X.; Zhang, Y.; Huang, L.; Li, Q., *ACS Applied Materials & Interfaces* **2016,** *8* (10), 6411-6422.

203.   López-Noriega, A.; Hastings, C. L.; Ozbakir, B.; O'Donnell, K. E.; O'Brien, F. J.; Storm, G.; Hennink, W. E.; Duffy, G. P.; Ruiz-Hernández, E., *Advanced Healthcare Materials* **2014,** *3* (6), 854-859.

204.   Hyun, H.; Kim, Y. H.; Song, I. B.; Lee, J. W.; Kim, M. S.; Khang, G.; Park, K.; Lee, H. B., *Biomacromolecules* **2007,** *8* (4), 1093-1100.

205.   Sosnik, A.; Cohn, D., *Biomaterials* **2004,** *25* (14), 2851-2858.

206.   Lee, K. Y.; Bouhadir, K. H.; Mooney, D. J., *Macromolecules* **2000,** *33* (1), 97-101.

207.   McGillicuddy, F.; Lynch, I.; Rochev, Y.; Burke, M.; Dawson, K.; Gallagher, W.; Keenan, A., *Journal of Biomedical Materials Research Part A* **2006,** *79* (4), 923-933.

208.   Molinos, M.; Carvalho, V.; Silva, D. M.; Gama, F. M., *Biomacromolecules* **2012,** *13* (2), 517-527.

209.   Sivakumaran, D.; Maitland, D.; Hoare, T., *Biomacromolecules* **2011,** *12* (11), 4112-4120.

210.   Lynch, I.; Dawson, K. A., *The Journal of Physical Chemistry B* **2004,** *108* (30), 10893-10898.

211.   Lynch, I.; de Gregorio, P.; Dawson, K., *The Journal of Physical Chemistry B* **2005,** *109* (13), 6257-6261.

212.   Lynch, I.; Dawson, K. A., *The Journal of Physical Chemistry B* **2003,** *107* (36), 9629-9637.

213.   Brazel, C. S.; Peppas, N. A., *Macromolecules* **1995,** *28* (24), 8016-8020.

214.   Bruce, E. E.; Bui, P. T.; Rogers, B. A.; Cremer, P. S.; Van Der Vegt, N. F., *Journal of the American Chemical Society* **2019,** *141* (16), 6609-6616.

215.   Caykara, T.; Kiper, S.; Demirel, G., *European Polymer Journal* **2006,** *42* (2), 348-355.

216.   Sumaru, K.; Ohi, K.; Takagi, T.; Kanamori, T.; Shinbo, T., *Langmuir* **2006,** *22* (9), 4353-4356.

217.   Xulu, P. M.; Filipcsei, G.; Zrínyi, M., *Macromolecules* **2000,** *33* (5), 1716-1719.

218.   Kim, S. J.; Park, S. J.; Lee, S. M.; Lee, Y. M.; Kim, H. C.; Kim, S. I., *Journal of Applied Polymer Science* **2003,** *89* (4), 890-894.

219.   Carter, M. C.; Sorrell, C. D.; Serpe, M. J., *The Journal of Physical Chemistry B* **2011,** *115* (49), 14359-14368.

220.   Liu, J.; Soo Yun Tan, C.; Lan, Y.; Scherman, O. A., *Journal of Polymer Science Part A: Polymer Chemistry* **2017,** *55* (18), 3105-3109.

221.   Xue, W.; Hamley, I. W., *Polymer* **2002,** *43* (10), 3069-3077.

222.   Lee, W.-F.; Chiu, R.-J., *Materials Science and Engineering: C* **2002,** *20* (1-2), 161-166.

223.   Frei, E.; Karon, M.; Levin, R. H.; Freireich, E. J.; Taylor, R. J.; Hananian, J.; Selawry, O.; Hollan, J. F.; Hoostraten, B.; Wolman, I. J., *Blood* **1965,** *26* (5), 642-656.

224.   Hersh, E. M.; Carbone, P. P.; Wong, V. G.; Freireich, E. J., *Cancer Research* **1965,** *25* (7 Part 1), 997-1001.

225.   Guarneri, V.; Conte, P. F., *European Journal of Nuclear Medicine and Molecular Imaging* **2004,** *31* (1), S149-S161.

226.   Lehár, J.; Krueger, A. S.; Avery, W.; Heilbut, A. M.; Johansen, L. M.; Price, E. R.; Rickles, R. J.; Short Iii, G. F.; Staunton, J. E.; Jin, X., *Nature Biotechnology* **2009,** *27* (7), 659.

227.   Wu, J.-L.; Wang, C.-Q.; Zhuo, R.-X.; Cheng, S.-X., *Colloids and Surfaces B: Biointerfaces* **2014,** *123*, 498-505.

228.   He, Q.; Gao, Y.; Zhang, L.; Zhang, Z.; Gao, F.; Ji, X.; Li, Y.; Shi, J., *Biomaterials* **2011,** *32* (30), 7711-7720.

229.   Shin, H.-C.; Alani, A. W.; Rao, D. A.; Rockich, N. C.; Kwon, G. S., *Journal of Controlled Release* **2009,** *140* (3), 294-300.

230.   Guo, Y.; He, W.; Yang, S.; Zhao, D.; Li, Z.; Luan, Y., *Colloids and Surfaces B: Biointerfaces* **2017,** *151*, 119-127.

231.   Cho, H.; Kwon, G. S., *Journal of Drug Targeting* **2014,** *22* (7), 669-677.

232.   Salmaso, S.; Semenzato, A.; Bersani, S.; Matricardi, P.; Rossi, F.; Caliceti, P., *International Journal of Pharmaceutics* **2007,** *345* (1-2), 42-50.

233.   Wang, Q.; Zhang, H.; Xu, H.; Zhao, Y.; Li, Z.; Li, J.; Wang, H.; Zhuge, D.; Guo, X.; Xu, H., *Theranostics* **2018,** *8* (16), 4429.

234.   Vecchione, R.; Coppola, S.; Esposito, E.; Casale, C.; Vespini, V.; Grilli, S.; Ferraro, P.; Netti, P. A., *Advanced Functional Materials* **2014,** *24* (23), 3515-3523.

235.   Wang, W.; Wat, E.; Hui, P. C.; Chan, B.; Ng, F. S.; Kan, C.-W.; Wang, X.; Hu, H.; Wong, E. C.; Lau, C. B., *Scientific Reports* **2016,** *6*, 24112.

236.   Liu, M.; Song, X.; Wen, Y.; Zhu, J.-L.; Li, J., *ACS Applied Materials & Interfaces* **2017,** *9* (41), 35673-35682.

237.   Appel, E. A.; Tibbitt, M. W.; Webber, M. J.; Mattix, B. A.; Veiseh, O.; Langer, R., *Nature Communications* **2015,** *6*, 6295.

238.   Han, L.; Lu, X.; Wang, M.; Gan, D.; Deng, W.; Wang, K.; Fang, L.; Liu, K.; Chan, C. W.; Tang, Y., *Small* **2017,** *13* (2), 1601916.

239.   Han, L.; Yan, L.; Wang, K.; Fang, L.; Zhang, H.; Tang, Y.; Ding, Y.; Weng, L.-T.; Xu, J.; Weng, J., *NPG Asia Materials* **2017,** *9* (4), e372.

240.   Van Tran, V.; Park, D.; Lee, Y.-C., *Environmental Science and Pollution Research* **2018,** *25* (25), 24569-24599.

241.   Plank, T. N.; Skala, L. P.; Davis, J. T., *Chemical Communications* **2017,** *53* (46), 6235-6238.

242.   Culver, H. R.; Clegg, J. R.; Peppas, N. A., *Accounts of Chemical Research* **2017,** *50* (2), 170-178.

243.   Chen, P.; Wang, S.; Inci, F.; Güven, S.; Tasoglu, S.; Demirci, U., Cell-encapsulating Hydrogels for Biosensing. In *GELS HANDBOOK: Fundamentals, Properties and Applications Volume 3: Application of Hydrogels in Drug Delivery and Biosensing*, World Scientific: 2016; pp 327-356.

244.   Medeiros, S.; Santos, A.; Fessi, H.; Elaissari, A., *International Journal of Pharmaceutics* **2011,** *403* (1-2), 139-161.

245.   Cheng, R.; Meng, F.; Deng, C.; Klok, H.-A.; Zhong, Z., *Biomaterials* **2013,** *34* (14), 3647-3657.

246.   Zhang, Q. M.; Serpe, M. J., *ACS Applied Materials & Interfaces* **2015,** *7* (49), 27547-27553.

247.   Islam, M. R.; Li, X.; Smyth, K.; Serpe, M. J., *Angewandte Chemie International Edition* **2013,** *52* (39), 10330-10333.

248.   Baek, K.; Jeong, J. H.; Shkumatov, A.; Bashir, R.; Kong, H., *Advanced Materials* **2013,** *25* (39), 5568-5573.

249.   Veiseh, O.; Doloff, J. C.; Ma, M.; Vegas, A. J.; Tam, H. H.; Bader, A. R.; Li, J.; Langan, E.; Wyckoff, J.; Loo, W. S., *Nature Materials* **2015,** *14* (6), 643.

250.   Rivest, C.; Morrison, D.; Ni, B.; Rubin, J.; Yadav, V.; Mahdavi, A.; Karp, J.; Khademhosseini, A., *Journal of Mechanics of Materials and Structures* **2007,** *2* (6), 1103-1119.

251.   Fu, G.; Soboyejo, W., *Materials Science and Engineering: C* **2011,** *31* (5), 1084-1090.

252.   Meng, Z.; Smith, M. H.; Lyon, L. A., *Colloid and Polymer Science* **2009,** *287* (3), 277-285.

253.   Ayed, L.; Cheriaa, J.; Laadhari, N.; Cheref, A.; Bakhrouf, A., *Annals of Microbiology* **2009,** *59* (2), 267.

254.   Patel, K. R.; Tang, H.; Grever, W. E.; Ng, K. Y. S.; Xiang, J.; Keep, R. F.; Cao, T.; McAllister II, J. P., *Biomaterials* **2006,** *27* (8), 1519-1526.

255.   Lewis, W. J.; Alexander, D., *Grafting and budding: A Practical Guide for Fruit and Nut Plants and Ornamentals*. Landlinks Press: 2008.

256.   Darikova, J. A.; Savva, Y. V.; Vaganov, E. A.; Grachev, A. M.; Kuznetsova, G. V., *Журнал Сибирского федерального университета. Серия: Биология* **2011,** *4* (1), 54-63.

257.   Vršič, S.; Pulko, B.; Kocsis, L., *Scientia Horticulturae* **2015,** *181*, 168-173.

258.   Bromberg, L. E.; Ron, E. S., *Advanced Drug Delivery Reviews* **1998,** *31* (3), 197-221.

259.   Ayano, E.; Karaki, M.; Ishihara, T.; Kanazawa, H.; Okano, T., *Colloids and Surfaces B: Biointerfaces* **2012,** *99*, 67-73.

260.   Zavgorodnya, O.; Serpe, M. J., *Colloid and Polymer Science* **2011,** *289* (5-6), 591-602.

261.   Karg, M.; Lu, Y.; Carbó-Argibay, E.; Pastoriza-Santos, I.; Pérez-Juste, J.; Liz-Marzán, L. M.; Hellweg, T., *Langmuir* **2009,** *25* (5), 3163-3167.

262.   Niikura, K.; Iyo, N.; Matsuo, Y.; Mitomo, H.; Ijiro, K., *ACS Applied Materials & Interfaces* **2013,** *5* (9), 3900-3907.

263.   Zhang, Q. M.; Li, X.; Islam, M. R.; Wei, M.; Serpe, M. J., *Journal of Materials Chemistry C* **2014,** *2* (34), 6961-6965.

264.   Fischer, W.; Quadir, M. A.; Barnard, A.; Smith, D. K.; Haag, R., *Macromolecular Bioscience* **2011,** *11* (12), 1736-1746.

265.   Sahoo, B.; Devi, K. S. P.; Banerjee, R.; Maiti, T. K.; Pramanik, P.; Dhara, D., *ACS Applied Materials & Interfaces* **2013,** *5* (9), 3884-3893.

266.   Kwon, I. C.; Bae, Y. H.; Kim, S. W., **1991**.

267.   Ge, J.; Neofytou, E.; Cahill III, T. J.; Beygui, R. E.; Zare, R. N., *ACS Nano* **2011,** *6* (1), 227-233.

268.   Slowing, I. I.; Trewyn, B. G.; Giri, S.; Lin, V. Y., *Advanced Functional Materials* **2007,** *17* (8), 1225-1236.

269.   Nadrah, P.; Maver, U.; Jemec, A.; Tišler, T.; Bele, M.; Dražić, G.; Benčina, M.; Pintar, A.; Planinšek, O.; Gaberšček, M., *ACS Applied Materials & Interfaces* **2013,** *5* (9), 3908-3915.

270.   Chu, L. Y.; Yamaguchi, T.; Nakao, S.-i., *Advanced Materials* **2002,** *14* (5), 386-389.

271.   Hoare, T.; Pelton, R., *Langmuir* **2008,** *24* (3), 1005-1012.

272.   Zhang, J.; Yuan, Z.-F.; Wang, Y.; Chen, W.-H.; Luo, G.-F.; Cheng, S.-X.; Zhuo, R.-X.; Zhang, X.-Z., *Journal of the American Chemical Society* **2013,** *135* (13), 5068-5073.

273.   Wu, C.; Zhou, S., *Macromolecules* **1995,** *28* (24), 8381-8387.

274.   Zhang, G.; Wu, C., *Journal of the American Chemical Society* **2001,** *123* (7), 1376-1380.

275.   Ma, X.; Cui, Y.; Zhao, X.; Zheng, S.; Tang, X., *Journal of Colloid and Interface Science* **2004,** *276* (1), 53-59.

276.   Rubio-Retama, J.; Zafeiropoulos, N. E.; Serafinelli, C.; Rojas-Reyna, R.; Voit, B.; Lopez Cabarcos, E.; Stamm, M., *Langmuir* **2007,** *23* (20), 10280-10285.

277.   Islam, M. R.; Serpe, M. J., *Macromolecules* **2013,** *46* (4), 1599-1606.

278.   Islam, M. R.; Serpe, M. J., *Chemical Communications* **2013,** *49* (26), 2646-2648.

279.   Smiley-Wiens, J. B.; Serpe, M. J., *Colloid and Polymer Science* **2013,** *291* (4), 971-979.

280.   Hu, L.; Serpe, M. J., *Polymers* **2012,** *4* (1), 134-149.

281.   Islam, M. R.; Serpe, M. J., *Biosensors and Bioelectronics* **2013,** *49*, 133-138.

282.   Islam, M. R.; Serpe, M. J., *APL Materials* **2013,** *1* (5), 052108.

283.   Islam, M. R.; Gao, Y.; Li, X.; Serpe, M. J., *Journal of Materials Chemistry B* **2014,** *2* (17), 2444-2451.

284.   Burmistrova, A.; von Klitzing, R., *Journal of Materials Chemistry* **2010,** *20* (17), 3502-3507.

285.   Ferguson, J.; Smith, E.; Weimer, A.; George, S., *Journal of The Electrochemical Society* **2004,** *151* (8), G528-G535.

286.   Deng, X.; Mammen, L.; Butt, H.-J.; Vollmer, D., *Science* **2012,** *335* (6064), 67-70.

287.   Kobayashi, Y.; Katakami, H.; Mine, E.; Nagao, D.; Konno, M.; Liz-Marzán, L. M., *Journal of Colloid and Interface Science* **2005,** *283* (2), 392-396.

288.   Mitchell, D.; Clark, K.; Bardwell, J.; Lennard, W.; Massoumi, G.; Mitchell, I., *Surface and Interface Analysis* **1994,** *21* (1), 44-50.

289.   Kneuer, C.; Sameti, M.; Haltner, E. G.; Schiestel, T.; Schirra, H.; Schmidt, H.; Lehr, C.-M., *International Journal of Pharmaceutics* **2000,** *196* (2), 257-261.

290.   Lu, Y.; Yin, Y.; Mayers, B. T.; Xia, Y., *Nano Letters* **2002,** *2* (3), 183-186.

Appendix A: Supporting Information for Chapters
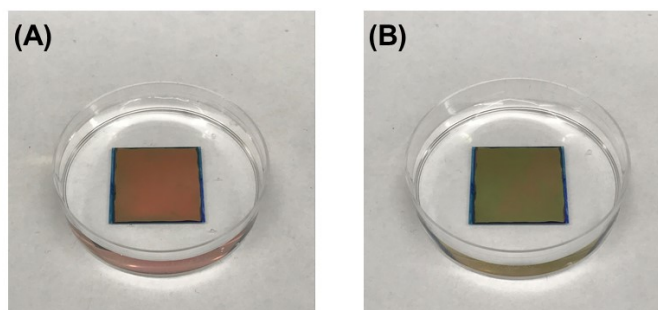
Figure A-1. Photographs of pNIPAm-*co*-AAc microgel-based etalon soaking in (A) pH 6.5 and (B) pH 3 solutions (2-mM NaCl).
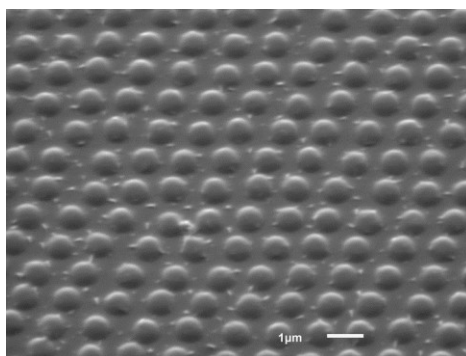
Figure A-2. A SEM image of CV-loaded pNIPAm-*co*-AAc microgels. (Scale bar = 1 μm)
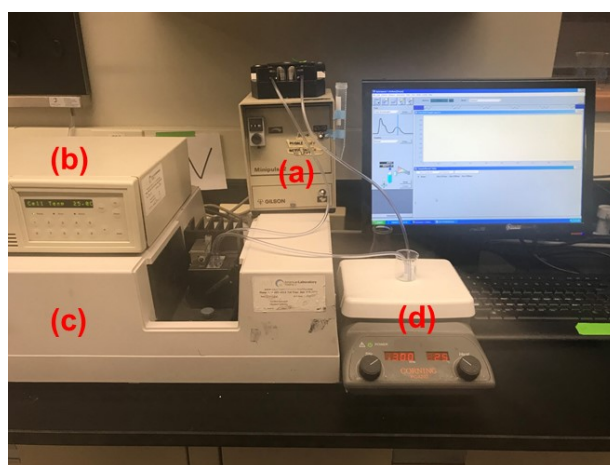
Figure A-3. A photograph of an instrumental setup for the CV release experiments. (a) Peristatic pump, (b) Temperature controller, (c) UV-Vis spectrometer, and (d) Heating/stirring plate.
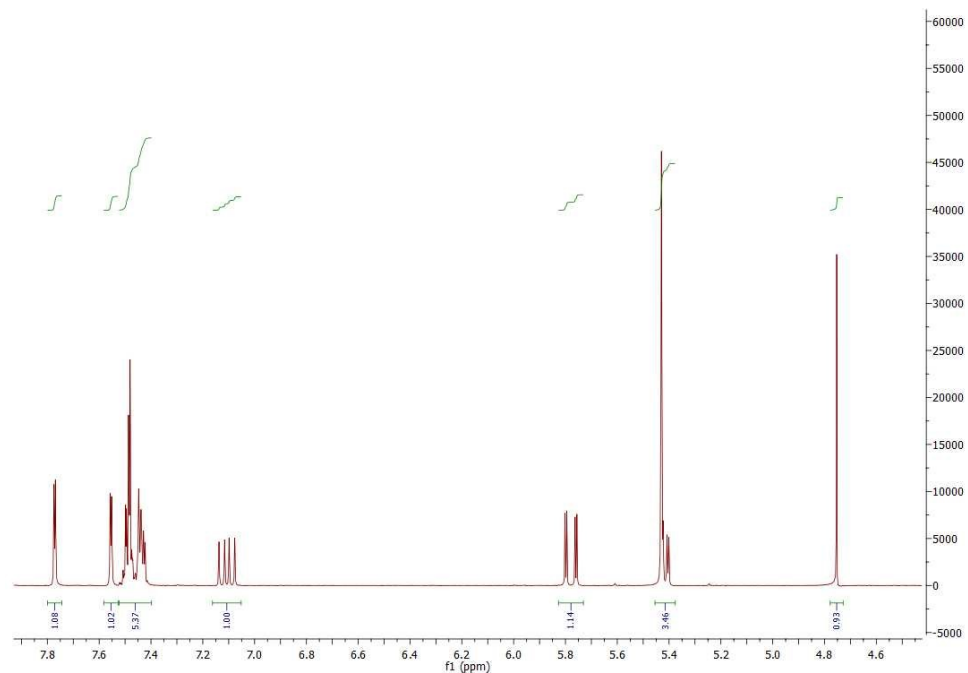
Figure A-4. ^{1}H NMR spectrum (400 MHz, D$_2$O) of 1-benzyl-3-vinylimidazolium bromide (BVB).
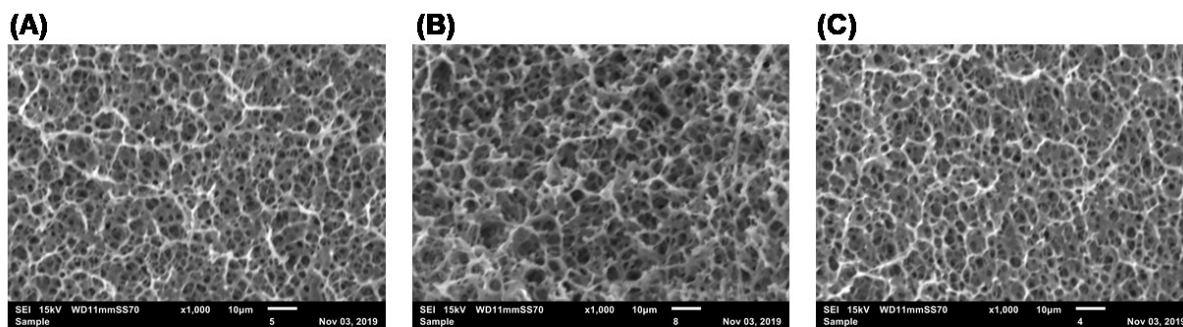
Figure A-5. SEM images of (A) HMC-5BISa, (B) HMC-10OMA, and (C) HMC-10HEAm.

Appendix B: Controlled Release Kinetics from a Surface Modified Microgel-Based Reservoir Device

B.1 Introduction

Stimuli responsive polymer-based materials are often referred as "smart materials" due to their ability to respond to external stimuli, e.g., temperature,[258] pH,[82, 259-261] light,[262-264] magnetic field,[265] and electrical field.[266-267] In the last few decades, functional stimuli responsive materials such as porous materials,[268-270] microgels,[271] and nanogels[272-273] have been used to encapsulate and release small molecules (or drugs) in a controlled and triggered fashion. Among stimuli responsive polymers, poly (N-isopropylacrylamide) (pNIPAm) is by far the most extensively studied to date; a direct result of its thermoresponsivity.[8, 94, 273-274] Specifically, pNIPAm exhibits a lower critical solution temperature (LCST) of 32°C in water, which is close to physiological temperature. Above the LCST, pNIPAm undergoes a transition from a random coil (extended state) to a globule (collapsed state), expelling its solvating water in the process.

PNIPAm can be crosslinked into a polymer network, and hydrogel particles (nanogels or microgels, depending on diameter) can be synthesized. These networks also undergo a swollen-to-collapsed transition in water at elevated temperature. Specifically, pNIPAm-based microgels transition from a swollen (large diameter) to a collapsed (small diameter) state at elevated temperature.[219, 275-276] Like all temperature induced conformational state changes of pNIPAm, the transition for pNIPAm-based microgels is fully reversible over many cycles. PNIPAm-based microgels can also be made responsive to other stimuli, in addition to temperature. For example, copolymerization of functional

monomers or crosslinkers into the pNIPAm network can make them responsive to, e.g., pH, light and/or electric field.[261, 263, 267] A well-known pH responsive pNIPAm-based microgel is pNIPAm-*co*-acrylic acid (pNIPAm-*co*-AAc), which is made by simply adding AAc at the time of synthesis.[82] AAc exhibits a pK_a of 4.25, therefore pNIPAm-*co*-AAc microgels are negatively charged at pH > 4.25, while they are neutralized at pH < 4.25. The charge switchability of the pNIPAm-*co*-AAc microgels allows them to bind and release positively charged molecules at pH > pK_a, and pH < pK_a, respectively.[177]

In previous work, we showed that optical devices, known as etalons, could be generated by "sandwiching" a homogeneous monolayer of pNIPAm-*co*-AAc microgels between two thin Au layers.[82, 177, 179, 181, 186, 219, 277-281] The structure of this device can be seen in Figure B-1. The optical properties of these devices have been studied in great detail, and they have been used for sensing a variety of species.[282-283] We also found that the structure could be used for controlled and triggered drug delivery. Importantly, we determined that the release rate depended greatly on the thickness of the Au layer covering the microgel layer (Au overlayer), which systematically varied the pore size. Therefore, thick Au layers slowed the release properties compared to thin Au layers.[177]
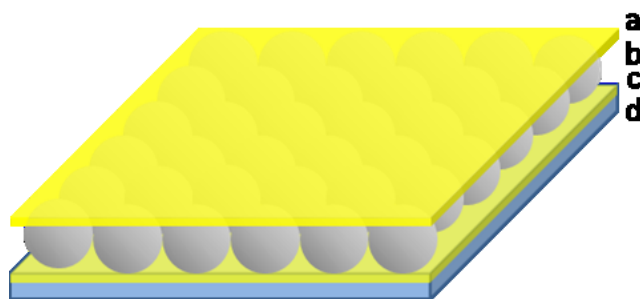
Figure B-1. Structure of a pNIPAm microgel-based etalon. (a) 50 nm Au layer (with 2 nm Cr adhesion layer) sandwiching (b) a microgel layer all on a (c,d) glass substrate coated with 15 nm Au layers (with 2 nm Cr adhesion layer). (Reprinted with permission from RSC)

In those studies, we used Au layer thicknesses of up to 700 nm, which increases the device's cost and fabrication time dramatically. Therefore, new ways to control release rates are needed. In this submission, we modify the Au overlayer porosity by adding a layer of silica via the hydrolysis of tetraethyl orthosilicate (TEOS) vapor with water in the presence of ammonia. Using this approach, we were able to decrease the Au overlayer thickness to below 50 nm and subsequently modify the Au layer with silica to control the release rates. By varying the silica layer thickness by varying the modification time, the release rate could be effectively controlled and tuned, i.e., long modification time leads to slow release rates. This low-cost and effective method provides an alternative way to control and trigger drug release by using the microgel-based drug reservoir systems.

B.2 Experimental Section

B.2.1 Materials

N-isopropylacrylamide (NIPAm) was purchased from TCI (Portland, Oregon) and purified by recrystallization from hexanes (ACS reagent grade, EMD, Gibbstown, NJ) prior to use. *N,N'*-methylenebisacrylamide (BIS) (99%), acrylic acid (AAc) (99%), and ammonium persulfate (APS) (98+%) were obtained from Sigma-Aldrich (St. Louis, MO) and were used as received. Tris (4-(dimethylamino)phenyl)methylium chloride (Crystal Violet, CV) and tetraethyl orthosilicate (TEOS, 98%) were obtained from Sigma-Aldrich (St. Louis, MO). Sodium chloride was obtained from EMD (Millipore, Billerica, MA), and deionized (DI) water with a resistivity of 18.2 M$\Omega \times$cm was used. Cr/Au annealing was done in a Thermolyne muffle furnace from ThermoFisher Scientific (Ottawa, Ontario). Anhydrous

ethanol was obtained from Commercial Alcohols (Brampton, Ontario). Sodium hydroxide (NaOH, 99.8%) and hydrochloric acid were purchased from Caledon Chemicals (Georgetown, Ontario) and were used as received. Fisher's finest glass coverslips were 25 × 25 mm and obtained from Fisher Scientific (Ottawa, Ontario). Cr was 99.999% and obtained from ESPI as flakes (Ashland, OR), while Au was 99.99% and obtained from MRCS Canada (Edmonton, AB).

B.2.2 Microgel Synthesis

Temperature-ramp, surfactant-free, free radical precipitation polymerization was used to synthesize mcirogels, as previously described.[284] Briefly, a 3-necked round- bottom flask was fitted with a reflux condenser, nitrogen inlet, and temperature probe, and charged with a solution of monomer mixture, comprised of NIPAm (11.9 mmol) and BIS (0.703 mmol) in 99 mL of deionized water, previously filtered through a 0.2 μm filter. The solution was bubbled with N_2 while stirring and heated to 70 °C over ~1 hour. 99 μL of AAc (1.43 mmol) was added to the heated reaction mixture with micropipette in one aliquot. The reaction was then initiated with an ammonium persulfate (APS) solution, prepared by dissolving 0.2 mmol APS in 1mL of deionized water. The reaction was then allowed to proceed at 70℃ for 4 hours under a blanket of nitrogen and vigorous stirring. The resulting suspension was allowed to cool overnight while stirring, and then filtered through glass wool to remove any large aggregates. About 12 mL of the microgel suspension was then distributed into centrifuge tubes and washed via centrifugation at ~8500 rcf for 45 min to form a pellet at the bottom of centrifuge tubes, followed by removal of the supernatant. And then the pellet of microgel was re-suspended with original volume, 12 mL, of deionized water. This

process was repeated to a total of six times to remove any unreacted monomers. The purified microgels were recombined and stored in a brown glass jar.

B.2.3 CV Loaded Etalon Fabrication

CV loaded etalons were fabricated by using a previously reported protocol with slight modification.[219] The process is shown in Figure B-2. To fabricate the Au coated glass substrates (etalon underlayer), 2 nm Cr and 15 nm of Au was sequentially thermally evaporated at a rate of 0.2 Å s^{-1}, and 0.1 Å s^{-1}, respectively, (Torr International Inc., thermal evaporation system, Model THEUPG, New Windsor, NY) onto a 25 x 25 mm DI water/ethanol rinsed and N$_2$ gas dried glass substrate (Fisher's Finest, Ottawa, ON). The Cr/Au coated substrates were annealed at 250 °C for 3 h (Thermolyne muffle furnace, Ottawa, ON) and cooled down to room temperature prior to microgel film painting. The annealed substrate was washed with deionized water and ethanol followed by drying with N$_2$ gas. Then a 40 µL aliquot of the concentrated microgels was dispensed onto the substrate and then spread toward each edge using the side of a micropipet tip. The substrate was rotated 90°, and the microgel solution was spread again. The spreading and rotation continued until the microgel solution became too viscous to spread due to drying. The microgel solution was allowed to dry completely on the substrate for 2 h with the hot plate temperature set to 35 °C. After that, the dry film was rinsed copiously with DI water to remove any excess microgels not directly bound to the Au. The microgel painted substrate was then placed into a DI water bath and allowed to incubate overnight on a hot plate set to 30 °C. Following this step, the substrate was again rinsed with DI water to further remove any microgels not bound directly to the Au substrate surface. The samples were

then dried with N$_2$, and soaked in CV solution (4 mg/mL, pH of 6.5) for 5 hours. The substrates were again rinsed with pH 6.5 solution (to maintain the microgel-CV interaction) to remove excess CV not bound to the microgels, and incubated in pH 6.5 solution for 1 hour followed by drying with N$_2$ gas. Finally, another 2 nm Cr and 50 nm of Au metal layers were deposited on the microgel layer.
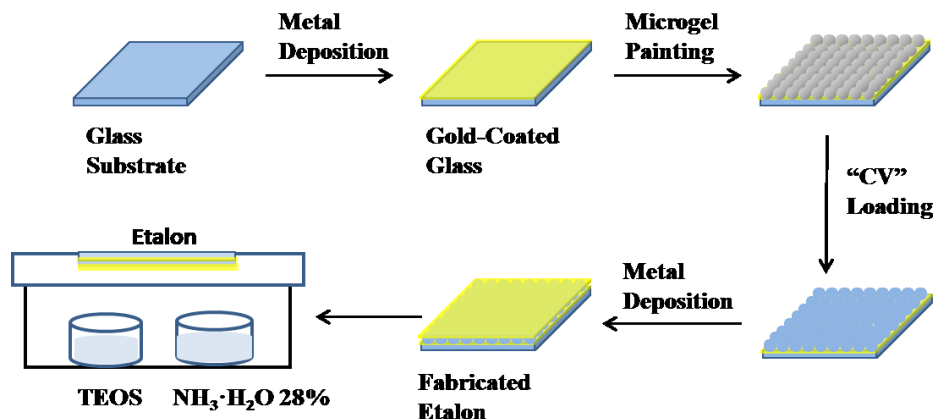
Figure B-2. Schematic showing the fabrication of the reservoir devices. (Reprinted with permission from RSC)

B.2.4 Au Overlayer Modification with Silica

Two 0.5 mL glass vessels were placed inside of a glass Petri dish. 0.4 mL of TEOS and NH$_3$ (28% in water) were added separately into each vessel. Another Petri dish, with a CV-loaded device secured inside, was placed on top of the above Petri dish such that the Au overlayer was facing the TEOS/NH$_3$ vessels. Parafilm was used to completely seal the system. The whole apparatus was held at room temperature, for different periods of time, to yield SiO$_2$ (silica) layers with various thicknesses. After silica layer formation, the etalon edges were sealed with clear nail polish, to ensure CV could only exit the microgel layer through the Au/silica overlayer.

B.2.5 CV Release Experiments

A Petri dish filled with 20 mL of water at pH 3 (ionic strength=2 mM) was placed on a hot plate, and the solution temperature was maintained at 25℃. The solution in the Petri dish was stirred continuously at 400 rpm using a magnetic stir bar. A peristaltic pump was used to pump the solution through a quartz cuvette in an Agilent 8453 UV-Vis spectrophotometer, equipped with an 89090A temperature controller and Peltier heating device. The absorbance spectrum of the solution was collected every minute. The flow rate of the solution was set to a constant value, 0.042 mL/s (as measured).

B.3 Results and Discussion

PNIPAm microgel-based etalons loaded with the small molecule tris (4-(dimethylamino)phenyl)methylium chloride (Crystal Violet, CV) were generated. The procedure is outlined in Figure B-2 and detailed above. Briefly, microgels attached to a Au coated glass substrate were loaded with CV, by soaking them in a CV solution with a pH 6.5 that renders the microgels negatively charged, and the CV positively charged. This layer was subsequently coated with another layer of Cr and Au, and the "sandwich" structure exposed to TEOS for various times. The reaction of TEOS with water to form silica is shown below, and has been utilized previously for coating surfaces. [285-287]

$$Si(OCH_2CH_3)_4 + H_2O \xrightarrow{NH_3 \text{ catalyst}} (SiO_2)_n + CH_3CH_2OH$$
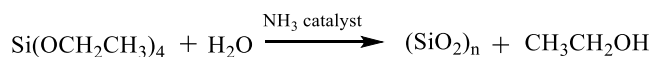
A schematic depiction of the silica layer generation is shown in Figure B-3. We hypothesize that the silica layer covers the surface of the Au overlayer and fills in the Au overlayer pores to block the path of CV exiting the microgel layer to enter the surrounding

solution. As the modification time is increased, the silica layer thickness should likewise increase, and more of the Au pores should be filled. The surface morphology of the resulting devices was investigated using atomic force microscopy (AFM, tapping mode, Asylum Research, Santa Barbara, CA) at room temperature. The images are shown in Figure B-4. From the images it can be seen that the microgel curvature is obvious before silica layer formation, while the curvature is diminished after silica layer formation. From the image, the apparent microgel diameter (diameter that can be measured, not necessarily the absolute diameter) before silica layer deposition was ~500 nm, while it appears to increase to ~700 nm as a result of silica layer deposition. The surface morphology is also clearly affected by the silica layer deposition. These observations allow us to conclude that the silica layers are forming on the Au overlayer.
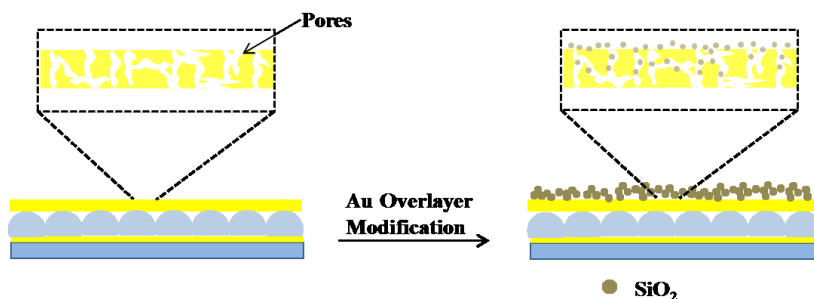
Figure B-3. Schematic illustrating the pores in Au layers that allow CV to be transferred from the microgel layer to the system, and how this is changed by the addition of the silica layers. (Reprinted with permission from RSC)

(a)
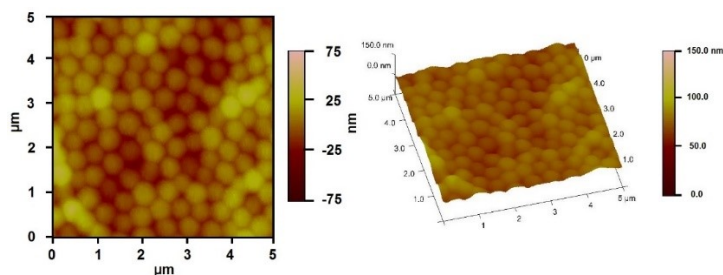
(b)
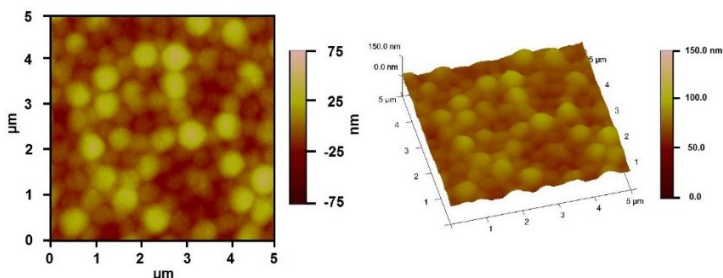
Figure B-4. AFM images of surface morphology of the reservoir devices (a) before, and (b) after 9 h silica layer growth. (Reprinted with permission from RSC)

X-ray photoelectron spectroscopy (XPS) was also used to confirm the elemental composition of the overlayers after silica layer deposition, and how the atomic mole percent of silicon was affected by deposition time. The signal at 104 eV from the XPS spectrum (data not shown) was used to determine the atomic mole percent of Si^{4+}, which is evidence of the oxide state.[288] Figure B-5 shows that as the silica layer "growth" time increased, the amount of Si^{4+} also increased, with a concomitant decrease in the Au signal due to the silica layer covering it. Also, the Second Ionization Mass Spectroscopy (SIMS) images of unmodified, 3-hour modified, and 9-hour modified samples (Figure B-6) illustrate the formation of a homogeneous silica layer covering the Au surface. These data are consistent with thicker silica layers being deposited on the device's Au overlayer as a function of increasing deposition time.
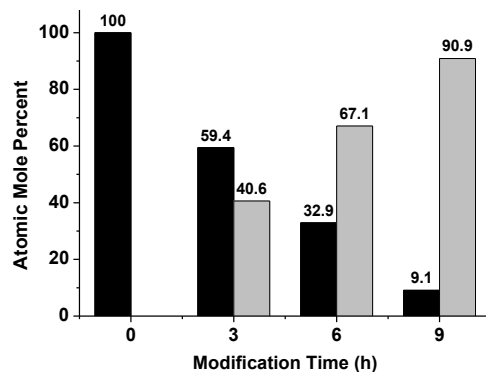
Figure B-5. Atomic mole percent of (black) Au and (grey) Si as a function of modification time, as determined from XPS analysis. (Reprinted with permission from RSC)

(a)

(b)

(c)
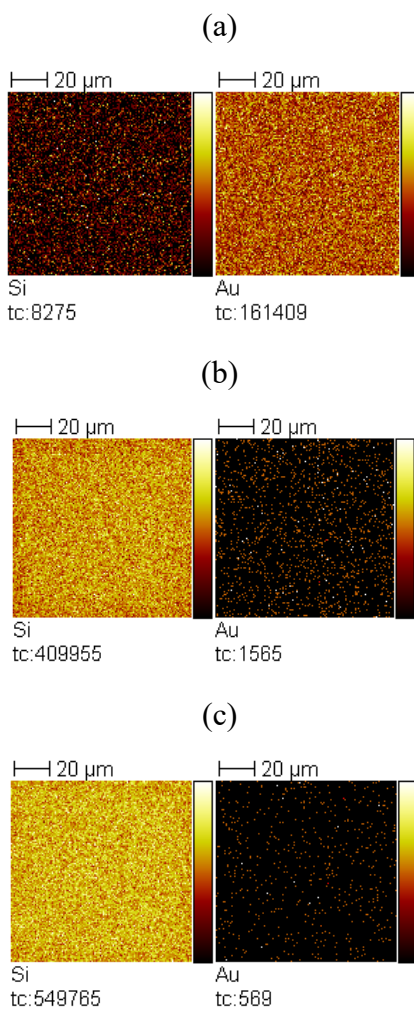
Figure B-6. SIMS images of (a) unmodified sample, (b) 3-hour modified sample, and (c) 9-hour modified sample. Field of view is 100×100 μm². (Reprinted with permission from RSC)

The electron penetration depth of SIMS and XPS are 5 nm and 10 nm, respectively. From the SIMS analysis results, very low signal from Au on a 3-hour modified sample can be observed (Figure B-6(b)). On the other hand, based on the data of XPS (Figure B-5), a significant amount of signal intensity is from Au, on a 9-hour modified sample. Conclude from these data, estimation can be made that the thickness of the silica layer is between 5 nm to 10 nm; and it's possibly greater than 10 nm when the modification time is longer than 9 hours.

Once silica layers were deposited on the device Au overlayers, the CV release kinetics were investigated. We determined the release kinetics for devices with no silica layer, and devices after 3, 6, and 9 h TEOS exposure. These experiments were completed by adding CV loaded devices to a Petri dish containing 20 mL of pH 3.0 aqueous solutions. This pH neutralizes the microgel AAc groups allowing the CV to exit the devices. Solution from the Petri dish was pumped into a cuvette held in a UV-Vis spectrometer, which was setup acquire a spectrum every 1 min for 240 min (4 h). The flow rate of the liquid was fixed at a constant value of 0.042 mL/s. CV, a water soluble dye, has a maximum absorbance at ~590 nm. Therefore, based on Beers' law, and the constant solution volume, the magnitude of the absorbance at 590 nm is proportional to the amount of CV released. Representative UV-Vis absorbance spectra from the 3 h modified sample are shown in Figure B-7a. Figure B-7b shows the full set of release kinetics. As is clearly seen, the release kinetics from the unmodified device is much faster than the modified devices. The device exposed to TEOS for 9 h clearly has the slowest release kinetics, releasing only half the CV that the unmodified devices do in the given time period.

145
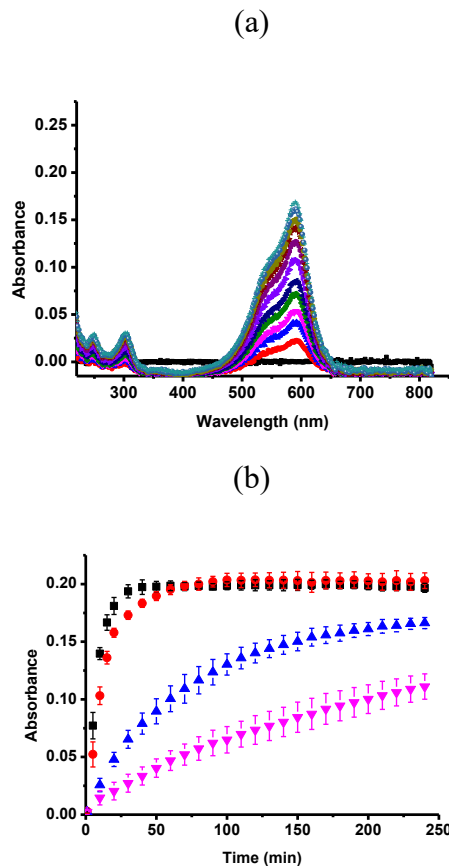
Figure B-7. (a) UV-Vis absorbance spectra for the 3h modification device as a function of time -- as time increases, the absorbance likewise increases. (b) Release profiles for the microgel-based devices in pH 3.0 solution. The modification time periods were (■) 0 hour, (●) 3 hours, (▲) 6 hours, and (▼) 9 hours. Each data point is the average of three individual measurements from three individual devices, while the error bars are the standard deviations. (Reprinted with permission from RSC)

We went on to determine the long-term release characteristics of the devices. The release kinetics of samples modified for 6 and 9 h were monitored up to 1200 minutes. The highest value of absorbance was reached by 6-hour samples at around 650 min and by 9-hour samples at around 1000 min. The final absorption values of solutions for all samples (modified and unmodified) are within the range of 0.185-0.205 after full release. Based on this result, we can conclude that the silica layers do not block CV from being released from

the devices, it simply reduces the rate at which it can enter the solution from the microgels. To further quantify this, we determined the time it takes for each device to release 50 % of total amount of loaded CV; the plot can be seen in Figure B-8. As expected, it takes devices longer to release 50% of CV when the silica layer thickness increases.
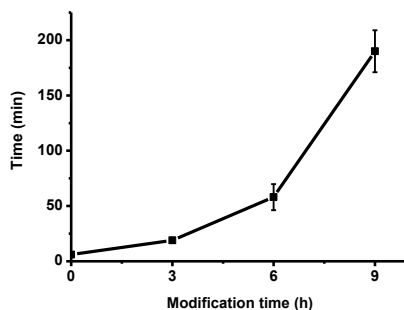
Figure B-8. Time required to release 50% of the loaded CV in pH 3.0 solutions as a function of silica modification time. Each data point is the average from three individual measurements from three individual devices, while the error bars are the standard deviations. (Reprinted with permission from RSC)

B.4 Conclusion

In this investigation, we show that pNIPAm-*co*-AAc microgel-based devices coated with silica layers are very effective at controlling the release kinetics of small molecules to a system. The layers were characterized by atomic force microscopy, which showed the devices were being modified. We also showed by XPS analysis that the amount of silica deposited on the devices was directly related to the device modification time. Finally, the release kinetics were determined, which showed that the devices released CV slower as the amount of silica on the devices increased. In the future, these silica modified devices could be used for controlled and triggered drug delivery.[289-290]

Appendix C: Preparation of a Metal-Free Free-Standing Microgel Monolayer for pH-Triggered Drug Delivery

C.1 Introduction

In this project, we prepared a free-standing microgel monolayer on a polymer film, by utilizing the self-assembling of pNIPAm-based microgels on a thermal evaporation deposited Au surface. Specifically, microgels were deposited on the Au surface, followed by spin coating a layer of polycaprolactone (PCL). When the PCL was peeled off from the substrate, microgels would be attached on the PCL film to form a free-standing microgel monolayer. This free-standing microgel monolayer exhibit its potential to be used for drug delivery applications.

Since there is a strong interaction between microgel layer and the Au surface, the removal of the microgel layer from the Au surface by the peeling-off of the PCL film is not always complete. In order to make this process more efficient, alkanethiol modifications was utilized to weaken the microgel-Au interaction. SEM images and surface plasma resonance (SPR) data show that this surface modification approach is very efficient to weaken the interaction, and the easiness of the microgel removal is related to the polarity and chain length of alkanethiol molecules.

C.2 Experimental Section

4 nm of Cr and 15 nm of Au were deposited on an ethanol rinsed, N_2 gas dried glass substrate. Then, the metal coated substrate needs to be re-rinsed with DI water and 95% ethanol, followed by incubating in 1-hexadecanethiol solution (10 mM in anhydrous ethanol). After 8 h of modification, substrates were rinsed copiously with 95% of ethanol and dried with N_2 gas.

When the pNIPAm-*co*-AAc microgel layer has been deposited on the Au-coated glass substrate with the procedure mentioned in Chapter 2, 150 µL of 8% (w/w) PCL/ethyl acetate solution was spin-coated on the microgel-coated substrate. Spin coater was set to 2000 rpm. Then the spin-coated PCL film was left in air for 5 h to make the solvent evaporate completely. Finally, the PCL film attached with the microgel layer can be peeled off from the substrate.

C.3 Schematic Diagrams
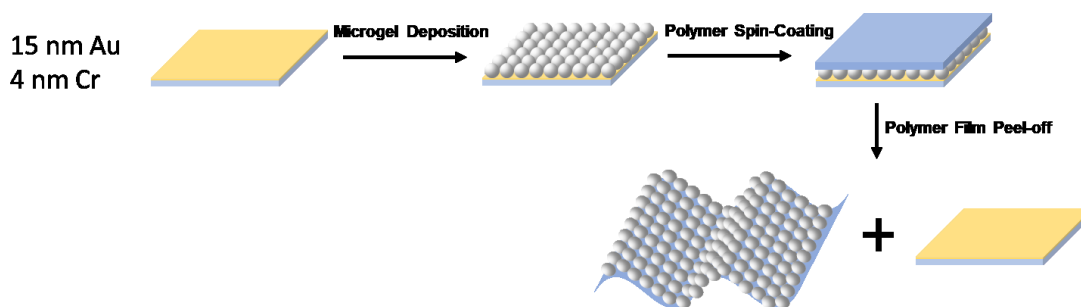
Scheme C-1. A schematic diagram of preparation steps of the free-standing metal-free microgel monolayer.
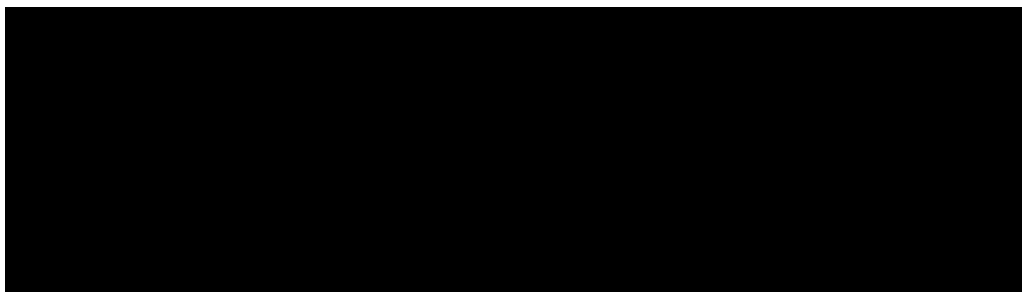
Figure C-1. Structures and names of selected alkanethiol molecules.
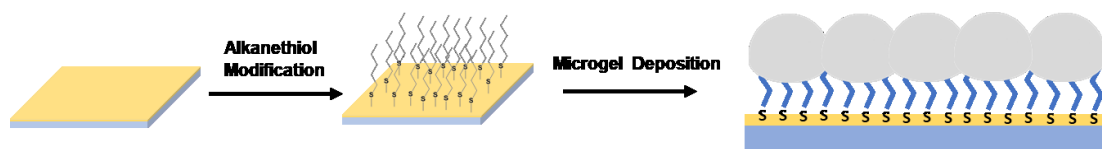
Scheme C-2. A schematic diagram of the alkanethiol layer in the self-assembled microgel monolayer on a substrate.

C.4 Preliminary Experimental Results
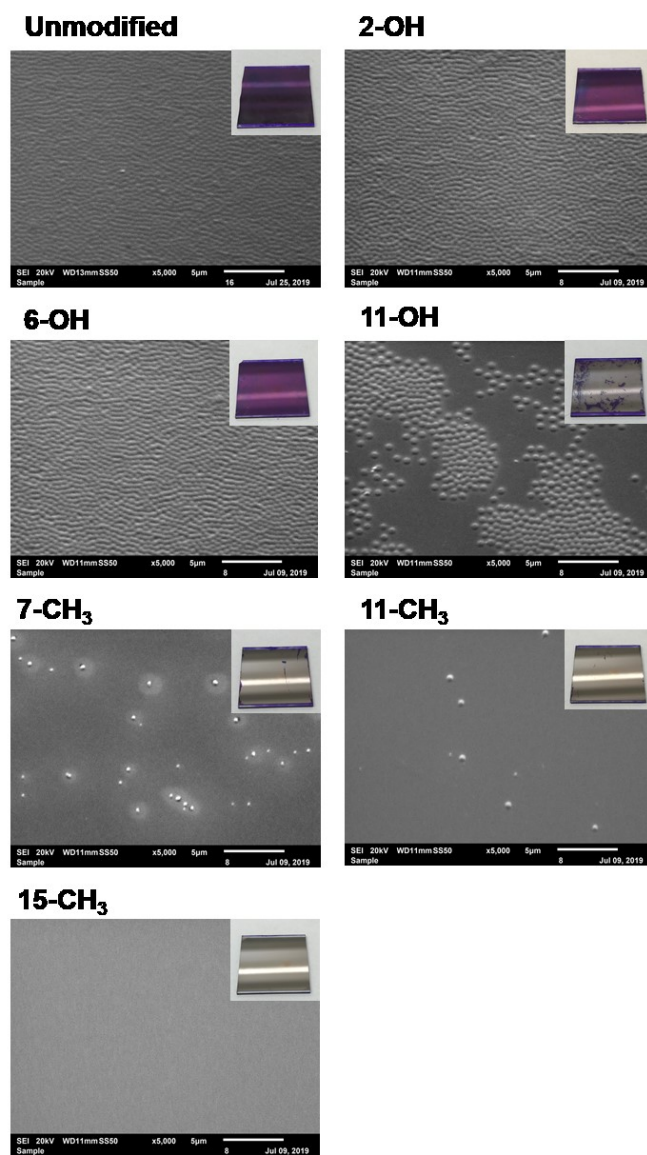
Figure C-2. SEM images of the Au surfaces after PCL film peeling-off. Sub-images are the photographs of CV-dyed leftover substrates. (Any microgels remained on the surface are dyed to violet color.)
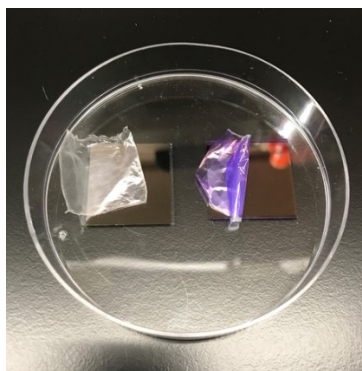
Figure C-3. A photograph of comparing free-standing metal-free microgel monolayers with (left) and without (right) CV.
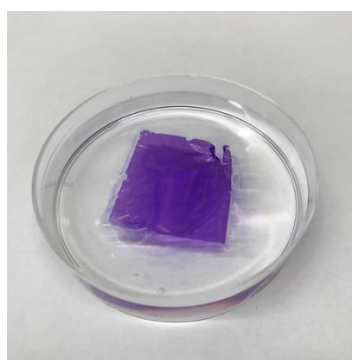
Figure C-4. A photograph of a CV-loaded free-standing microgel monolayer floating on water.
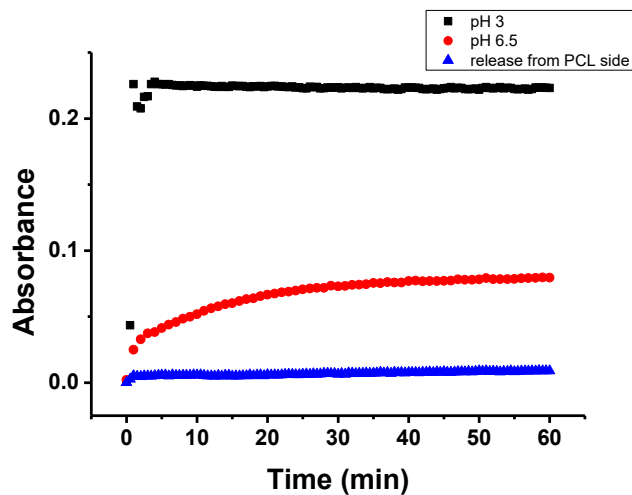
Figure C-5. CV release profiles of the CV-loaded free-standing microgel monolayer from the microgel side at pH 3 (black square), pH 6.5 (red circle), and from the PCL side (blue triangle).

Appendix D: Enhanced Hydrogel Toughness from pNIPAm-Based Microgel Supramolecular Crosslinking

D.1 Introduction

There is a widely investigated supramolecular assembly based on the trimer formed with cucurbituril [8] (CB [8]), methyl viologen (MV) moiety, and naphthalene (Nap) moiety (Scheme D-1 and D-2). CB [8] is a macrocyclic molecule that can bind to various of molecular structures and/or moieties with host-guest interactions. In this research, a microgel-based supramolecular crosslinker was synthesized to prepare a self-healable toughness enhanced hydrogel, as the pNIPAm-based microgel has hyperbranched and porous microstructures.
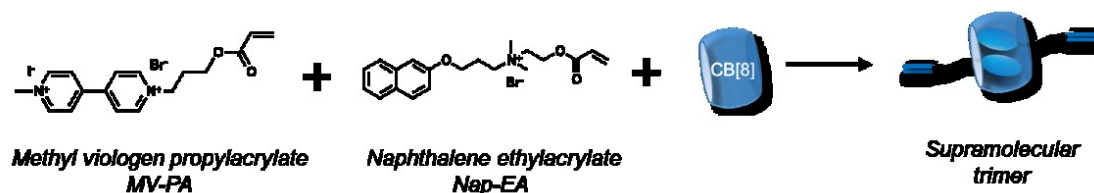
Scheme D-1. Schematic diagram of the supramolecular assembly between CB [8], methyl viologen, and naphthalene.
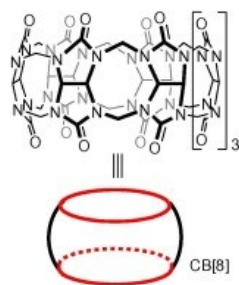
Scheme D-2. Structure and cartoon of a CB [8] molecule.

D.2 Experimental Sections

Specifically, pNIPAm-based microgels were functionalized with methyl viologen groups with the experimental procedure shown in Scheme D-3. Then the MV-functionalized microgels were used to prepare the microgel-crosslinked hydrogel (MCH) as a macromolecular crosslinker, and polyacrylamide was used as the polymer back chain, shown in Figure D-4. As a comparison, a supramolecular hydrogel (SH) was prepared with the small-molecule supramolecular crosslinker as a control sample. The orange color observed from both two hydrogels are from the charge transfer (CT) interaction between the MV and Nap in the cavity of a CB [8], and the cloudy appearance of the MCH is due to the presence of microgels.
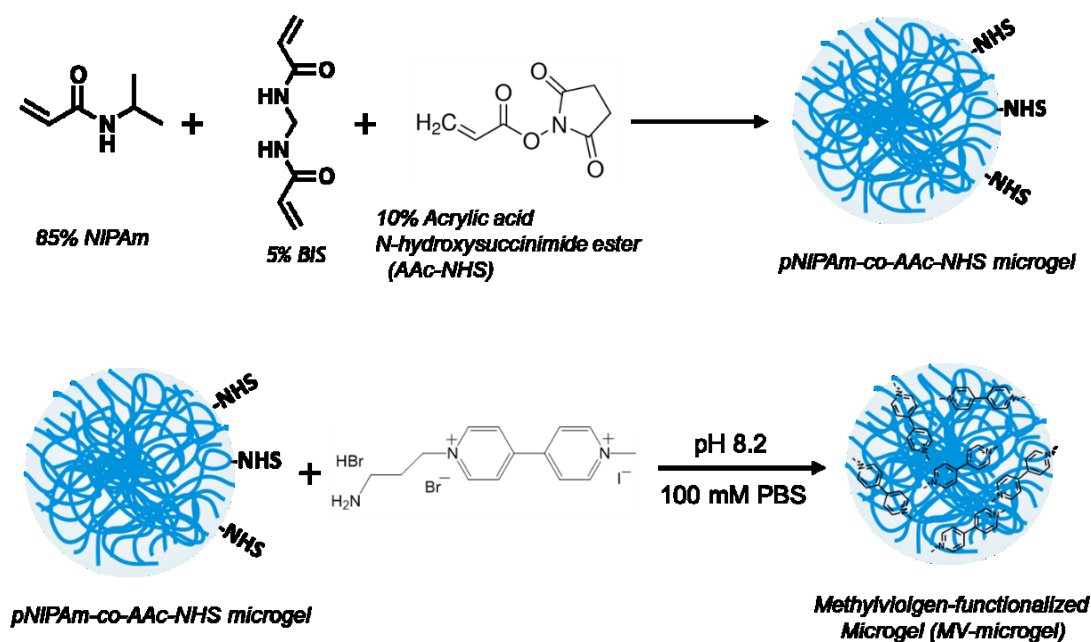
Scheme D-3. Schematic diagrams of synthesis and functionalization of MV-microgels.
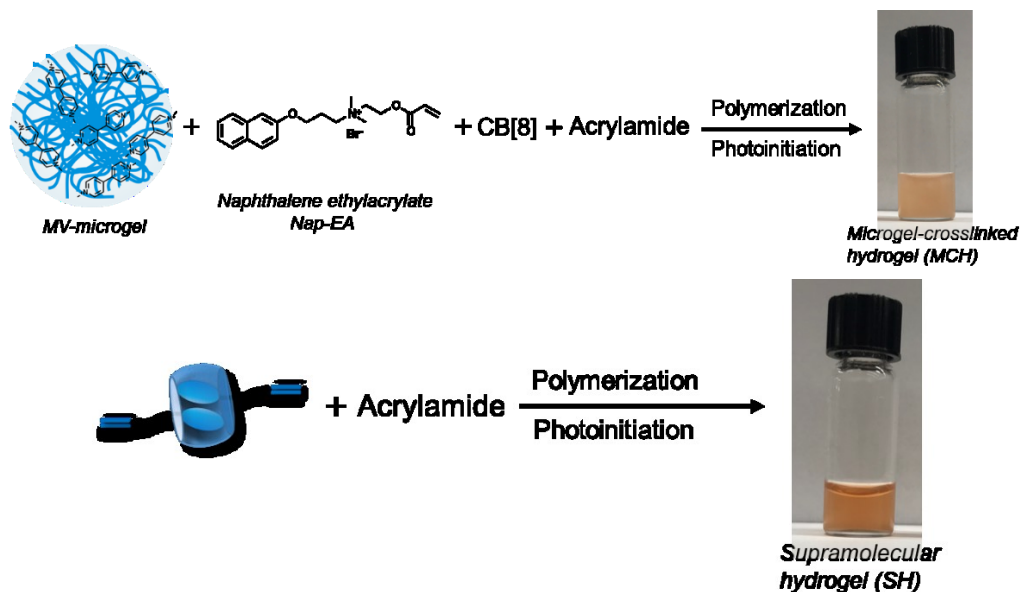
Scheme D-4. Schematic diagrams of supramolecular hydrogel preparation.

D.3 Preliminary Experimental Results
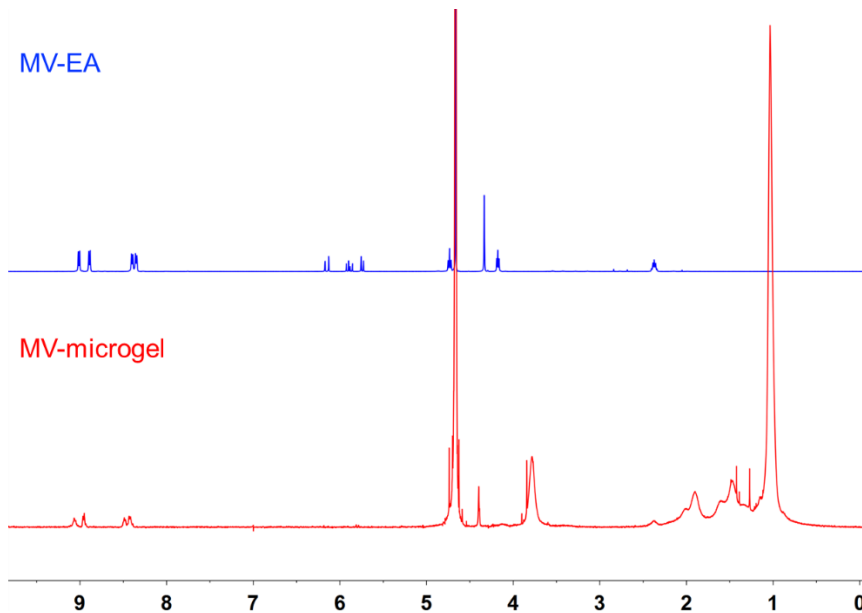
Figure D-1. H^1 NMR spectrum (400 MHz, D$_2$O) of MV-EA monomer and MV-functionalized microgels.
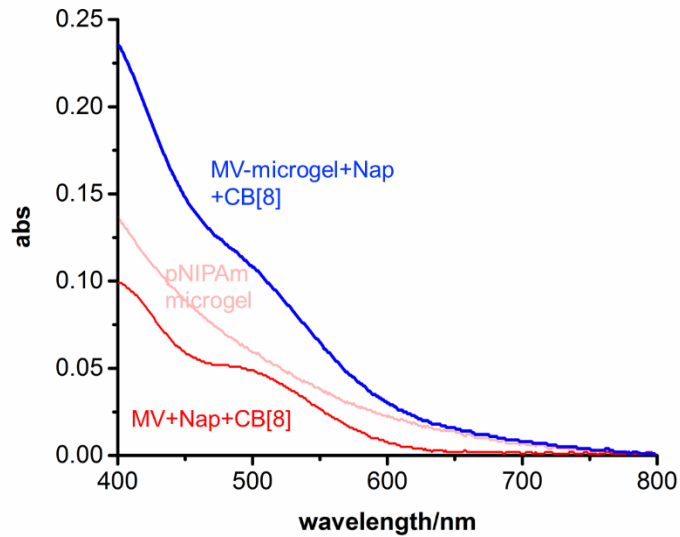
Figure D-2. UV-Vis spectrum of the supramolecular trimer, supramolecular trimer formed with MV-microgels, and normal pNIPAm-based microgels.
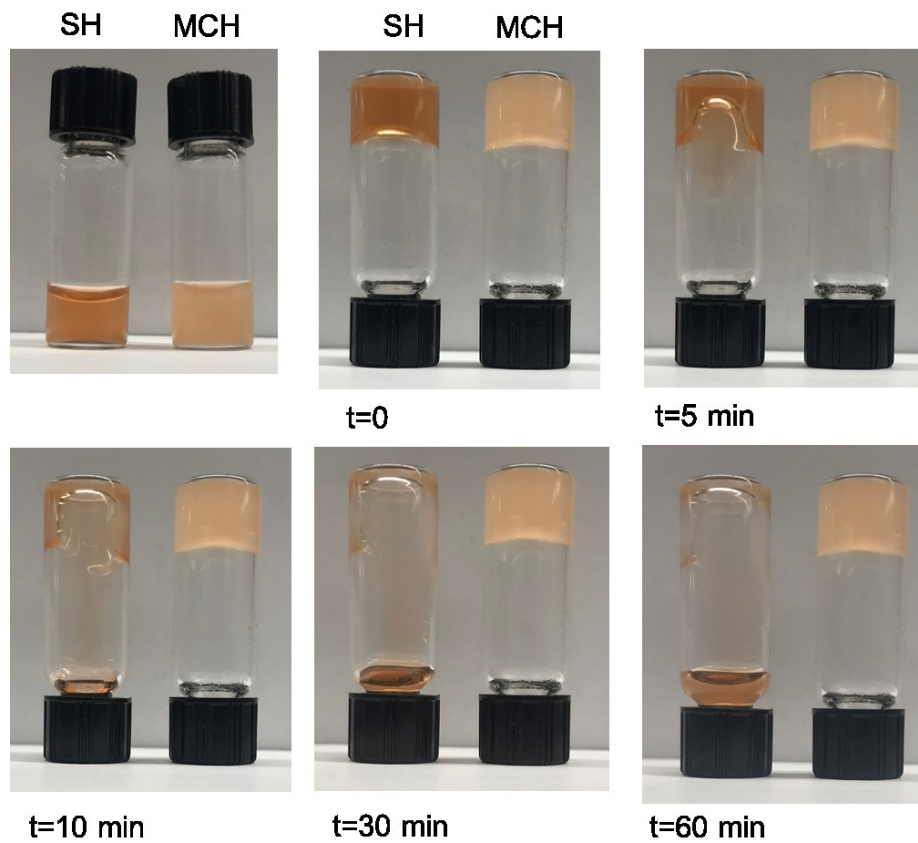
Figure D-3. Viscosity test on SH and MCH.